Application of circulating cell-free tumor DNA profiles for therapeutic monitoring and outcome prediction of metastatic melanoma

Inaugural Dissertation

for

the Doctoral Degree of

Dr. rer. nat.

from the Faculty of Biology

University of Duisburg-Essen,

Germany

Submitted by

Renáta Váraljai (M.Sc.)

from Ózd, Hungary

August 2018

© Renáta Váraljai, 2018

ALL RIGHTS RESERVED

DuEPublico
Duisburg-Essen Publications online

UNIVERSITÄT DUISBURG ESSEN
Offen im Denken

ub | universitäts bibliothek

Diese Dissertation wird über DuEPublico, dem Dokumenten- und Publikationsserver der Universität Duisburg-Essen, zur Verfügung gestellt und liegt auch als Print-Version vor.

DOI: 10.17185/duepublico/47600
URN: urn:nbn:de:hbz:464-20191128-080933-4

Alle Rechte vorbehalten.

Die der vorliegenden Arbeit zugrunde liegenden Experimente wurden an der Klinik für Dermatologie, Universitätsklinikum Essen (Westdeutsches Tumorzentrum, Partnerstandort des Deutsches Konsortium für Translationale Krebsforschung) der Universität Duisburg-Essen in Deutschland angefertigt.

1. Gutachter: Prof.Dr. Ralf Küppers

2. Gutachter: Prof.Dr. Alexander Rösch

3. Gutachter: Asst.Prof.Dr. Nelleke Gruis

Vorsitzender des Prüfungsausschusses: Prof. Dr. Michael Ehrmann

Tag der mündlichen Prüfung: November 19, 2018

Remarks

I hereby declare that this submitted thesis for the consideration of Dr. rer. nat award has been composed by myself. The data presented in this thesis is my own, except where stated and referenced otherwise in the text. This work has not been submitted for the award of any other degree.

Parts of this this thesis (Chapter 4.2) have been submitted for publication as follows:

Renáta Váraljai, Kilian Wistuba-Hamprecht, Teofila Seremet, Joey Mark S. Diaz, Jérémie Nsengimana, Antje Sucker, Klaus Griewank, Jan-Malte Placke, Peter A. Horn, Nils von Neuhoff, Batool Shannan, Heike Chauvistré, Felix Vogel, Susanne Horn, Jürgen C. Becker, Julia Newton-Bishop, Andreas Stang, Bart Neyns, Benjamin Weide, Dirk Schadendorf, Alexander Roesch: *Application of circulating cell-free tumor DNA profiles for therapeutic monitoring and outcome prediction in genetically heterogeneous metastatic melanoma*. (JCO PO)

Table of Contents

1. Abstract 1

2. Introduction 5

2.1. Epidemiology of melanoma 5

2.2. Risk factors of melanoma 6

2.2.1. Environmental risk factors 6

2.2.2. Genetic risk factors 7

2.3. The process of melanomagenesis 8

2.4. Classification of melanoma 9

2.4.1. Histopathological classification 9

2.4.2. Genomic classification of melanoma 11

2.4.3. The AJCC classification (7th edition, 2009) and staging procedures 13

2.5. Prognosis 17

2.5.1. Localized melanoma (stage I and stage II) 17

2.5.2. Metastatic melanoma (stage III and IV) 17

2.6. Current treatments of melanoma 17

2.6.1. Management of the primary tumor 17

2.6.2. Management of metastatic melanoma 18

2.7. Currently approved molecular diagnostics in metastatic melanoma and limitations of tissue-based assays 22

2.8. The field of liquid biopsies 23

2.8.1. Circulating tumor cells (CTCs) 24

2.8.2. Circulating nucleic acids 24

2.9. Methods for ctDNA monitoring 27

2.9.1. Targeted amplicon-based next generation sequencing 27

2.9.2. Droplet Digital PCR 27

2.10. Aims of the study 29

3. Materials and Methods 30

3.1. Materials 30

3.1.1. Patients and clinical data collection 32

3.2. Methods 33

3.2.1. Cell culture of human melanoma cell lines 33

3.2.2. Blood samples 34

3.2.3. DNA extraction and quantification 34

3.2.4. DNA quantification and storage 36

3.2.5. Serum assays 36

3.2.6. Routine mutational analysis of melanoma tissue samples 36

3.2.7. Amplicon-based next generation sequencing of ctDNA samples 37

3.2.8. NGS assay validation experiments 39

3.2.9. Quantitative real-time PCR (qPCR) 39

3.2.10. qPCR analysis 40

3.2.11. Droplet Digital PCR (ddPCR) 40

3.2.12. Droplet generation and thermal cycling conditions 42

3.2.13. ddPCR data analysis 44

3.2.14. Assay sensitivity and false positive rate determination 45

3.2.15. Statistical analysis 46

4. Results 49

4.1. Targeted amplicon-based next generation sequencing of ctDNA samples ..49

4.1.1. Analytical sensitivity of the TA-NGS protocol using cell line derived DNA 49

4.1.2. Validation of the ctDNA TA-NGS protocol in patient derived plasma samples 50

4.1.3. Optimization of the ctDNA TA-NGS protocol in patient derived plasma samples 53

4.2. Application of ddPCR for monitoring therapy responses in metastatic melanoma patients 56
4.2.1. Selection and validation of ctDNA assays 56
4.2.2. Patient characteristics and cohort summary 61
4.2.3. Background levels of mutant-specific ctDNA in healthy donors 64
4.2.4. The ctDNA level correlates with melanoma tumor burden and is a risk factor for disease progression at baseline 66
4.2.5. The ctDNA profiles of melanoma patients correlate with radiologic response and tumor progression under therapy 69
4.2.6. Changes in the ctDNA profile indicate therapy response and failure earlier than radiologic scans 76
4.2.7. ctDNA dynamics in the validation cohort 78
4.2.8. Baseline $NRAS^{Q61}$ ctDNA is an independent predictor of progressive disease and overall survival in MAPKi-treated patients 80
5. Discussion 84
5.1. Targeted amplicon based next generation sequencing of ctDNA samples 84
5.2. Application of ddPCR for monitoring therapy responses in metastatic melanoma patients 86
5.2.1. ddPCR is a sensitive tool to detect low frequency mutations 87
5.2.2. Impact of sample processing and storage conditions on mutation detection 88
5.2.3. ctDNA thresholds have predictive value at baseline 88
5.2.1. ctDNA thresholds have predictive value during therapy 89
5.2.2. The dynamic ctDNA changes reflect response to therapy 90
5.2.3. Baseline $NRAS^{Q61}$ ctDNA is an independent predictor of survival in MAPKi-treated patients 90
5.3. Future prospects 92
6. References 94
7. Appendices 109

8. Acknowledgements 114

9. Curriculum vitae.....115

10. Statutory declarations 117

List of tables

Table 2.1 Summary of AJCC 7th edition (2009) TNM categories 15
Table 2.2 Clinical and pathological AJCC TNM stage grouping 16
Table 2.3 Summary of follow-up guidelines 16
Table 3.1 List of materials 30
Table 3.2 List of human melanoma cell lines 32
Table 3.3 Mutational profiles of cell lines 34
Table 3.4 Multiplex PCR master mix preparation 37
Table 3.5 End Prep master mix preparation 38
Table 3.6 Adapter ligation master mix preparation 38
Table 3.7 Index primer master mix preparation 38
Table 3.8 qPCR primers 40
Table 3.9 Reaction set up for detection *BRAF*^{V600E} mutation (96 wells) 42
Table 3.10 Reaction set up for detection *NRAS*^{Q61} mutation (96 wells) 43
Table 3.11 Reaction set up for detection of *TERT*^{C228T} or *TERT*^{C250T} mutation (96 wells) 43
Table 3.12 Thermal cycling conditions for the *BRAF*^{V600E} and *NRAS*^{Q61} assays 43
Table 3.13 Thermal cycling conditions for the *TERT*^{prom} assays 44
Table 4.1 Characteristics of patient derived plasma samples for TA-NGS analyses .51
Table 4.2 Elevated baseline ctDNA is a risk factor for disease progression 69
Table 4.3 Changes in ctDNA levels identify therapy responders and non-responders 74
Table 4.4 *NRAS*^{Q61} baseline ctDNA is a risk factor for disease progression 81

List of figures

Figure 2.1 Overview of the top 10 cancer rates in the European and German populations. 6
Figure 2.2 The evolutionary process of melanomagenesis....9
Figure 2.3 Overview of the frequently occurring mutations in the TCGA melanoma dataset. 12
Figure 2.4 PD-1 and CTLA-4 immunotherapies for the treatment of cutaneous melanoma....19
Figure 2.5 Signaling targeted therapies for the treatment of cutaneous melanoma...21
Figure 2.6 Origin and range of genetic alterations in cell-free DNA....25
Figure 4.1 Validation of the ctDNA amplicon-based NGS assay sensitivity....50
Figure 4.2 Detectable mutations in ctDNA with TA-NGS....52
Figure 4.3 Detectable mutations in ctDNA with TA-NGS using the optimized settings 54
Figure 4.4 qPCR analysis of genes supposedly falsely detected by TA-NGS 55
Figure 4.5 Frequency of somatic mutations in melanomas....56
Figure 4.6 Technical validation of *BRAF*^{V600E} and *NRAS*^{Q61} mutation detection with ddPCR....58
Figure 4.7 Technical validation of *TERT*^{prom} mutation detection using ddPCR 59
Figure 4.8 False positive detection rate of ddPCR assays 60
Figure 4.9 Patient enrollment in the training cohort 61
Figure 4.10 Basic characteristics of melanoma patients with *BRAF*^{V600E}, *NRAS*^{Q61} and *TERT*^{prom} mutations 62
Figure 4.11 Detection of melanoma specific ctDNA using ddPCR 65
Figure 4.12 Correlation of baseline ctDNA levels with metastatic stage in the training cohort....67
Figure 4.13 Correlation of ctDNA levels with routine serum markers in the training cohort....68
Figure 4.14 ctDNA as a marker of tumor load and its predictive value for occurrence of radiologic tumor burden in melanoma patients 70
Figure 4.15 Changes of the *BRAF*^{V600E} ctDNA levels correlate with therapy response and progression free survival....71
Figure 4.16 Changes of *NRAS*^{Q61} and *TERT*^{prom} ctDNA levels correlate with therapy response and progression free survival. 73
Figure 4.17 *BRAF*^{V600E} ctDNA percentiles predict PFS....75

Figure 4.18 Time gain in assessment of disease progression in the training cohort..77
Figure 4.19 Independent validation cohort.....79
Figure 4.20 Detection of *NRAS*^{Q61} at baseline is a predictor of worse clinical outcome in MAPKi-treated patients.....81
Figure 4.21 Overview of matched tumor tissue and plasma genotypes.....82

List of equations

Equation 1: Gene copies per milliliter of plasma 44
Equation 2: Calculation of standard deviation 45
Equation 3: Assay sensitivity calculation 45
Equation 4: ctDNA normalization 46
Equation 5: ctDNA percent change per week 47

List of appendices

Appendix 1 ROC analysis coordinates of *BRAF*^{V600E}, *NRAS*^{Q61} and *TERT*^{prom} ctDNA assays (related to Figure 4.11) 109
Appendix 2 ROC parameters of ctDNA measurement in correlation to the radiologically assessed tumor load (CT/MRI scans) (related to Figure 4.14).....110
Appendix 3 Contingency table of treatment response of *BRAF*^{V600E} patients (related to Figure 4.15E).....111
Appendix 4 Contingency table of 6 months PFS of *BRAF*^{V600E} patients (related to Figure 4.15F) 111
Appendix 5 Contingency table of 6 months PFS of *NRAS*^{Q61} patients (related to Figure 4.16E).....111
Appendix 6 Contingency table of 6 months PFS of *TERT*^{prom} patients (related to Figure 4.16F) 112
Appendix 7 Contingency table of treatment response of *NRAS*^{Q61} patients (related to Figure 4.16G) 112
Appendix 8 Contingency table of treatment response of *TERT*^{prom} patients (related to Figure 4.16H).....112
Appendix 9 Contingency table of treatment response of patients in the validation cohort (related to Figure 4.19C).....113
Appendix 10 Contingency table of 6 months PFS of patients in the validation cohort (related to Figure 4.19D).....113

Symbols and units

°C: degree Celsius

∆: increment

µ: micro

µl: microliter

µM: micromole

F: capacitance

g: relative centrifugal force

L: liter

ml: milliliter

pM: picomole

V: voltage

λ: lambda (wavelength)

σ: sigma (standard deviation)

Abbreviations

ACD: Shelterin complex subunit and telomerase recruitment factor

AJCC: American joint committee on cancer

ALM: Acral lentiginous melanoma

ATG: adenine, guanine, cytosine (start codon)

AUC: area under the curve

AXL: AXL receptor tyrosine kinase

BAP1: BRCA1 associated protein 1

BEAMing: beads, emulsion, amplification and magnetics

bp: Base pair

BRAF: V-raf murine sarcoma viral oncogene homolog B1

BRAFi: BRAF inhibitor

BRCA1: BRCA1, DNA repair associated

CCND1: Cyclin D1

CD274: CD274 molecule (programmed cell death 1ligand 1)

CDK4: Cyclin dependent kinase 4

CDKN2A: Cyclin dependent kinase inhibitor 2A

cfDNA: Circulating cell-free DNA

chr: Chromosome

CI: Confidence interval

CKIT: Proto-oncogene c-kit

CLND: Completion lymphadenectomy

CNA: Copy number alteration

CR: Complete response

CT: Computed tomography

Ct: Cycles threshold

CTC: Circulating tumor cells

ctDNA: Circulating cell-free tumor DNA

CTLA-4: Cytotoxic T lymphocyte-associated protein 4

CXC: Chemokine receptor

ddPCR: Droplet digital PCR

DLBCL: Diffuse large B-cell lymphoma

DM: Desmoplastic melanoma

dUTP: 2´-Deoxyuridine, 5´-Triphosphate

EMT: Epithelial to mesenchymal transition

EpCAM: Epithelial cell adhesion molecule

FAM: 6-carboxyfluorescein

FDA: Food and Drug Administration

FFPE: Formalin fixed paraffin embedded

gDNA: Genomic DNA

GRCh37: Genome reference consortium human build 37

HEX: Hexachloro-fluorescein

HR: Hazard ratio

IDH1: Isocitrate dehydrogenase (NADP(+)) 1, cytosolic

IFN: Interferon

IL-2: Interleukin-2

KIT: KIT proto-oncogene receptor tyrosine kinase

LDH: Lactate dehydrogenase

LMM: Lentigo maligna melanoma

LOD: Limit of detection

MAF: Mutant allele frequency

MAP2K1: Mitogen-activated protein kinase kinase 1

MAP2K2: Mitogen-activated protein kinase kinase 2

MAPK: Mitogen activated protein kinase

MAPKi: MAPK inhibitor

MC1R: Melanocortin receptor 1

MDM2: MDM2 proto-oncogene

MEKi: MEK inhibitor

Melan-A: Protein melan-A

MET: MET proto-oncogene

miR-21: MicroRNA 21

MITF: Melanogenesis associated transcription factor

mo: monthly

MRI: Magnetic resonance imaging

mt: Mutant

NF1: Neurofibromin 1

NGS: Next generation sequencing

NMM: Nodular melanoma

NRAS: Neuroblastoma RAS viral oncogene homolog

nt: Nucleotide

ntc: No template control

OS: Overall survival

PAP: pyrophosphorolysis activated polymerization

PCR: Polymerase chain reaction

PD: Progressive disease

PD-1: Programmed cell death protein 1

PD-L1: Programmed cell death 1 ligand 1

PD-L2: Programmed cell death 1 ligand 2

PET: Positron emission tomography

PFS: Progression free survival

pH: Potential of hydrogen

POT1: Protection of telomeres 1

PR: Partial response

PTEN: Phosphatase and tensin homolog

qPCR: Quantitative real-time polymerase chain reaction

RAC1: Ras-related C3 botulinum toxin substrate 1

RB1: Retinoblastoma 1

RNA: Ribonucleic acid

ROC: Receiver operating characteristics

RT: Room temperature

rxn: reaction

S100: S100 Calcium binding protein family

SD: Stable disease

sd: Standard deviation

SEM: Standard error of the mean

SLNB: Sentinel lymph node biopsy

SMM: Superficial spreading melanoma

TCGA: The Cancer Genome Atlas

TERF2IP: Telomeric repeat binding factor 2 interacting protein

TERT: Telomerase reverse transcriptase

TNM: primary tumor (T), lymph nodes (N) and distant organ metastasis (M)

TP53: Tumor protein 53

US: Ultrasound

UV: Ultraviolet

VEGF: Vascular endothelial growth factor

WES: Whole exome sequencing

wt: Wild-type

1. Abstract

The implementation of precision oncology requires novel disease and therapy monitoring technologies that are non-invasive, sensitive and specific. Circulating cell-free tumor DNA (ctDNA) reflects the heterogeneous spectrum of specific mutations, especially in systemic disease. Specifically, this thesis aimed to establish and validate plasma-based assays that allow the dynamic quantitative detection of ctDNA as a prognostic biomarker for tumor load and prediction of therapy response in melanoma patients using droplet digital PCR (ddPCR) and next generation sequencing (NGS).

ctDNA monitoring by ddPCR showed excellent sensitivity and high reproducibility. After technical validation of ddPCR with cell line-derived DNA (sensitivity 0.01%), plasma-derived ctDNA was analyzed from a large training cohort (*N*=96) of advanced stage melanoma patients with assays for the *BRAF*^{V600E} and *NRAS*^{Q61} driver mutations as well as *TERT*^{C250T} and *TERT*^{C228T} promoter mutations. An independent patient cohort (*N*=35) was used to validate the clinical utility of ctDNA monitoring under MAPK-targeted or immune checkpoint inhibition therapies.

In contrast, the establishment of an amplicon based NGS protocol in ctDNA samples was hindered by technical issues related to low sensitivity, discrepancies in mutation detection, and poor agreement in mutational status of tumor tissues vs. plasma. In dilution series, using cell line-derived DNA, the lowest limit of detection was 1,000 mutant copies in the background of 10,000 wild-type copies resulting in only 10% analytical sensitivity.

The ddPCR ctDNA results were evaluated with various statistical methods, including ROC and Kaplan Meier analyses, where ctDNA levels were correlated with radiologic treatment response and patient survival. Elevated plasma ctDNA at baseline (i.e. before treatment) was an independent prognostic factor of disease progression when compared with serum S100 and LDH levels in multivariable analysis (HR 7.43, 95% CI 1.01-55.19, *P*=0.05). Changes in ctDNA levels during therapy correlated with treatment response. For example, in patients with the *BRAF*^{V600E} mutation, which drives about half of the melanomas, increasing ctDNA levels were predictive for shorter progression free survival (PFS) (HR 7.28 95% CI 3.64-14.53, *P*<0.0001), and predicted earlier disease progression compared to routine radiological scans (*P*<0.05) with a mean lead-time of 3.5 months.

In *BRAF*^{V600} patients treated with signaling targeted therapies, the occurrence of secondary *NRAS*^{Q61} mutation is associated with treatment failure due to therapy resistance. Accordingly, *NRAS* mutant ctDNA was detected in a significant proportion of samples from patients with *BRAF* mutant tumors under therapy, but unexpectedly also already at baseline. *In vitro* sensitivity studies suggested that this represents higher than expected intra-tumoral heterogeneity with pre-existence of small subclones of NRAS-mutated cells. Furthermore, the detection of plasma *NRAS*^{Q61} ctDNA in baseline samples of MAPKi-treated *BRAF*^{V600E} patients significantly correlated with shorter PFS (HR 3.18 95% CI 1.31-7.68, *P*=0.03) and shorter overall survival (OS) (HR 4.08 95%CI 1.57-10.58, *P*=0.01).

Overall, these results show the potential clinical utility of ddPCR based ctDNA assays as a sensitive monitoring tool, and that ctDNA assessment is a clinically applicable prediction tool for the early assessment of disease progression and therapeutic response in metastatic melanoma patients.

Zusammenfassung

Die Präzisionsonkologie erfordert innovative Methoden zur Beurteilung des Krankheitsverlaufs von Tumorpatienten und des therapeutischen Ansprechens, die möglichst nicht-invasiv, aber hochsensitiv und -spezifisch sind. Die zirkulierende zellfreie Tumor-DNA (ctDNA) spiegelt hierbei das heterogene Spektrum spezifischer onkogener Mutationen wider, insbesondere bei Patienten im Stadium der Organmetastasierung. Das Ziel der vorliegenden Dissertation war die Etablierung und Validierung von plasmabasierten Messmethoden mittels *digital droplet PCR* (ddPCR) und *next generation sequencing* (NGS) zum quantitativen Nachweis von ctDNA und deren Rolle als Biomarker für die Tumorlast und Prädiktion des therapeutischen Ansprechens bei Melanompatienten.

Das ctDNA-Monitoring via ddPCR zeichnete sich durch eine hohe Sensitivität und Reproduzierbarkeit aus. Nach technischer Validierung der ddPCR an DNA aus Zelllinien (0,01 % Sensitivität), erfolgte die ctDNA-Analyse von Plasmaproben einer großen Patientenkohorte (*N*=96) mit fortgeschrittenem Melanom mittels spezifischer ddPCR-Assays für $BRAF^{V600E}$ und $NRAS^{Q61}$ Treiber-Mutationen sowie $TERT^{C250T}$ und $TERT^{C228T}$ Promoter-Mutationen. Eine unabhängige Kontrollkohorte (*N*=35) diente der Validierung der klinischen Anwendbarkeit des ctDNA-Monitoring unter zielgerichteter Therapie mit MAPK- oder Immun-Checkpoint-Inhibitoren.

Im Gegensatz zur ddPCR war die Etablierung des Amplicon-basierten NGS-Protokolls durch eine sehr geringe Sensitivität und Diskrepanzen im Mutationsnachweis sowie durch eine schwache Korrelation des Mutationsstatus im Tumorgewebe mit dem Mutationsstatus im Plasma gekennzeichnet. In einer Verdünnungsreihe mit DNA aus Zelllinien betrug die untere Nachweisgrenze lediglich 1,000 mutierte DNA-Kopien in einem Hintergrund aus 10,000 Wildtyp-DNA-Kopien, was einer Sensitivität von nur 10% entsprach.

Die Ergebnisse der ddPCR-basierten ctDNA-Analyse wurden mit verschiedenen statistischen Tests, einschließlich ROC- und Kaplan Meier-Analysen, ausgewertet. Hierbei wurden die ctDNA-Spiegel sowohl mit der radiologischen Beurteilung des Therapieerfolges als auch mit der Überlebenszeit korreliert. In der univariaten Analyse erwies sich ein erhöhter ctDNA-Ausgangswert im Plasma (d.h. vor Therapieeinleitung) als unabhängiger prognostischer Faktor für das Fortschreiten der Erkrankung und war deutlich der Bestimmung von S100 und LDH im Serum

überlegen (HR 7.43, 95% CI 1.01-55.19, *P*=0.05). Veränderungen der ctDNA-Spiegel während der Behandlung korrelierten eindeutig mit dem Therapieansprechen. Bei Patienten mit *BRAF*^{V600E} Mutation, die bei etwa der Hälfte aller Melanome als Treiber-Mutation fungiert, stellte der ctDNA-Anstieg einen prädiktiven Faktor für ein signifikant kürzeres progressionsfreies Überleben (PFS) dar (HR 7.28 95% CI 3.64-14.53, *P*<0.0001). Die ctDNA-basierte Erkennung des Tumorprogresses war im Durchschnitt 3,5 Monate früher als radiologische Standarmethoden (*P*<0.05).

Bei Patienten mit *BRAF*^{V600}-Mutation, die mit zielgerichteten Therapien behandelt werden, ist das Auftreten von sekundären *NRAS*$^{Q61-}$Mutationen häufig mit Therapieresistenz assoziiert. Dementsprechend wurde *NRAS*-mutierte ctDNA auch in unseren Patienten mit BRAF-mutierten Tumoren in einer erheblichen Anzahl der Proben unter Therapie nachgewiesen. Völlig unerwartet jedoch wurde bei einigen Patienten auch bereits vor Therapiebeginn *NRAS*^{Q61}-ctDNA detektiert. *In vitro* Sensitivitätsstudien ließen vermuten, dass dies auf eine unerwartet hohe intratumorale Heterogenität, sprich der *a priori* Existenz einzelner NRAS-mutierter Subklone, zurückzuführen ist. Darüber hinaus korrelierte der Nachweis von *NRAS*^{Q61} ctDNA im Plasma von MAPK-Inhibitor-naiven Patienten mit *BRAF*^{V600E}-Mutation mit signifikant kürzerem PFS (HR 3.18 95% CI 1.31-7.68, *P*=0.03) und kürzerer Gesamtüberlebenszeit (OS) (HR 4.08 95%CI 1.57-10.58, *P*=0.01).

Insgesamt unterstreichen die Ergebnisse dieser Arbeit den klinischen Nutzen der ctDNA-Bestimmung mit ddPCR als einer hochsensitiven Methode sowohl zur Therapieverlaufskontrolle als auch zur frühzeitigen Beurteilung der Tumorprogression und zur Prädiktion des therapeutischen Ansprechens bei Patienten mit metastasiertem Melanom.

2. Introduction

2.1. Epidemiology of melanoma

Melanoma is the most life-threatening form of skin cancer that develops from the uncontrolled growth of melanocytes, and it is one of the most treatment-resistant human tumors. Melanocytes are pigment producing cells stemming from pluripotent neural crest cells (1). The majority of melanomas are sporadic (i.e. randomly occurring), and around 10% of melanomas are caused by genetic inheritance (familial melanoma) (2,3). Regarding localization, the most common type of melanoma develops from melanocytes in the epidermis (cutaneous melanoma); but melanoma can also develop from melanocytes residing in mucosal surfaces (mucosal melanoma) and in the eye (uveal melanoma) (2). The focus of this research project was cutaneous melanoma; thus, only the biology, epidemiology, classification, and prognosis of cutaneous melanoma are highlighted in this chapter.

Cutaneous melanoma is reported as the 7th most common cancer type in the European Union with an estimated incidence rate of 10.2 and mortality rate of 1.4 per 100,000 inhabitants (4,5) (**Figure 2.1A**). In Germany, the estimated incidence and mortality rate is 11.4 and 1.4; accounting for 16,884 new cases and 2,671 deaths per year, respectively (4,5) (see **Figure 2.1B**). Specifically, in North-Rhine-Westphalia (the largest federal state of Germany), the estimated incident rate of cutaneous melanoma was 14.6 in men, and 16.4 in women in 2015, resulting in an estimated annual increase of 3.8% (6). Importantly, the incidence of melanoma has been increasing worldwide over the past decades in an alarming rate (7). Therefore, there is a high need for preventative efforts in order to reduce the global burden of melanoma.

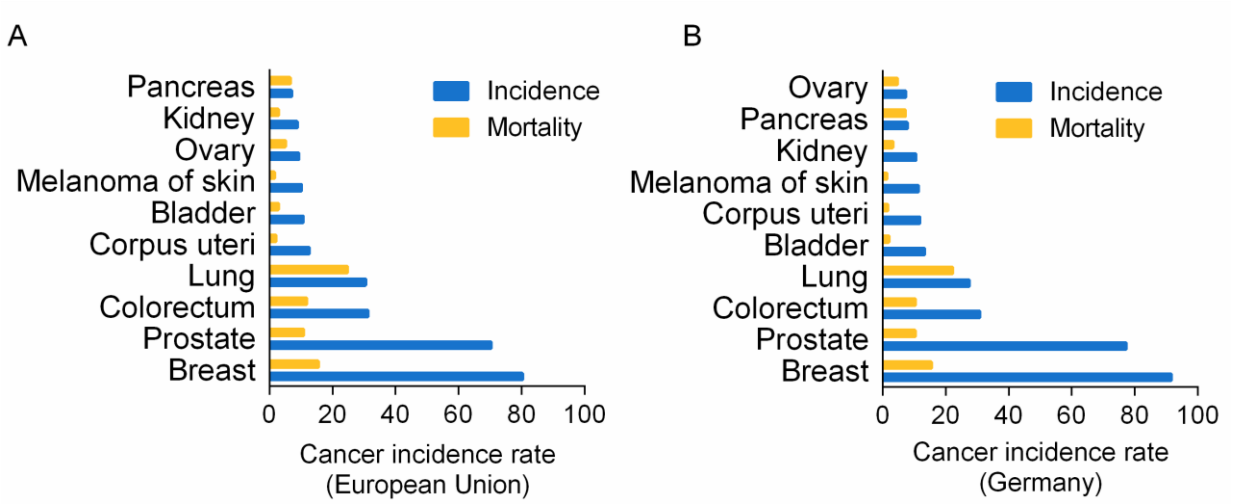

Figure 2.1 Overview of the top 10 cancer rates in the European and German populations.

Incidence and mortality rates per 100,000 inhabitants per year shown for **A.** the European Union and **B.** Germany. Estimated incidence and mortality rates for both sexes in 2012, age standardized rates (European). Graph was created based on the GLOBOCAN 2012 data source (4,5).

2.2. Risk factors of melanoma

2.2.1. Environmental risk factors

The main environmental risk factor of cutaneous melanoma is exposure to ultraviolet (UV) light from the sun. The three types of UV rays are classified by their wavelengths: UV-A (λ=320-400 nM), UV-B (λ=280-320 nM) and UV-C (λ=200-280 nM). Current scientific views suggest that UV radiation plays a role in premature skin aging, sunburn, eye damage, harmful effects on the immune system, and skin cancer (8).

The worldwide melanoma incidence rates are influenced by the differences in UV exposure. In fact, incidence rates of melanoma are higher in regions close to the equator and where the ozone layer is reduced (9). Intense and intermittent sun exposure is associated with a higher risk for melanoma compared to continuous sun exposure (10–13). Moreover, multiple episodes of sunburn during childhood or adolescence can significantly contribute to an increased risk of getting melanoma (12,13). But sunlight isn't the only source of UV radiation. Tanning salons are popular worldwide, and several reports presented association between sunbed usage and risk of skin cancer including melanoma (14). Age and sex also represent a risk factor

for developing melanoma. The incidence of melanoma is higher in females in their younger ages, while, in males, it is more common in middle aged or older individuals (15). Other environmental risk factors like smoking have not been shown to significantly correlate with melanoma (7,16).

UV rays are well known to be mutagenic for the DNA resulting in UV signature mutations, characterized by C>T or CC>TT substitutions, at di-pyrimidine sites. Meta-analyses of 333 patients with cutaneous melanoma revealed the presence of UV signature mutations in 76% of primary melanomas and in 84% of metastatic samples (17). When these genetic aberrations occur in tumor suppressor genes or oncogenes, and are not restored by the DNA repair machinery, it can lead to uncontrolled growth of skin cells including melanocytes. Specifically, in the *TP53* (tumor protein 53) tumor suppressor gene, which is altered in many human cancers including melanoma, high number of UV mutations were identified (the highest frequency across all known genetic melanoma drivers) (18). Moreover, it has been shown that UV radiation accelerated the most common genetic melanoma subtype, i.e. *BRAF* (V-raf murine sarcoma viral oncogene homolog B1)-mutated melanomas (see below), through the interaction with *TP53.* Thus the UV induced damages in *TP53* play a key role in the melanomagenesis (19).

2.2.2. Genetic risk factors

Approximately 10% of melanomas occur due to hereditary predisposition (3). Familial melanoma is characterized by two or more first-degree (e.g. parent, child) affected family members. Most familial melanomas are associated with germline mutations in the *CDKN2A* and *CDK4* genes with 19.39 % and 0.68 % frequency, respectively (20–22). Other germline mutations with high penetrance are described in the *BRCA1*, *BAP1*, *POT1*, *CXC*, *ACD*, *TERF2IP* and *TERT* genes (22). UV exposure plays a role also in familial melanoma, however, mostly in individuals with low penetrance mutations. For example, Caucasian individuals with red hair and freckles who carry variations in the *MC1R* gene (an important regulator of pigmentation) are prone to sunburn and melanoma (23). To date, genetic testing is available for *CDKN2A* (24) and there is growing focus on *CDK4* predispositions. The extensive research done in this field paves the way for new tests and genetic counseling of risk populations. In addition, protection from UV radiation and examination of existing pigmented skin

tumors (including benign melanocytic nevi) play a central part in the prevention of melanoma (25).

2.3. The process of melanomagenesis

An important risk factor for both sporadic and familial melanoma is the total number of benign and atypical melanocytic nevi (26,27). Nevi are benign cutaneous neoplasms caused by proliferating melanocytes. The most known form, the common acquired nevus, is particularly frequent in Caucasians (28). While the risk of progression to melanoma is low for a single benign nevus, the likelihood of progression increases with the total number of nevi. In fact, Gandini *et al* demonstrated in a meta-analysis that those individuals who showed a nevus count above 100 had a significantly increased risk of melanoma (29). Shain *et al* recently unraveled on a genetic and histological level the sequential evolutionary process of melanomagenesis (**Figure 2.2).** His analyses revealed that in most benign melanocytic nevi the first genetically altered (activated) driver is the *BRAF*^{V600E} mutation. So-called intermediate nevi, i.e. the next step in melanomagenesis, were characterized by the presence of more mutated driver genes and had a higher total mutational burden (comprising of also UV signature mutations). Intermediate nevi were additionally associated with the occurrence of another *BRAF* hotspot variant, *BRAF*^{V600K}, and *NRAS* (Neuroblastoma RAS viral oncogene homolog) mutations. *TERT* (Telomerase reverse transcriptase) promoter mutations (termed *TERT*^{prom}*)* seemed to be selected also relatively early during the process of melanocytic transformation. In fact, 77% of the analyzed intermediate nevi and melanomas *in situ* contained *TERT*^{prom} mutations. *CDKN2A* loss was predominantly seen at a more advanced level of melanoma progression and invasion. There, also mutations in the *SWI/SNF* chromatin remodeling genes and a loss of *TP53* and *PTEN* (phosphatase and tensin homolog) tumor suppressor genes were detected (**Figure 2.2**).

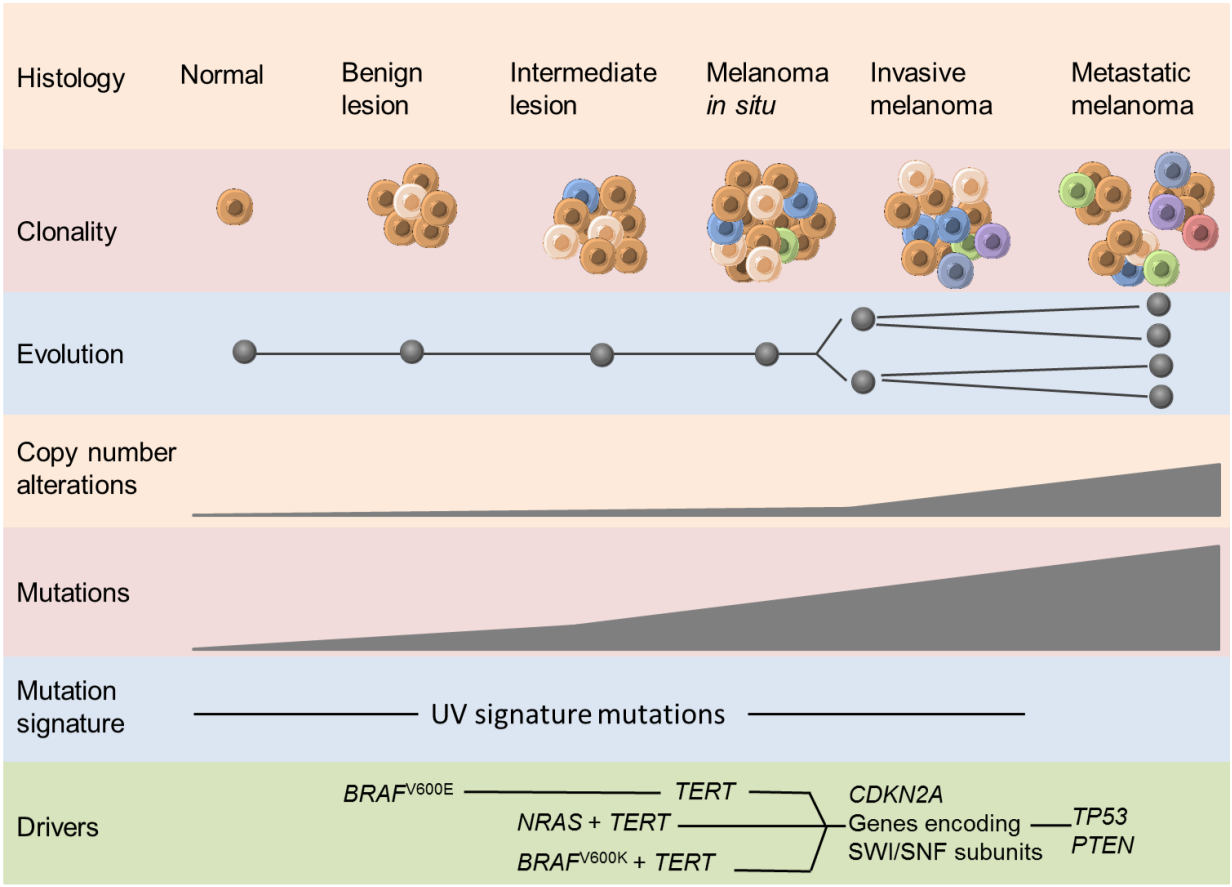

Figure 2.2 The evolutionary process of melanomagenesis

Adapted from Shain *et al* 2015 and Shain *et al* 2016 (28,30). The figure was created using Servier Medical Art (31).

2.4. Classification of melanoma

2.4.1. Histopathological classification

According to histopathological characteristics, melanoma can be classified mainly into the following subtypes:

2.4.1.1. Superficial spreading melanoma (SSM)

SSM is the most common subtype in Caucasians, accounting for 75% of the melanomas and is associated with intermittent sun exposure (15,32). As the name suggests, SSM grows on the surface of the epidermis for a while, before invading into deeper skin layers. It is histologically characterized by the lateral spread of transformed melanocytes along the epidermis. It is often localized on the back of men and on the legs of women. It can show various colors including pink, tan, brown, black or sometimes blue. SSM can arise from a previously benign nevus (15,32).

2.4.1.2. Lentigo Maligna Melanoma (LMM)

LMM accounts for 4-15% of melanomas and it is associated with long-term sun exposure (15). LMM is characterized by small, often hyperchromatic proliferating cells along the dermal epidermal junction. It shows also a variety of colors, such as tan, brown or black with irregular outline. LMM is often located on the head or neck of elderly people (15,32).

2.4.1.3. Nodular Melanoma (NMM)

NMM occurs in approximately 5% of all cutaneous melanoma cases and it is associated with intermittent sun exposure (15,32). NMM is often ulcerated and characterized by rapidly proliferating tumor cell aggregates in a vertical growth phase. It is mostly localized on the trunk, legs and arms of middle-aged and elderly adults. NMM can be brown, black or sometimes blue with irregular outlines (15,32).

Less common melanoma subtypes include acral lentiginous melanoma and desmoplastic melanoma.

2.4.1.4. Acral lentiginous melanoma (ALM)

ALM is a rare subtype, which accounts for less than 5% of melanomas. It is found on acral surfaces, often in the nail bed (15). ALM is characterized by single hyperchromatic, and often spindle shaped cells along the dermal epidermal junction. It appears in brown or black discoloration within the nails, on the palms or on the soles of the feet. Commonly it affects elderly Asians, African Americans and Hispanics (15,32).

2.4.1.5. Desmoplastic melanoma (DM)

DM often occurs in chronically sun damaged cutaneous surfaces. DM is morphologically heterogeneous, but it is often characterized by dispersed, separating spindle shaped single melanocytes in a collagen-rich stroma. It can appear as pale pink nodules or plaques that lack pigmentation. DM mainly effects elderly people, particularly men (15,32).

Other, even rarer types include balloon cell melanoma, which is composed of large, clear cells; rhabdoid melanoma characterized by polygonal neoplastic cells; and

myxoid melanoma is myxoid stroma which is associated with mucin production (33–36).

2.4.2. Genomic classification of melanoma

During the recent years, large-scale genomic analyses revealed heterogeneous genetic subtypes and molecular characteristics of melanoma, providing new possibilities including targeted therapy rationales for personalized medicine. Particularly, The Cancer Genome Atlas (TCGA) provided insights into the different genomic subtypes, and revealed the significance of frequently occurring genetic alterations in melanoma analyzing 333 patients' samples [primary tumors (20%) and metastatic sites (80%)] (17).

The TCGA framework identified significantly mutated genes using whole exome sequencing (WES), and found that melanomas can be categorized into three subtypes: the *BRAF*-mutated, *NRAS*-mutated and *NF1* (Neurofibromin 1)-mutated subtype. The mutant *BRAF* subtype accounting for 52% of the samples was the largest identified subtype, followed by the mutant *NRAS* subtype with 28% frequency. *NF1* mutations have been found in 14% of the cases. Altogether, these three subtypes cover 94% of all melanoma genotypes. A fourth subtype was referred to as triple wild-type. Triple wild-type melanomas represent a highly heterogeneous subgroup with non-hotspot mutations in 11 additional genes (**Figure 2.3A**). UV signature mutations were detected in 30% of triple wild-type melanomas, and in more than 90% of the cases in the other three subtypes. Additionally, UV signature mutations were seen in *RAC1*, *IDH1*, *TP53* and *RB1.* Regarding somatic copy number alterations (CNA), triple wild-type melanomas had significantly more CNAs in *KIT*, *CDK4*, *CCND1, MDM2* and *TERT*. *BRAF*, *MITF,* and *CD274* (*PD-L1*) amplifications were associated with the *BRAF* subtype, while *NRAS* amplifications occurred in the *NRAS* subtype only.

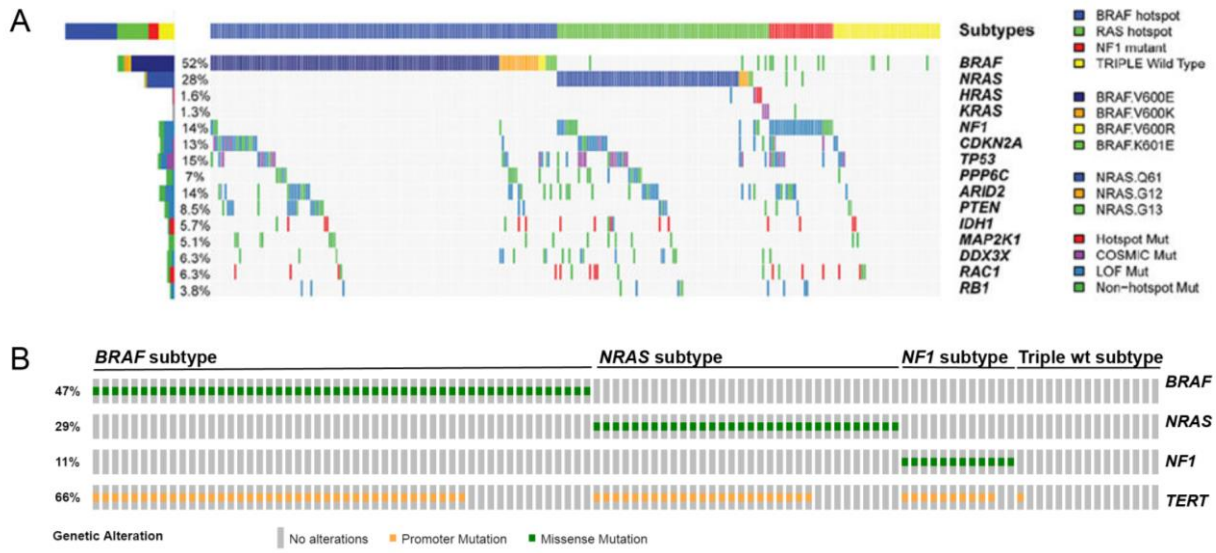

Figure 2.3 Overview of the frequently occurring mutations in the TCGA melanoma dataset.

A. Overview of the melanoma driver mutations across the TCGA dateset. Figure taken from The Cancer Genome Atlas Network (17). **B.** Frequency of *TERT* promoter mutations across 111 samples from the TCGA dataset [map was created with OncoPrinter tool (37,38) based on data from The Cancer Genome Atlas Network (17)]. The percentage of samples altered per gene is indicated on the left side. Each column represents one sample. Subcategories are represented in a color-coded manner.

2.4.2.1. The most frequently occurring hotspot mutations in melanoma

In the TCGA melanoma cohort, the majority of the samples carried mutations in the mitogen-activated protein kinase (MAPK) signaling pathway. The hyperactivation of the MAPK pathway is a driving force of the oncogenic transformation process in many cancers and is mainly caused by upregulated *BRAF* and *NRAS* due to missense mutations. Within the most prominent *BRAF* melanoma subtype (52% of all cases; see **Figure 2.3A**), most mutations occurred at the V600 codon (46% of all cases). More specifically, 85% of the V600 codon mutations accounted for the V600E variant, which results in a substitution of valine (V) to glutamic acid (E) (17,39). Less common variants at V600 included V600K; [valine (V) to lysine (K)], V600R [valine (V) to arginine (R)] with 12% and 0.02% frequency of all V600 cases, respectively [18]. Although not seen in the TCGA melanoma dataset, there are other less frequent V600 hotspot mutations, such as V600D [valine (V) to aspartic acid (D)], or the V600M [valine (V) to leucine (M)] mutations (39). Mutations in non-V600 hotspot

locations also occur in melanoma, however only in a minority of the cases [0.03% frequency (17)].

The second most frequent melanoma subtype was characterized by mutations in *RAS* family members. *NRAS* mutations occurred in the vast majority of cases (28%; see **Figure 2.3A**) with variants at the Q61 codon being the most prominent (98%). Of these, Q61R [glutamine (Q) to arginine (R)], and Q61K [glutamine (Q) to lysine (K)], mutations occurred in 40% and 32% of all Q61 hotspot cases. Less frequently, the Q61L [glutamine (Q) to leucine (L)], and Q61H [glutamine (Q) to histidine (H)] mutations were detected with 0.12 and 0.04% frequencies, respectively. Non-Q61 hotspot mutations in *NRAS* were reported in only a few cases, corresponding to 0.08% of all *NRAS*-mutated cases (17).

A large proportion of samples had hotspot mutations in the promoter region of the *TERT* gene (66 % of the analyzed samples, see **Figure 2.3B**). Within all promoter mutations the $TERT^{C228T}$ and $TERT^{C250T}$ were the most prominent, accounting for 23.5% and 42.5% of all cases, respectively. $TERT^{prom}$ mutations co-occurred in over 70% of the *BRAF* and *NRAS* subtypes and in 83% of the *NF1* subtype. $TERT^{prom}$ mutations were also detected in triple wild-type melanomas, however at significantly lower rate (17).

In summary, the above described *BRAF*, *NRAS*, $TERT^{prom}$ hotspot mutations occur in a considerable proportion of melanomas and a combination of these, e.g. when used as a genetic biomarker, would cover approximately 85% of all melanoma patients.

2.4.3. The AJCC classification (7th edition, 2009) and staging procedures

The American Joint Committee on Cancer (AJCC) tumor classification is a cancer-specific clinicopathologic staging system. It is essential in guiding treatment recommendations and stratification of patients for clinical trial eligibility.

The classification system is evaluating three factors: primary tumor (T), lymph node metastasis (N), and distant organ metastasis (M). M stage evaluation additionally includes serum lactate dehydrogenase (LDH) measurement, which is a general surrogate for tumor burden. Meanwhile an updated version, the AJCC 2017, 8th edition, is being introduced into the clinics. However, since all work presented in the thesis is based on biomaterial annotated to AJCC 2009 stages (all patients were

diagnosed before December 31st of 2017), this update is not considered here. The AJCC 2009, 7th edition classification is summarized in **Table 2.1.** and **Table 2.2.** (40)**.**

The T stage is assessed by evaluation of the primary tumor after surgical excision and is mainly based on the measurement of tumor thickness, which is determined in millimeter and referred to as Breslow thickness. Ulceration of the primary tumor and the mitotic rate are provided as additional prognostic parameters. The metastatic lymph node infiltration (N stage) is either assessed histologically after surgical removal or imaged *in situ* by ultrasound (US) or radiologic assessment such as computed tomography (CT) or magnetic resonance imaging (MRI). The spread of metastasis into distant organs (M stage) is evaluated by radiologic imaging, mostly CT and MRI, but occasionally also whole-body scintigraphy or positron emission tomography (PET). Depending on respective disease stages and national guidelines, melanoma patient follow-up is done at different time intervals. In **Table 2.3**, the German recommendations are explained according to which patients at the Department of Dermatology at the University Hospital Essen are being examined for follow-up.

Table 2.1 Summary of AJCC 7th edition (2009) TNM categories

Table was created based on AJCC 7th edition, adapted from Balch *et al* (40).

TNM staging categories		
Classification		
T	**Thickness (mm)**	**Ulceration/Mitosis**
Tis	N/A	N/A
T1	≤1.00	a: without ulceration and mitosis < 1/mm^2 b: with ulceration or mitoses ≥ 1/mm^2
T2	1.01-2.00	a: without ulceration b: with ulceration
T3	2.01-4.00	a: without ulceration b: with ulceration
T4	≥4.00	a: without ulceration b: with ulceration
N	**Metastatic nodes (*N*)**	**Nodal metastatic burden**
N0	0	N/A
N1	1	a: micrometastasis* b: macrometastasis**
N2	2-3	a: micrometastasis* b: macrometastasis** c: in transit metastasis/satellites without metastatic nodes
N3	4+, or in transit/satellite metastatic nodes	
M	**Site**	**Serum LDH**
M0	No distant metastases	N/A
M1a	Distant skin, subcutaneous, or nodal metastases	Normal
M1b	Lung metastases	Normal
M1c	All other visceral metastases	Elevated

Tis: T *in situ*, *N*: number, N/A: not applicable, LDH, lactate dehydrogenase. *Micrometastases are diagnosed after sentinel lymph node biopsy. **Macrometastases are defined as clinically detectable nodal metastases confirmed pathologically.

Table 2.2 Clinical and pathological AJCC TNM stage grouping

Table was created based on AJCC 7th edition, adapted from Balch *et al* (40).

Stage	Clinical grouping	Pathological grouping
Stage 0	Tis N0 M0	Tis N0 M0
Stage I		
Stage IA	T1a N0 M0	T1a N0 M0
Stage IB	T1b–T2a N0 M0	T1b–T2a N0 M0
Stage II		
Stage IIA	T2b–T3a N0 M0	T2b–T3a N0 M0
Stage IIB	T3b–4a N0 M0	T3b–4a N0 M0
Stage IIC	T4b N0 M0	T4b N0 M0
Stage III		
Stage IIIA		T1–4a N1a/N2a M0
Stage IIIB	Any T N>N0 M0	T1b–T4b N1a-N2c M0
Stage IIIC		T1–T4b N1b-N3 M0
Stage IV	Any T Any N M1	Any T Any N M1

Tis: T in situ

Table 2.3 Summary of follow-up guidelines

Table was created based on the S3 recommendations of the German Cancer Society and German Dermatologic Society, adapted from the published guidelines (41).

Stage	Physical examination			Lymph node US			Laboratory (S100B)			Imaging examination		
Years	**1-3**	**4+5**	**6-10**	**1-3**	**4+5**	**6-10**	**1-3**	**4+5**	**6-10**	**1-3**	**4+5**	**6-10**
IA	6-mo	12-mo	12-mo	-	-	-	-	-	-	-	-	-
IB-IIB	3-mo	6-mo	6-12 mo	6-mo**	-	-	3-mo	-	-	-	-	-
IIC-IV*	3-mo	3-mo	6-mo	3-mo	6-mo	-	3-mo	6-mo	-	6-mo	-	-

US: ultrasound, mo: monthly. *in case of complete resection, ** in case of pathological confirmation of SLNB, otherwise refer to stage IIC.

2.5. Prognosis

2.5.1. Localized melanoma (stage I and stage II)

Tumor thickness (Breslow) is the most important prognostic marker in melanoma. Early diagnosis of the primary lesion correlates with improved prognosis. For example, patients with thin primary tumors without ulceration (T1a, stage IA) have significantly better 5- and 10-year survival rates (97% and 93%, respectively) as compared to patients with melanomas thicker than 4 mm and ulceration (T4b, IIC). The 5- and 10-year survival rates of these patients are 53% and 39%, respectively (40). The mitotic rate is the second most important predictor of survival, where an increasing mitotic rate significantly correlate with worse survival rates (40).

2.5.2. Metastatic melanoma (stage III and IV)

The number of lymph nodes affected by either (histologically detected) micrometastases (N1a, N2a) or macrometastases (N1b, N2b) is another independent predictor of survival (40). For example, patients with T1N1a stage have a 70% 5-year survival rate and, thus, significantly better as compared to the 39% survival rate of patients with T1N3 stage (40). The prognosis of stage IV melanoma differs with regard to the location of distant metastasis and LDH status. For example, patients with M1a stage (metastases in the skin and subcutaneous regions with normal LDH) have better 1-year survival rates (62%) compared to M1b stage (lung metastasis or lung and skin or subcutaneous metastases with normal LDH (53%); M1c stage (any other visceral organs and elevated LDH) patients have the worst 1-year survival rates with 33% (40).

2.6. Current treatments of melanoma

2.6.1. Management of the primary tumor

Patients with primary cutaneous melanoma and with no evidence of lymph node metastasis are usually treated by surgery. Excision margins are dependent on Breslow thickness (tumor thickness ≤1-2mm → 1 cm safety margin, 2,01- >4mm → 2 cm safety margin). Based on the primary tumor stage, sentinel lymph node biopsy (SLNB) is performed. High-risk primary melanomas can be additionally treated with

adjuvant therapy regimens which include interferon (IFN) or novel signaling pathway targeted or immune therapies (2).

2.6.2. Management of metastatic melanoma

2.6.2.1. Surgery

In stage III melanoma, still the first choice is surgical removal of the affected lymph nodes, however only if a complete resection of the tumor(s) is possible. Completion lymphadenectomy (CLND) is performed after histological confirmation of melanoma infiltration in the resected lymph nodes. In case of unresectable lymph node metastases, patients may receive immunotherapy or targeted therapies, and less frequently radiotherapy. In stage IV melanoma, surgical removal of metastatic organs is mostly dependent on the location and number of the metastases. Metastases that cannot be removed may be treated with radiotherapy, immunotherapy, targeted or combination therapies. Adjuvant therapy options with targeted or immune therapies are about to become approved for clinical use (2).

2.6.2.2. Chemotherapy and radiotherapy

Modern cancer therapies demonstrated significant improvement in survival compared to classic chemotherapies (e.g. dacarbazine) (2,42). Radiotherapy is commonly applied in the treatment of skin, bone and brain metastasis (43). Since the approval of immune checkpoint and targeted inhibitors, chemotherapy and radiotherapy is being rather applied in 2^{nd}, 3^{rd} or 4^{th} line scenarios, or in combination with these modern cancer treatments in clinical trials (2,42,44) .

2.6.2.3. Immunotherapies and resistance

In the past 30 years, immunotherapies in melanoma predominantly focused on the T-cell activating cytokine Interleukin-2 (IL-2), or interferon alpha (IFNα) which is an activator of many different immune effector cell types. The success rate of these treatments was relatively low, while the toxicity rates were high (45,46). Other immunotherapy approaches involved vaccination or adoptive cell therapies in order to activate the immune system. Despite extensive research efforts, real success in the immunotherapy field only came in the recent years with the use of immune checkpoint inhibitors (**Figure 2.4**).

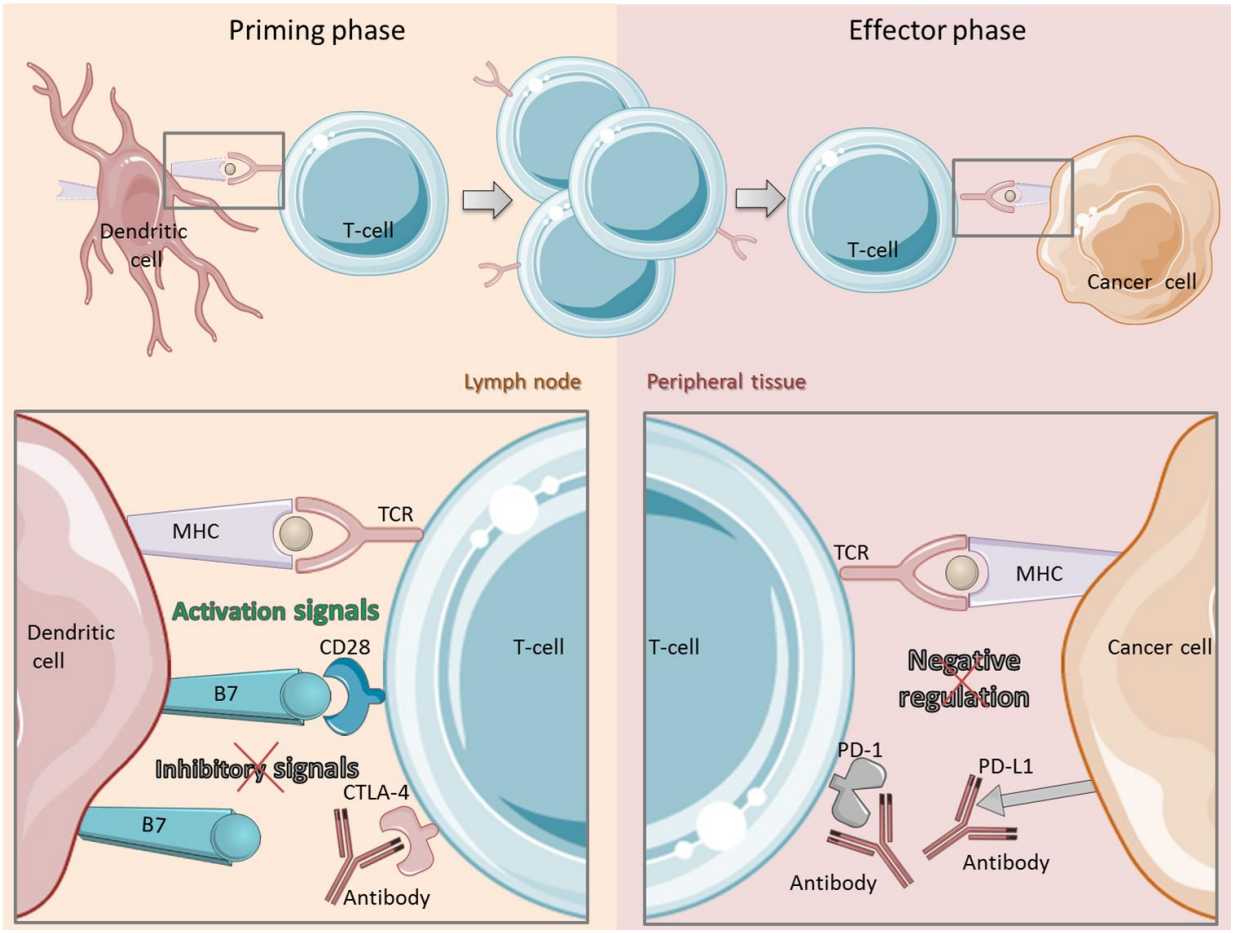

Figure 2.4 PD-1 and CTLA-4 immunotherapies for the treatment of cutaneous melanoma

CTLA-4 inhibition is effective in the priming phase of the T-cell response within the lymph nodes (left panel). PD-1 and PD-L1 inhibition are effective in the effector phase of the T cell response within the peripheral tissue (right panel). Adapted from Ribas, 2012 (47). The figure was created using Servier Medical Art (31).

The development of a cytotoxic T lymphocyte-associated protein 4 (CTLA-4) blocking humanized monoclonal antibody and antibodies specific to programmed cell death-1 (PD-1) expressed on T-cells resulted in significant improvement of patients' survival (42). CTLA-4 is an inhibitory checkpoint receptor expressed on T-lymphocytes that blocks T-cell activation by inhibiting IL-2 secretion and inducing cell cycle arrest (48,49). The CTLA-4 blocker ipilimumab showed good responses in stage IV melanoma patients with a 50.4% overall survival (OS) rate at 12 months (42). PD-1 has two ligands, PD-L1 which is found on tumor cells, and PD-L2 found on antigen presenting cells (50–52). The PD-1 monoclonal antibodies pembrolizumab and nivolumab showed better clinical responses compared to CTLA-4 blockade resulting in an average 72.2% OS rate at 12 months. The combination of CTLA-4 plus PD-1

blockade showed an OS rate of even 73.1% at 12 months (42). Treatment strategies targeting PD-L1 also showed good responses and low toxicities (53). Other modern immunotherapies, like the anti-CD137 antibody urelumab, showed good responses, too, with a 70% disease control rate in early phase clinical studies in combination with nivolumab (54). Despite the good response rates seen across pharmaceutical studies and in clinical routine, many immunotherapy-treated patients do not respond or progress after initial response due to acquired resistance. This happens mainly due to impaired immune infiltration, impaired presentation of antigens (e.g. due to alterations in β2-microglobulin), attenuated IFN signaling (e.g. caused by alterations in the JAK/STAT signaling pathway), or severe T-cell exhaustion (55). Many more immune checkpoint blockers are tested in currently ongoing clinical trials, particularly in combination with each other or with targeted therapies, which perhaps could further increase the overall survival of patients (44).

2.6.2.4. Signaling pathway targeted therapies and resistance

Targeted therapies employ small molecules against the activity of disease-driving proteins (**Figure 2.5**). The identification of activating mutations in the MAPK signaling pathway, particularly *BRAF* mutations at the V600 codon, and the development of matching molecular inhibitors have significantly improved the PFS and the OS of metastatic melanoma patients. The first approved $BRAF^{V600}$ inhibitor (BRAFi) vemurafenib showed a significant improvement of clinical responses in V600-mutated melanoma patients resulting in a 84% survival rate at 6 months of treatment (56). Next generation BRAFi, like dabrafenib and encorafenib, also showed pronounced effects. In average, 63.4% of patients were alive at 12 months when treated with these BRAFi (42). The *MAP2K1* or *MAP2K2* (MEK1/2) targeting compounds trametinib and cobimetinib, working downstream of *BRAF*, particularly resulted in improved clinical outcomes of patients with *NRAS* mutant melanoma. The combination of MEK inhibitors (MEKi) with BRAFi in $BRAF^{V600}$-positive patients showed even better responses as compared to single BRAFi treatment, where 76.9% OS rates were reported at 12 months (42). Despite the initial success of MAPK pathway-targeted therapies, the majority of treated patients experienced tumor recurrence (after a median of 6-8 months of response) due to developing treatment resistance. BRAFi/MEKi resistance of melanoma cells happens due to a variety of mechanisms, but mainly due to molecular MAPK pathway reactivation by either

BRAF splice variants, *BRAF* amplifications, or mutations at the Q61 codon of *NRAS*, and mutations in MEK1/2 genes (57).

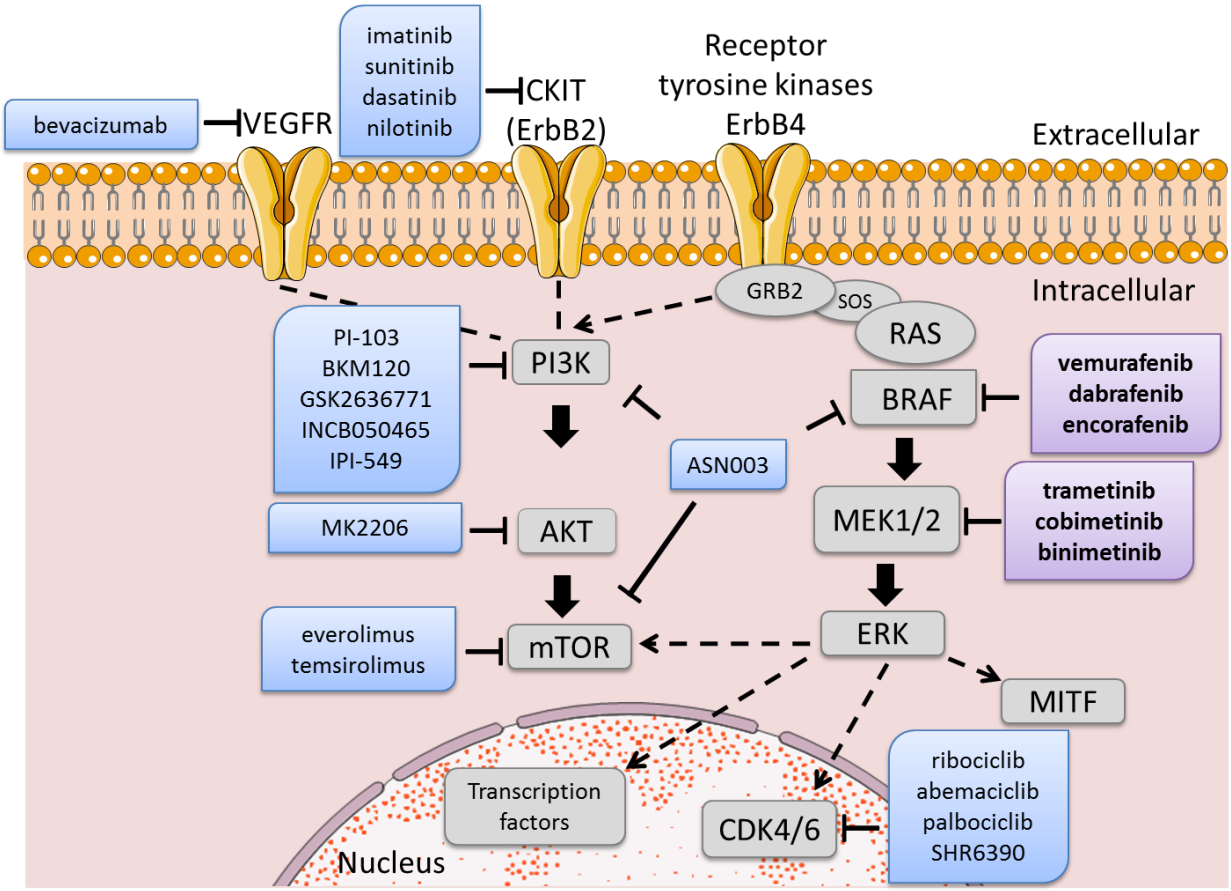

Figure 2.5 Signaling targeted therapies for the treatment of cutaneous melanoma

Approved therapies (BRAFi, MEKi) are shown in purple boxes, while therapies investigated in clinical trials are shown in blue boxes. Adapted from Domingues *et al* (58). The figure was created using Servier Medical Art (31).

For *NF1*-mutated patients, currently no targeted therapeutic approach is available. *CKIT* mutations have been reported in a smaller proportion of cutaneous melanoma patients, but promising targeted approaches are available based on tyrosine kinase inhibitors such as imatinib. Imatinib resulted in less pronounced effects in melanoma survival as compared to MAPKi, but new multikinase *KIT* inhibitors are being evaluated in clinical trials aiming for improved survival (44,59). For patients with wild-type melanomas, treatment with the vascular endothelial growth factor (VEGF) monoclonal antibody bevacizumab provided some survival benefit, with a 25.5% response rate and 12.3 months median overall survival (60); however other clinical

trials are ongoing, which evaluate the efficacy of bevacizumab in combination with chemotherapies or immunotherapies (44).

Given that the success of modern cancer treatment is mostly transient, identification of novel biomarkers and technologies for real-time therapy monitoring, i.e. early detection of response and resistance, is a major task in current oncology. Such new monitoring tools would dramatically improve the timing of treatment and the development of combination strategies for the management of disease progression.

2.7. Currently approved molecular diagnostics in metastatic melanoma and limitations of tissue-based assays

The use of MAPK signaling-targeted drugs and CTLA-4 or PD-1 immune checkpoint inhibitors has dramatically improved the survival of patients with advanced melanoma. Patients can now be offered different and consecutively applicable treatment options, e.g. in case of developing therapy resistance (2). At the same time, large-scale sequencing efforts have revealed the mutational landscape of melanomas and identified oncogenic drivers such as *BRAF*^{V600E} or *NRAS*$^{Q61R/L/K/H}$ providing the basis for therapeutic stratification strategies (18,61,62).

Crucial for the prognosis of melanoma is to know the presence of driver mutations or expression of immune checkpoint molecules in the tumor tissue. The first FDA (Food and Drug Administration) approved *BRAF*^{V600} hotspot mutation test was the COBAS 4800 BRAF V600 Mutation Test (Roche Molecular Systems, Inc., 2011), which was based on real-time PCR and is still used by some centers for selecting patients for treatment with BRAFi. Other real-time PCR assays followed in 2013. The THXID BRAF ASSAY KIT (bioMérieux, Inc) was applied for selecting patients with *BRAF*^{V600E} mutations for the treatment with dabrafenib and patients with *BRAF*$^{V600E/K}$ mutations for the treatment with trametinib (63). The latest approved companion diagnostic test is used for the detection of *BRAF*^{V600} hotspot mutations on the FoundationOne CDx™ platform (Foundation Medicine, Inc, approved in 2017), which is a next generation sequencing panel of 324 genes and is used to identify patients eligible for signaling targeted therapies (63). All FDA approved diagnostic tests are established on DNA isolated from formalin-fixed paraffin embedded (FFPE) tissue biopsies. The usefulness of immunohistochemical anti-PD-L1 staining for patient selection for anti-PD1 treatment is still highly controversially discussed, not least due to the

inconsistent staining quality of the different antibody assays available (e.g. PD-L1 IHC 28-8, PharmDx or PD-L1 IHC 22C3 PHARMDX, DAKO).

To date there is no molecular tool available that could precisely monitor melanoma progression and resistance, especially not in real-time. Although tumor biopsy-based molecular procedures are reliable for diagnosis of melanoma and for decision making for the initiation of therapy, there are serious limitations with regard to the characterization of tumor dynamics. Melanoma is a highly diverse tumor with notoriously high genetic and epigenetic heterogeneity (64). Inter-metastatic heterogeneity exists within the same patient and intra-tumor heterogeneity exists in different areas even of the same tumor. As a consequence, the analysis of a single biopsy may not adequately represent the other tumor areas, e.g. which may have undergone branched evolution into a different genetic/biologic pathway. These limitations considerably challenge precision medicine and individualized therapy decisions, especially in the case of drug resistance.

Individualized treatment plans require continuous monitoring of the patient's tumor status with repetitive updates on both the tumor burden and current tumor biology (e.g. mutational status, biomarker expression, etc.) to detect tumor evolution and possible development of resistance to therapy. At the moment, the tumor burden of melanoma patients who receive systemic treatment is commonly monitored by radiologic imaging (e.g. CT/MRI or PET scans), serum LDH, and S100 assessment, but additional strategies which provide tumor biologic information, are not yet routinely integrated. Performing recurrent tissue biopsies, especially in case of multiple disseminated metastases with heterogeneous therapy responses, is not feasible and usually not accepted by patients. Instead, peripheral blood-based (liquid) biopsies appear much more feasible for longitudinal monitoring and may even better assess the full genetic heterogeneity of solid cancers at the systemic disease level.

2.8. The field of liquid biopsies

As compared to focal tumor tissue biopsies, 'liquid biopsies', i.e. the blood-based assessment of tumors and their biology, have the potential to better characterize the systemic magnitude of cancer, capturing the biosignals from all tumor sites within an individual. Liquid biopsy is non-invasive and allows for frequent monitoring. Besides,

a diverse range of genetic and epigenetic alterations can be found in the different subclasses of liquid biopsy.

2.8.1. Circulating tumor cells (CTCs)

CTCs are shed by primary and metastatic tumors and can be found in the blood circulation of cancer patients. CTCs were first identified in 1969 in blood samples of a patient with breast cancer (65). Since then, CTCs have been detected in various cancers based on the surface expression of markers such as the epithelial cell adhesion molecule EpCAM (mainly prominent in epithelial carcinomas), while they are rare in healthy individuals (66). The number of circulating tumor cells is usually very low, ranging from 1-10 CTCs per milliliter of blood (66). Thus, capturing of CTCs can be challenging due to the limited CTC count and high background of blood cells. The development of CTC capturing techniques is constantly evolving, employing antibody-based and physical property (size, density) guided approaches **(reviewed in 55)**. Scientifically, CTC research is highly interesting since it allows an in-depth analysis of the biologic processes happening in the disseminating tumor cells. However, the clinical application of CTC isolation techniques, particularly in melanoma patients, is still hampered by the absence of reliable and consistently expressed cell surface markers.

2.8.2. Circulating nucleic acids

There is growing interest on the characterization and utilization of circulating nucleic acids in cancer diagnostics. Several types of circulating nucleic acids have been reported to be present in the blood stream of cancer patients, such as circulating cell-free DNA, RNA, and microRNAs or nucleic acids derived from exosomes and extracellular vesicles (68).

2.8.2.1. Cell-free circulating tumor DNA

Small fragments of DNA can be found circulating in the cell-free component of the blood. Cell-free DNA (cfDNA) is released into the bloodstream from normal and tumor cells that are undergoing apoptosis and necrosis (69). The fragment length of cfDNA is approximately 166 base pairs corresponding to the size of nucleosomal DNA, further indicating that apoptosis is the main mechanism responsible for cfDNA release (70). Various genetic alterations can be found in cfDNA, including point

mutations, chromosomal rearrangements, copy number alterations and methylation marks (**Figure 2.6**) (71).

Previous reports showed the significant correlation between the amounts of cfDNA in the blood, the tumor stage, size, and number of metastases in various cancer types (72). Specifically in melanoma, the increase in the total cfDNA concentration was found as a significant prognostic factor and as a biomarker of treatment response (73). Valpione *et al* demonstrated in a cohort of 43 metastatic melanoma patients the clinical utility of total cfDNA concentration measurement. Patients with high tumor burden had increased total cfDNA concentrations; moreover, a cut off value of 89 pg/µl stratified patients in two significantly different prognostic groups (HR=2.22 for high cfDNA, *P*=0.004) (73). Therefore, measurement of total cfDNA concentrations could serve as a prognostic tool and be easily implemented in routine diagnostics.

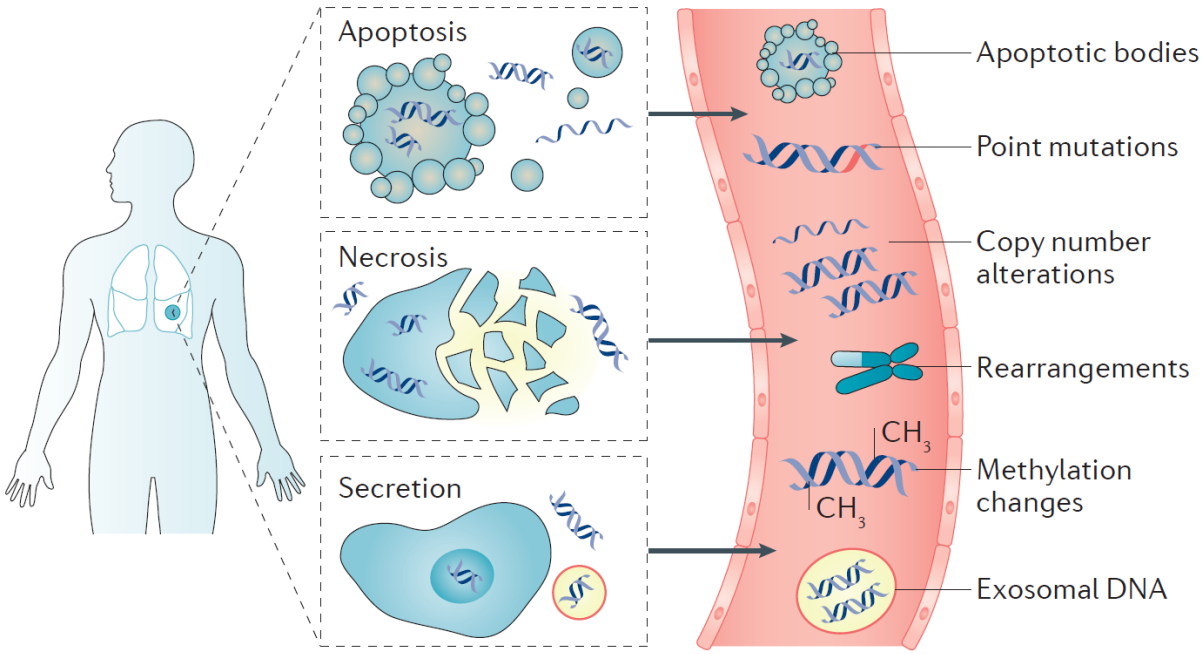

Figure 2.6 Origin and range of genetic alterations in cell-free DNA

Normal and tumor cells release cfDNA into the bloodstream by apoptosis, necrosis and secretion. Tumor specific genomic information can be analyzed and used to characterize the systemic magnitude and biology of cancer. Figure taken from Wan *et al* (71).

The tumor-specific sub-fraction of cfDNA is termed circulating tumor DNA (ctDNA). ctDNA is released from all parts of a tumor and all tumor sites, thus, reflecting the full spectrum of specific mutations in a systemically progressed cancer. This makes ctDNA a powerful candidate for molecular biomarking and monitoring. The advances in PCR-based approaches like ddPCR and NGS expanded the possibility of detecting single point-mutations and rare cancer specific mutant variants.

Particularly in melanoma, ctDNA has emerged as a potential non-invasive blood biomarker for monitoring tumor load and detecting clinically actionable driver and resistance mutations in patients receiving therapy (74–88). Most studies published on ctDNA in melanoma so far were -in essence- proof-of-principle reports investigating technical feasibility or focusing on ctDNA courses of individual (mostly *BRAF*^{V600E}-positive) patients based on retrospective sample and data collections. Furthermore, the mutational status of melanoma tissue biopsies was mostly used as the gold standard or reference for ctDNA analyses. However, the adaptation of liquid biopsy in clinical routine is slow and it has not yet been established in therapy monitoring of melanoma patients, not least due to the lack of studies including high numbers of patients allowing reliable statistical considerations.

2.8.2.2. Exosomes

Exosomes are actively released microvesicles ranging from 40-100 nm in diameter (89). They contain DNA, RNA, microRNAs lipids, and proteins (90,91). Exosomes are supposedly involved in the communication between cells to stimulate proliferation, angiogenesis and suppress the immune response (92,93). The most common isolation technique is based on differential centrifugation, but new methods are constantly being developed to facilitate diagnostic feasibility (94). A possible clinical utility of exosomes was suggested by Peinado *et al*, highlighting the prognostic value of blood derived exosomes that educate bone marrow progenitor cells towards a pro-metastatic phenotype (95). However, further translational research is needed for the identification, validation and clinical implementation of exosomal biomarkers.

2.8.2.3. MicroRNAs

MicroRNAs are small (around 22 nucleotides) naturally occurring, single stranded, non-protein coding nucleic acids. They are reported to have an impact on many biological processes, including proliferation, differentiation, and cancer development

(96). Circulating microRNAs have been detected in plasma of both healthy subjects and cancer patients, thus, both normal and tumor cells release microRNAs into the bloodstream by apoptosis and necrosis (97). For example, miR-21 was identified as a prognostic biomarker in diffuse large B-cell lymphoma (DLBCL) (98), and it was found to be significantly increased in breast cancer, especially on metastatic disease level (99,100). So far, large studies on miRNA-based approaches in melanoma are lacking.

2.9. Methods for ctDNA monitoring

2.9.1. Targeted amplicon-based next generation sequencing

Targeted amplicon (TA) sequencing is a high-throughput next generation sequencing (NGS) method that is ideal for analysis of multiple genomic regions of interest. TA-NGS involves two-step PCR amplification of a targeted gene region (amplicon), which results in tagged amplicons. Hundreds to over a thousand of amplicons per reaction could be multiplexed and with the suitable sequencing platform high coverage and an estimated 1% sensitivity can be achieved (101). The NGS workflow contains four steps. The first step is the library preparation, in which the fragmented and pre-amplified DNA is ligated to adaptors on both ends. In the cluster amplification step, the library is loaded on the flow cell and the fragments are hybridized to the surface of the flow cell. After amplification, the fragments are clustered and ready for sequencing. In this step, the emission wavelength of the fluorescently labeled nucleotides is digitally imaged throughout the sequencing cycles. The number of cycles is recorded as reads at a particular base position. Finally, the reads are aligned to the reference genome and data is analyzed using bioinformatics tools (according to Illumina®'s description).

2.9.2. Droplet Digital PCR

Droplet digital PCR is a method for performing digital PCR that is based on the water-oil emulsion droplet technology. By combining microfluidics and surfactant chemistries, this technique has the ability to detect single point mutations with 0.01% or lower assay sensitivity. On the Bio-Rad ddPCR platform, a sample is fractionated into approximately 20,000 droplets and PCR amplification of the template molecule with mutant and wild-type specific probes occurs in each individual droplet. Following PCR, each droplet is read in a flow cytometer to determine the fraction of probe-

positive droplets. These data are then analyzed using Poisson statistics to determine the target DNA template concentration in the original sample. Even very low quantities of DNA can be analyzed with ddPCR as its dynamic range is from 1 to 100,000 copies per reaction (101).

2.10. Aims of the study

In order to make precision oncology a reality for melanoma patients, the overall aim is to identify highly predictive, non-invasive monitoring technologies. Melanoma has been shown to be a genetically heterogeneous systemic disease and the emergence of therapy-surviving tumor clones is known to predict secondary mutation-driven resistance. Recent publications indicate that ctDNA is a promising biomarker for the assessment of tumor progression, therapeutic response, and resistance in this clinical context. However, the adaptation of liquid biopsy in clinical routine is slow and it has not yet been established in therapy monitoring, not least due to the lack of studies including high numbers of patients allowing reliable statistical considerations. To establish genetic profiles of plasma-derived ctDNA of advanced stage melanoma patients under therapy, TA-NGS and ddPCR were proposed as molecular tools.

Specifically, this study aimed at:

(i.) establishing a sensitive technological platform at the Essen University Hospital allowing ctDNA monitoring

(ii.) establishing and validating ctDNA assays that allow the dynamic quantitative detection of ctDNA as a prognostic biomarker for tumor load and prediction of therapy response in melanoma patients

(iii.) assessing whether ctDNA levels indicate metastasis earlier than radiologic imaging or serum marker measurements (like the serum tumor load markers S100 or LDH)

(iv.) establishing predictive ctDNA thresholds and statistical procedures that facilitate the transfer of ctDNA assays into the clinical routine.

3. Materials and Methods

3.1. Materials

Table 3.1 List of materials

Name	Catalog number (Vendor)
RPMI	12633-020 (Gibco™)
MCDB basal media	F 8105 (Merck)
Leibovitz's L-15 media	F 1315 (Merck)
L-glutamine	25030-081 (Gibco™)
Penicillin-streptomycin	A 2212 (Merck)
FBS	10500064 (Gibco™)
Trypsin/EDTA	L 2143 (Merck/Biochrom)
PBS	20012-019 (Gibco™)
Quick-cfDNA™ Serum & Plasma Kit	D4076 (Zymo Research)
QIAamp® DNA FFPE Tissue Kit	56404 (Qiagen®)
QIAamp® DNA mini kit	51304 (Qiagen®)
Qubit™ dsDNA HS Assay Kit	Q32851 (ThermoFisher Scientific™)
qPCR primers	Eurofins Scientific
Droplet Generation Oil for Probes	186-3005 (Bio-Rad Laboratories)
DG8 Gaskets for Droplet Generator	186-3009 (Bio-Rad Laboratories)
DG8 Cartridges for Droplet Generator	186-4008 (Bio-Rad Laboratories)
ddPCR Supermix for Probes (No dUTP)	186-3023/3024 depending on size (Bio-Rad Laboratories)
Pierceable Foil Heat Seal	181-4040 (Bio-Rad Laboratories)
ddPCR™ 96-Well Plates	12001925 (Bio-Rad Laboratories)
Droplet Reader Oil	186-3004 (Bio-Rad Laboratories)
PrimePCR™ ddPCR™ Mut. Assay: *BRAF* WT for p.V600E, Human	10031249 (Bio-Rad Laboratories)

PrimePCR™ ddPCR™ Mut. Assay: *BRAF* p.V600E, Human	10031246 (Bio-Rad Laboratories)
ddPCR™ *NRAS* Q61 Screening Kit	12001006 (Bio-Rad Laboratories)
ddPCR™ 2X Buffer Control Kit	1863052 (Bio-Rad Laboratories)
TERT C250T_113	dHsaEXD46675715 (Bio-Rad Laboratories)
TERT C228T_113	dHsaEXD72405942 (Bio-Rad Laboratories)
CviQI enzyme (10U/µl)	ER0211 (ThermoFisher Scientific™)
HindIII enzyme (10U/µl)	ER0505 (ThermoFisher Scientific™)
HaeIII enzyme (10U/µl)	ER0151 (ThermoFisher Scientific™)
Betaine solution – 5M, PCR Reagent	B0300-1VL (Sigma Aldrich®)
EDTA (0.5M), pH 8.0	AM9260G (ThermoFisher Scientific™)
Cartridge Illumina® Miseq® 300cycles v2	MS-102-2002 (Illumina®)
Gene Read Panel DNASeq Reagent v2	181942 (Qiagen®)
Agencourt AMPure XP Kit	A63881 (Beckman Coulter)
NEBNext Ultra DNA Library Prep Mastermix Set for Illumina	E7370 S (NEB)
NEBNext Multiplex Oligos for Illumina 1	E7335 S (NEB)
NEBNext Multiplex Oligos for Illumina 2	E7500 S (NEB)
PhiX v3 Illumina	FC-110-3001 (Illumina®)
Qubit dsDNA HS Assay	Q32851 (ThermoFisher Scientific™)
ThermoPrime Plus DNA Polymerase	AB0301B (ThermoFisher Scientific™)
100mM dNTP Mix	200415-51 (Stratagene)
DNA Lo bind tubes (0.5 and 1.5 ml, 2 ml)	0030108035, 0030108051, 0030108078 (Eppendorf)
Micro Amp8 Tube strip 0,2ml	N8010580 (ThermoFisher Scientific™)
Micro Amp 8 Cap strip	N8010535 (ThermoFisher Scientific™)
PCR plate	AB-0900 (ThermoFisher Scientific™)

Table 3.2 List of human melanoma cell lines

Name	Catalog number (Vendor)
MeWo cell line	ATCC® HTB-65™ (ATCC®)
MelJuso cell line	ACC 74 (DSMZ)
MaMel-007 cell line	SCABIO biobank
UKE-Mel-039a cell line	SCABIO biobank
WM3734 cell line	Wistar Institute
451-LuBR cell line	Wistar Institute

3.1.1. Patients and clinical data collection

Plasma samples from melanoma patients were collected as part of two different cohorts as described below.

3.1.1.1. Training cohort

In total, 560 plasma samples from 96 melanoma patients with advanced stage III or IV disease were obtained at the Department of Dermatology of the University Hospital Essen. Patients received tumor mutational testing, longitudinal blood sampling, and treatment as part of standard care or within clinical trials. Patients were treated with signaling targeted drugs (dabrafenib plus trametinib *N*=18, dabrafenib *N*=12, encorafenib plus binimetinib *N*=9, binimetinib *N*=5, encorafenib *N*=4, vemurafenib *N*=6, vemurafenib plus cobinetinib *N*=3, vemurafenib plus pexidartinib *N*=1) or signaling targeted therapy in combination with chemotherapy (pazopanib plus paclitaxel *N*=1, nintedanib plus paclitaxel *N*=4) or with immune checkpoint inhibition (ipilimumab *N*=13, nivolumab *N*=11, pembrolizumab *N*=6, nivolumab plus urelumab *N*=1, nivolumab plus ipilimumab *N*=2) between October 2013 and March 2017. Patients who had a minimum of 3 consecutive plasma samples during systemic therapy were included into ctDNA monitoring (baseline, during, and after therapy), and in the majority the first evaluation was at week 4±2, the second at week 10±5, and the third at week 18±8 after baseline. One sample was analyzed after therapy or in case of progressive disease, at the time point, when the tumor relapsed at week 35±18. Radiological imaging (CT, MRI, or US) was carried out at baseline and at every 6-12 weeks (±2 weeks of plasma sampling time points). The experiments were

approved by the Ethics Commission of the Medical Faculty of the University Duisburg-Essen (approval no. 16-7132-BO).

3.1.1.2. Independent validation cohort

In total, 104 plasma samples from 35 patients with advanced stage III or IV disease were prospectively collected either within pharmaceutical clinical trials, early access programs, or biobanking protocols at the Department of Dermatology of the Tübingen University Medical Center and the Department of Medical Oncology of the Universitair Ziekenhuis in Brussels (UZ Brussel). Informed consent procedures were followed (approval numbers 316/2018BO2 and BUN 143201421920, respectively). Patients from Tübingen were treated with pembrolizumab (*N*=17), nivolumab plus ipilimumab (*N*=4) between January 2016 and February 2017 at the Department of Dermatology of the Tübingen University Medical Center. The UZ Brussel patients were treated with pembrolizumab (*N*=14) between September 2014 and June 2016. Samples were collected at baseline, at week 6±2, and at week 12±3.

3.1.1.3. Healthy donors

Aliquots from standard plasma preparations from 96 healthy donors were provided by the Institute of Transfusion Medicine of the Essen University Hospital. According to routine pre-sampling questionnaires, plasma donors were negative for malignant diseases in their history. The experiments were approved by the Ethics Commission of the Medical Faculty of the University Duisburg-Essen (approval no. 16-7132-BO).

3.2. Methods

3.2.1. Cell culture of human melanoma cell lines

Human melanoma cell lines MeWo and MelJuso, MaMel-007 and UKE-Mel-039a were cultured in RPMI 1640 medium supplemented with 10% fetal bovine serum, 2 mM glutamine and 1% penicillin-streptomycin. The WM3734 and 451-Lu-BR cell lines were cultured in ‘Tu2%’ medium composed of 78% MCDB, 20% Leibovitz's L-15 media, 2% fetal bovine serum, and 1.68mM $CaCl_2$. All cells were maintained at 37°C in a humidified atmosphere with 5% CO_2. Cell lines were passaged using 0.05% trypsin/EDTA solution when they reached 70-80% confluence; media containing FBS

was used to quench trypsin/EDTA. Characteristics and details of cell lines are summarized in **Table 3.2 and 3.3**.

Table 3.3 Mutational profiles of cell lines

Cell line	*BRAF* mutation	MAF (%)	*NRAS* mutation	MAF (%)	*TERT*^{prom} mutation	MAF (%)
Ma-Mel-007	*BRAF*^{V600E}	99.9	wt	-	*TERT*^{C250T}	39.5
MelJuso	wt	-	*NRAS*^{Q61L}	47.9	*TERT*^{C250T}	61
MeWo	wt	-	wt	-	*TERT*^{C250T}	63.2
UKE-Mel-039a	wt	-	*NRAS*^{Q61L}	99.7	wt	-
WM3734	*BRAF*^{V600E}	74.5	wt	-	*TERT*^{C228T}	54.8
451-Lu-BR	*BRAF*^{V600E}	60.8	wt	-	*TERT*^{C250T}	98.9

MAF: Mutant allele frequency; wt: wild-type

3.2.2. Blood samples

The Essen blood samples (7.5 ml) were collected in 9 ml monovettes containing EDTA (K3E, Sarstedt) and were centrifuged within 2 hours of collection at a relative centrifugal force of 2,000 g for 15 minutes at room temperature (RT). The plasma phase was aliquoted into 2 ml low bind tubes and stored immediately at -80 °C until analysis.

Blood samples from Tübingen were collected in 9 ml monovettes containing EDTA (K3E, Sarstedt) and plasma was separated within 24 hours by gradient density centrifugation. Prior to isolation the EDTA-blood was diluted 1:1 with Hank's Balanced Salt Solution (Thermo Fisher). Plasma was aliquoted into 2 ml tubes then stored immediately at -80°C until analysis.

Blood samples from UZ Brussel were collected in 10 ml vacutainer tubes containing EDTA and were immediately centrifuged at 1410,63 g for 15 minutes at RT. The plasma phase was aliquoted into 1ml tubes and stored at -80°C until analysis.

3.2.3. DNA extraction and quantification

3.2.3.1. Circulating cell-free DNA isolation

Total cfDNA was extracted from 1-2 ml of plasma using the Quick-cfDNA^{TM} Serum & Plasma Kit. Plasma samples were centrifuged at 2,000 g for 5 minutes at RT. For

each ml of plasma 250 µl S&P 5X Digestion Buffer was added, followed by 100 µl Proteinase K and lysates were incubated at 55°C for 30 min. After incubation, 2 volumes of S&P Binding Buffer were added, and mixtures were transferred to the filter assembly in 50 ml conical tubes and were centrifuged at 1,000 g for 2 minutes at RT. Filter columns were transferred into clean 1.5 ml collection tubes and 400 µl S&P Prep Buffer was added and columns were centrifuged at 10,000g for 30 seconds at RT. The columns were transferred into new 1.5 ml collection tubes and after addition of 700 µl S&P DNA Wash Buffer; columns were centrifuged at 10,000 g for 30 seconds at RT. The previous step was repeated with 400 µl S&P DNA Wash Buffer and centrifuged at full speed (17,000 g) for 1 minute at RT to ensure complete removal of the ethanol-based wash buffer. Columns were transferred into low bind 1.5 ml tubes and 40 or 60 µl (depending on the input plasma volume) of DNA Elution Buffer (preheated to 70°C, to improve elution) was added directly to the matrix of the columns. After 3 minutes of incubation at RT the columns were centrifuged at full speed (17,000 g) for 30 seconds at RT.

3.2.3.2. Genomic DNA isolation from FFPE tissues

Genomic DNA (gDNA) from paraffin embedded tissues was isolated with QIAamp® DNA FFPE Tissue Kit according to the manufacturer's instruction. gDNA was isolated by the personnel of Essen SCABIO biobank.

3.2.3.3. Genomic DNA isolation from cell lines

gDNA from cell pellets was isolated with the QIAamp® DNA Mini Kit. Cell pellets from the WM3734 and 451-Lu-BR cell lines were previously prepared by the technician in our lab. Cell pellets were re-suspended in 200 µl of PBS, and then 20 µl of Proteinase K was added to each sample. After addition of 200 µl of Buffer AL and pulse-vortexing, samples were incubated at 55°C for 10 minutes. 200 µl of absolute ethanol was added and samples were pulse-vortexed. Mixtures were transferred into mini spin columns in 2 ml collection tubes and centrifuged at 6,000 g for 1 minute at RT. Columns were transferred into clean collection tubes and 500 µl Buffer AW1 was added, then samples were centrifuged at 6,000 g for 1 minute at RT. The previous step was repeated using 500 µl Buffer AW2 and samples were centrifuged at full speed (17,000 g) for 3 minutes at RT. To ensure complete removal of wash buffers, columns were transferred into new collection tubes, and were centrifuged at full

speed (17,000 g) for 1 minute at RT. Finally, 200 µl of Buffer AE was used to elute the DNA, incubated at RT for 5 minutes and centrifuged at 6,000 g for 1 minute at RT.

3.2.4. DNA quantification and storage

The extracted DNAs or libraries were quantified with the Qubit® dsDNA HS Assay Kit on the Qubit® 2.0 Fluorometer. Qubit® working solution was prepared for each sample and 2 standards by 1:200 dilution of the Qubit® dsDNA HS Reagent in Qubit® dsDNA HS Buffer. Standards (standard 1 and standard 2 provided with the kit) were prepared by mixing 190 µl of Qubit® working solution and 10 µl of standard. DNA samples were prepared by mixing 199 µl of Qubit® working solution and 1 µl of DNA. Mixtures were vortexed and incubated for 2 minutes at RT. After calibration of the Qubit® 2.0 Fluorometer by the measurement of the 2 standards, DNA samples were quantified, and results were recorded as ng/ml. DNA samples were kept at -20°C until used (<1 month) and at -80°C for long term storage.

3.2.5. Serum assays

Serum LDH and S100 measurements were routinely determined by the Central Laboratory of the Essen University Hospital, where the upper normal limit for LDH is 247 IU/L and for S100 0.15 µg/L. Serum assays were performed on samples collected on the same day or ±7 days from the plasma collection date. Measurement data was retrospectively reviewed in the medical database and recorded for the appropriate plasma time points.

3.2.6. Routine mutational analysis of melanoma tissue samples

Mutational tumor testing of the training cohort was processed with custom designed amplicon-based next generation sequencing panel according to standard operating procedures of the Dermatology Laboratory at the Essen University Hospital. Mutational tumor testing of the Tübingen sub-cohort was performed by Sanger sequencing. In the Brussels sub-cohort, mutational testing was carried out on the Idylla^{TM} system, allele-specific PCR, or amplicon-based next generation sequencing.

3.2.7. Amplicon-based next generation sequencing of ctDNA samples

3.2.7.1. Library preparation

Library preparation protocol was developed at the Department of Dermatology by the personnel of SCABIO biobank. For the amplification of *BRAF*, *NRAS*, *MAP2K1*, *MAP2K2*, *GNAQ* and *GNA11* loci, 64 ng of cfDNA were used in a 4-pool panel custom designed primer set as part of the GeneRead DNAseq Panel PCR Kit V2. For each primer panel a total of 20 µl reaction mixture was set up which consisted of 16 µl master mix and 4µl DNA (16 ng) according to **Table 3.4**. Samples were vortexed and spun in a mini-centrifuge. Manufacturer's recommended thermal cycling conditions were followed.

Table 3.4 Multiplex PCR master mix preparation

Reagent	per sample (µl)
Gene Read DNASeq Panel PCR Buffer (5X)	4.4
Primer Pool (A1-A4)	5.5
Hot Start Taq	1.5
DNase-free water	6.2
Total	17.6

Amplification of the *TERT*^{prom} region was performed in a separate 20 µl PCR reaction using the following primers: hTERT_short_F CAGCGCTGCCTGAAACTC and hTERT_short_R GTCCTGCCCCTTCACCTT (163 bp product) as previously described (102). Multiplex PCR products were pooled (4x20 µl=80 µl) together with *TERT*^{prom} PCR product (80 µl+20 µl=100 µl) in 1.5 ml tube. 50 µl of the PCR mix was used for following purification steps, and the remaining 50 µl was stored at -20°C for backup control. DNA was purified with AMPure XP beads following manufacturer's instructions. 25 µl of purified PCR product was cloned into a NEBNext Ultra DNA Library Prep Kit for Illumina® by adding 40 µl of master mix prepared according to **Table 3.5**, followed by manufacturer's recommended PCR protocol.

Table 3.5 End Prep master mix preparation

Reagent	per sample (µl)
End Prep Enzyme Mix	3
End Repair Reaction Buffer	6.5
Nuclease-free H_2O	30.5
Total	40

For adapter ligation, adapter reagent was diluted 1:30 and 18.5 µl the master mix (see **Table 3.6**) was added to the end prepped libraries. Mixtures were incubated at 20°C for 15 minutes. 3 µl of USER® enzyme was added to the reactions, and then samples were incubated at 37°C for 15 minutes.

Table 3.6 Adapter ligation master mix preparation

Reagent	per sample (µl)
Blunt/TA Ligase Master Mix	15
NEBNext Adapter (1:30)	2.5
Ligation Enhancer	1
Total	18.5

DNA was purified with AMPure XP beads in two rounds to select appropriate size of libraries according to manufacturer's instructions. Libraries were then labelled with index primers by adding 27 µl of master mix (see **Table 3.7**) and 2 µl of Index Primer (each sample was labelled a different index primer). Manufacturer's recommended thermal cycling conditions were followed.

Table 3.7 Index primer master mix preparation

Reagent	per sample (µl)
NEBNext Q5 Hot start HiFi Master Mix	25
Universal Primer	2
Total	27

Next, DNA was purified with AMPure XP beads according to manufacturer's instructions and quantified with the Qubit® dsDNA HS Assay Kit on a Qubit 2.0 Fluorometer (ThermoFisher™ Scientific). Finally, the libraries were mixed with 10% Phix Control v3 to provide a quality control for cluster generation, and pooled, barcoded libraries were processed on an Illumina® Miseq®.

3.2.8. NGS assay validation experiments

To determine the sensitivity of the 6-panel ctDNA NGS protocol increasing number of cells (1,000-10,000 cells) from *BRAF*^{V600E}-mutant Ma-Mel-007 (homozygous) cell line were lysed by electroporation and spiked into wild-type (wt) plasma from a healthy donor. Briefly, cells were trypsinized, counted, and diluted in 300 µl of serum-free media. Cells were pipetted into cuvettes, then electroporated according to the following setting: 500 µF (capacitance), 0.45 µV (voltage) for 10 seconds. Cells were then transferred into 50 ml conical tubes, where growth media (Tu2%) was added up to 1 ml final volume. Finally, 1 ml of healthy plasma was added to each cell dilution and cfDNA was isolated.

As a second approach, gDNA equivalent to 1-1,000 gene copies from Ma-Mel-007 cell line were spiked into a constant background (10,000 copies) of wt cfDNA from a healthy donor to create 100%, 10%, 1%, 0.1%, 0.01%, and 0% mutant concentration. The absolute limit of detection (LOD) was assessed, which is the lowest mutant concentration that can be detected. For each library preparation 16 ng of negative control (cfDNA from a healthy donor) and 16 ng of positive control (gDNA from Ma-Mel-007 cell line) were included. Experiments were confirmed by independent replicates.

3.2.9. Quantitative real-time PCR (qPCR)

3.2.9.1. Primer design

Forward and reverse primers covering the target amplicon regions of *CDK4* and *TP53* genes and at control genomic regions were designed on the IDT® PrimerQuest Tool (https://eu.idtdna.com/PrimerQuest/Home/Index). Primers were analyzed on the Primer-BLAST tool (https://www.ncbi.nlm.nih.gov/tools/primer-blast/) to check for sequence identities within the human genome database.

3.2.9.2. Oligonucleotides

All primers were purchased from Eurofins Scientific and were re-suspended to 100 pM/µl in PCR grade water and stored at -20°C prior to use. Primer designs are shown in **Table 3.8**.

Table 3.8 qPCR primers

Gene name	Target chr location	Amplicon length	Forward sequence	Reverse sequence
CDK4	12:57,751,648	96 bp	GGACTCTCACAC TCTTGAGG	CAGTGGCTGAAA TTGGTGTC
TP53	3` transcript	82 bp	CCAGAGTGCTG GGATTACAA	GCAGATGTGCTT GCAGAATG
Control region	7: 116,781,986-116,782,097	77 bp	CAAGTAGCCAAA GGCATGAAAT	TACATACAGTTT CTTGCAGCCA

bp: base pair, chr: chromosome

3.2.10. qPCR analysis

Real-time qPCR was performed using the iTaq™ Universal SYBR® Green Supermix (Bio-Rad Laboratories) on the StepOnePlus™ (ThermoFisher Scientific) system. qPCR amplifications (40 cycles) were carried out in a total of 10 µl reaction volume. Samples were run in triplicates and master mixes were prepared accordingly. The reaction mixtures were composed of 5 µl iTaq™ Universal SYBR® Green Supermix, 1 µl of primer pair (10 pM/µl stock concentration), 2 µl DNA (500 pg/µl stock concentration) and 2 µl of PCR grade water. DNA samples from cell lines with known genetic profiles were included as controls. Background was analyzed with PCR-grade water (ntc-no template control). Results were analyzed by the StepOne Software v.2.3 (ThermoFisher Scientific) and the results were reported as relative concentration of the target gene (Ct values).

3.2.11. Droplet Digital PCR (ddPCR)

3.2.11.1. DNA restriction enzyme digestion of reference samples

For ddPCR analysis, intact DNA requires restriction digestion for optimal performance, especially when more than 60 ng DNA is added into 20 µl ddPCR

reaction mix (manufacturer's instructions). For mutation detection assays, enzymes were chosen which digest the DNA outside of the target amplicon region.

Restriction enzyme digestion was carried out in separate reactions prior to ddPCR. 1 µg of gDNA was used in a 50 µl reaction volume, which was comprised of 10 U of restriction enzyme, buffer according to the manufacturer's recommendation at 1X final concentration, and PCR grade water. Reaction mixes were incubated at 37°C for 1 hour, and then the enzyme was inactivated at 65°C for 10 minutes. Digested gDNA samples were stored at -20°C until used.

For the *BRAF*^{V600E} ddPCR assay, gDNA from homozygous *BRAF*^{V600E}-positive Ma-Mel-007 and wt *BRAF* MelJuso gDNA cell lines were digested with HindIII. For the *NRAS*^{Q61} ddPCR assay, gDNA from homozygous *NRAS*^{Q61L}-positive Mel-039a and *NRAS* wt MeWo cell lines were digested with HaeIII. To detect mutations in the *TERT* promoter regions at chr5, 1,295,228 C>T (*TERT*^{C228T}) and 1,295,250 C>T (*TERT*^{C250T}), genomic DNA from the heterozygous *TERT*^{C228T}-positve WM3734 and the heterozygous *TERT*^{C250T}-positive 451-Lu-BR cell line were used and gDNA was digested with CviQI.

3.2.11.2. Detection of BRAF^{V600E} mutation

The ddPCR assays were performed with the PrimePCR^{TM} ddPCR^{TM} Mutation Detection Assay kit (Bio-Rad Laboratories) that amplifies a 91 base pair long region targeting the p.V600E c.1799T>A mutation (manufacturer's information).

3.2.11.3. Detection of NRAS^{Q61} mutations

Detection of mutations in *NRAS* at the Q61 hotspot was performed with the ddPCR^{TM} *NRAS*^{Q61} Screening kit (Bio-Rad Laboratories). The kit is designed to detect five mutations at codon 61 of the *NRAS* gene: Q61K, Q61L, Q61R, Q61H 183A>T and Q61H 183A>C (manufacturer's information).

3.2.11.4. Detection of TERT promoter mutations

The *TERT*^{C228T} promoter mutation at chr5, 1,295,228 (GRCh37, C>T, -124 bp from the ATG) and the *TERT*^{C250T} promoter mutation at chr5, 1,295,250 (GRCh37, C>T, -146 bp from the ATG) location were analyzed with expert-designed mutation detection assays (dHsaEXD72405942, dHsaEXD46675715 from Bio-Rad

Laboratories) both covering 113 base pair amplicon regions (manufacturer's information).

3.2.12. Droplet generation and thermal cycling conditions

Droplet generation was performed on the QX200™ Droplet Digital PCR System (Bio-Rad Laboratories) and PCR amplifications were carried out in a total of 20 µl reaction volume according to manufacturer's protocols. Samples were run in triplicates and master mixes were prepared accordingly. The reaction mixtures were composed of 10 µl 2X droplet digital PCR Super mix for probes (No dUTP), 1 µl of each (mutant and wild-type) primer/probe mix, 4 µl extracted cfDNA, and water adjusted to 20 µl total reaction volume (see **Table 3.9-3.11**). 20 µl of the reaction mixtures were transferred in the middle row of chambers on the DG8 cartridge designated for "Sample". 70 µl of Droplet Generator Oil was pipetted to the bottom row of the cartridge designated for "Oil". Cartridges were secured with rubber gaskets and droplets were generated on the QX200™ Droplet Generator. Following droplet generation, samples were carefully transferred onto 96-well plates. Plates were foil-sealed using the PX™ PCR Plate Sealer set to 180°C and for 5 seconds. Foil-sealed plates were run on thermocycler with the thermal cycling conditions compatible with the respective assays (see **Table 3.12-3.13**).

Table 3.9 Reaction set up for detection *BRAF*^{V600E} mutation (96 wells)

***BRAF*^{V600E} assay**	**Per rxn (µl)**	**MM for 105 rxn (µl)**
2X SuperMix (no dUTPs)	10	1050
20X FAM (mt)	1	105
20X HEX (wt)	1	105
DNA sample	4	
PCR grade H_2O	4	420
Total	20	1680

FAM: 6-carboxyfluorescein HEX: hexachloro-fluorescein, rxn: reaction, MM: master mix

Table 3.10 Reaction set up for detection *NRAS*^{Q61} mutation (96 wells)

***NRAS*^{Q61} assay**	**Per rxn (µl)**	**MM for 105 rxn (µl)**
2X SuperMix (no dUTPs)	10	1050
NRAS^{Q61} screening kit	1	105
DNA sample	4	
PCR grade H_2O	5	525
Total	20	1680

FAM: 6-carboxyfluorescein HEX: hexachloro-fluorescein, rxn: reaction, MM: master mix

Table 3.11 Reaction set up for detection of *TERT*^{C228T} or *TERT*^{C250T} mutation (96 wells)

***TERT*^{prom} assay**	**Per rxn (µl)**	**MM for 105 rxn (µl)**
2X SuperMix (no dUTPs)	10	1050
5M Betaine	2	210
80 mM EDTA (pH 8.0)	0.25	26.25
CviQI enzyme (10U/µl)	0.25	26.25
20X *TERT*^{prom} assay	1	105
DNA sample	4	
PCR grade H_2O	2.5	262.5
Total	20	1680

dUTP: 2´-Deoxyuridine, 5´-Triphosphate, U: unit, rxn: reaction, MM: master mix

Table 3.12 Thermal cycling conditions for the *BRAF*^{V600E} and *NRAS*^{Q61} assays

Step	**Temperature (°C)**	**Time**	**Cycles (n)**	**Ramp rate**
Enzyme activation	95	10 min	1	2 °C/sec
Denaturation	94	30 sec	40	
Annealing/extension	55	1 min	40	
Enzyme Deactivation	98	10 min	1	
Hold (optional)	4	infinite	1	

°C: degree Celsius, min: minute, sec: second, n: number

Table 3.13 Thermal cycling conditions for the *TERT*^{prom} assays

Step	Temperature (°C)	Time	Cycles (n)	Ramp rate
Enzyme activation	95	10 min	1	
Denaturation	96	30 sec	50	
Annealing/extension	62	1 min		2.5 °C/sec
Enzyme Deactivation	98	10 min	1	
Hold (optional)	4	infinite	1	1°C/sec

°C: degree Celsius, min: minute, sec: second, n: number

3.2.13. ddPCR data analysis

PCR plates were read on the QX200™ droplet reader and results were analyzed by the Quantasoft v.1.7.4.0917 software (Bio-Rad Laboratories). Automatic thresholds were examined under 1- and 2-dimensional plots, and, when necessary, thresholds were manually set based on the fluorescent amplitudes of background of control samples. Data from replicate wells were merged in Quantasoft and exported as csv files. Data was then analyzed in Excel and reported as copies per milliliter of plasma using the following calculation:

Equation 1: Gene copies per milliliter of plasma

$C = ((c \times r \times EV))/PV$, where

$C =$ copies per ml of plasma sample

$c =$ value of copies/µl data i.e. calculated by Quantasoft

$r =$ ratio of DNA to reaction volume, e.g. 4 µl DNA in 20 µl rxn equals to a ratio of 5.

$EV =$ plasma elution volume (µl)

$PV =$ plasma volume (ml) used for DNA extraction

Standard deviation was calculated for each sample to the final sample volume from merged Poisson 95% confidence intervals using the ConfMax and ConfMin values reported for the copies per microliter data (calculated by Quantasoft), according to the following formula:

Equation 2: Calculation of standard deviation

$\sigma = \frac{CImax - CImin}{2 \times 1.96} \times (r \times EV)$, where

$\sigma =$ standard deviation

$CImax =$ 95% confidence interval upper bound

$CImin =$ 95% confidence interval lower bound

$r =$ ratio of DNA to reaction volume, e.g. 4 µl DNA in 20 µl rxn equals to a ratio of 5

$EV =$plasma elution volume (µl)

3.2.14. Assay sensitivity and false positive rate determination

To determine the sensitivity of the ddPCR assays increasing amounts of gDNA equivalent to 1-1,000 gene copies from melanoma cell lines harboring the respective mutations were spiked into a constant background (10,000 copies) of wt gDNA. For the validation of the *BRAF*^{V600E} assay, gDNA was isolated from *BRAF*^{V600E}-mutant Ma-Mel-007 (homozygous) and wt *BRAF* MelJuso cells. For validation of the *NRAS*^{Q61} assay, gDNA from UKE-Mel-039a (homozygous *NRAS*^{Q61L}) and MeWo cells (wt *NRAS*) was used. Technical sensitivity in dilution series of DNA samples from above was calculated according to the following formula:

Equation 3: Assay sensitivity calculation

$\left(\frac{\boldsymbol{mt}}{\boldsymbol{wt}}\right) \times \mathbf{100}$, where

$\boldsymbol{mt} =$ detected mutant copies

$\boldsymbol{wt} =$ detected wild-type copies

For the validation of the *TERT* promoter assays gDNA were used from cell lines harboring the respective mutations, where increasing amounts of gDNA (equivalent of 1 to 1,000 gene copies) were tested in 20 µl of total reaction volume. The *TERT*^{C228T} assay was validated using 451-Lu-BR cells (heterozygous for *TERT*^{C228T}, wt for *TERT*^{C250T}) as mutation control and WM3734 cells (wt for *TERT*^{C228T}, heterozygous for *TERT*^{C250T}) as wild-type control. In case of the *TERT*^{C250T} assay, gDNA from WM3734 cells was used as mutation control and gDNA from 451-Lu-BR cells as wild-type control. For the *TERT* assays, instead of technical sensitivity, LOD

was assessed, which is the lowest target copy number in a reaction that can be detected, because the cell lines were heterozygous for the respective mutations. For each assay, the false positive rate of the mutation-specific probe was determined using the respective wt gDNA. For the *NRAS*^{Q61} and *BRAF*^{V600E} assays the amounts of wild-type gDNA ranged from 150 to 15,000 gene copies. For the *TERT*^{prom} assays, a lower range of gene copies was used (equivalent to 10-1,000 gene copies), because assay linearity was not maintained at higher copy numbers (above 10,000 gene copies per 20 µl reaction). This issue had no impact on the quantification of lower copy numbers. All experiments were run in triplicate reactions and confirmed by independent replicates.

3.2.15. Statistical analysis

For graphical presentation and statistical analyses samples with no detectable ctDNA levels were given a value of 1 copy per ml. For further statistical analyses, ctDNA levels from melanoma patients were normalized to the background ctDNA levels from healthy donors according to the following formula:

Equation 4: ctDNA normalization

$z = (x - \mu\_healthy)/\sigma\_healthy$, where

$z =$ normalized ctDNA level

$x =$ ctDNA copies/ml (melanoma)

$\mu =$ mean ctDNA copies/ml (healthy donors)

$\sigma =$ standard deviation (healthy donors)

To compare ctDNA levels between groups of melanoma patients or patients and healthy donors, the Mann-Whitney U test was applied. Corresponding contingency tables were analyzed with Fisher's exact test. The association between biomarkers and clinicopathological variables was assessed with 2 sample t-test (Welch's t-test). In box-and-whiskers plots the mean values are additionally indicated. Rank correlation of ctDNA and serum biomarkers was performed with the Spearman's correlation coefficient (rho). LDH and S100 values were included in the correlation analyses only if results were obtained on the same day or ±7 days from the plasma ctDNA collection date. The Wilcoxon signed rank test was used to evaluate differences in time lead between ctDNA and imaging. Receiver operating

characteristics (ROC) curve was computed to discriminate melanoma samples from healthy controls. To determine the accuracy of ctDNA as well as serum LDH and S100 measurements in predicting tumor presence as assessed by MRI/CT scans, ROC curves were computed. The optimal cut-off value was determined based on the Youden Index (103) equivalent to maximizing the sum of sensitivity and specificity. Areas under ROC curves were compared using the DeLong test statistic (104). Smoothing of the ROC curves was performed for better visualization using the default binormal function in the pROC R package. Kaplan-Meier survival plots were generated based on ctDNA profiles (increasing or decreasing levels), ctDNA percentiles, or ctDNA presence (detected vs. not detected). PFS and OS curves were compared by the log rank test. PFS was measured from the date of baseline blood collection to the date of radiologic disease progression, death, or last follow-up. OS was measured from the date of diagnosis of melanoma to the date of death, or last follow-up. The median follow-up in the study period was 24 months. The hazard ratios were estimated using Cox proportional hazard regression analysis. In uni- and multivariable analysis, binary variables (e.g. biomarkers below or above the threshold) were tested against PFS as a continuous outcome variable. Multivariable analysis included all variables from univariable analysis. Comparisons between ctDNA levels during therapy (average percent change per week relative to baseline) were carried out using unpaired t-test, where time-points were compared to baseline. The percent change per week was calculated according to the following formula:

Equation 5: ctDNA percent change per week

$\Delta ctDNA(\%) = 100 * \left(\frac{\Delta ctDNA_{t1} - \Delta ctDNA_{t0}}{tw * \Delta ctDNA_{t0}}\right)$, where

$\Delta ctDNA =$ ctDNA percent change relative to previous sampling time point

$ctDNAt1 =$ ctDNA measurement of first follow-up or following time point

$ctDNAt0 =$ ctDNA measurement of baseline or previous time point

$tw =$ weeks elapsed between the two sampling time points

The degree of agreement between plasma and tissue mutational status was assessed by Cohen's kappa.

All statistical analyses were performed using R Studio software (R-3.3.3 release) and GraphPad Prism (version 6.0), conducted at the two-sided significance level, where *P*

values of ≤0.05 were considered significant. The following packages were used in R: readxl, pROC, survival, survminer, ggplot2. Results were reported according to the REMARK criteria (105).

4. Results

4.1. Targeted amplicon-based next generation sequencing of ctDNA samples

4.1.1. Analytical sensitivity of the TA-NGS protocol using cell line derived DNA

The TA-NGS panel contained 6 frequently mutated genes in melanoma covering the hotspot mutation regions of *BRAF*, *NRAS*, *MAP2K1*, *MAP2K2*, *GNAQ* and *GNA11* genes. Additionally, the *TERT* promoter region was tested in separate PCR reactions for the following mutations: (GRCh37) chr5, 1,295,228 C>T, -124 bp from the ATG; 1,295,228 and 1,295,229 CC>TT, -124 ad -125 bp from the ATG; 1,295,242 and 1,295,243 CC>TT, -138 ad -139 bp from the ATG; 1,295,250 C>T, -50 bp from the ATG (see Methods). The customized 6-gene panel was specifically designed for the detection of mutations in ctDNA samples, with primers flanking short amplicons, but covering the whole gene. The most commonly occurring mutation in melanoma is the $BRAF^{V600E}$ mutation (106), thus the first step in the establishment process involved a titration approach, where the Ma-Mel-007 melanoma cell line (harboring the $BRAF^{V600E}$ mutation; see Methods; **Table 3.2**) was used to assess the lowest limit of detection of the TA-NGS protocol. Known quantities of electroporated cells ranging from 1,000 copies up to 10,000 copies were spiked into 1 ml of plasma from a healthy donor. The mutant allele fraction proportionally increased with increasing mutant copies in the constant background of unknown copies of wt *BRAF* (**Figure 4.1A**). Next, gDNA isolated from the Ma-Mel-007 cell line was used to spike mutant DNA copies ranging from 1 copy up to 1,000 copies into a background of 10,000 copies of wt *BRAF* DNA, isolated from plasma of a healthy donor. The experiment revealed that the lowest limit of detection was 1,000 $BRAF^{V600E}$ copies in the background of 10,000 copies of wt *BRAF* (**Figure 4.1B**). This indicated an analytical sensitivity of the TA-NGS method in our setting of (only) 10% (see Methods; **Equation 3**). Since the rest of the 5 genes of the 6-panel TA-NGS protocol are amplified in the same 4-pool PCR reaction, I assumed that the overall amplification efficiency is similar for all 6 genes and continued the assay establishment with patients' plasma samples.

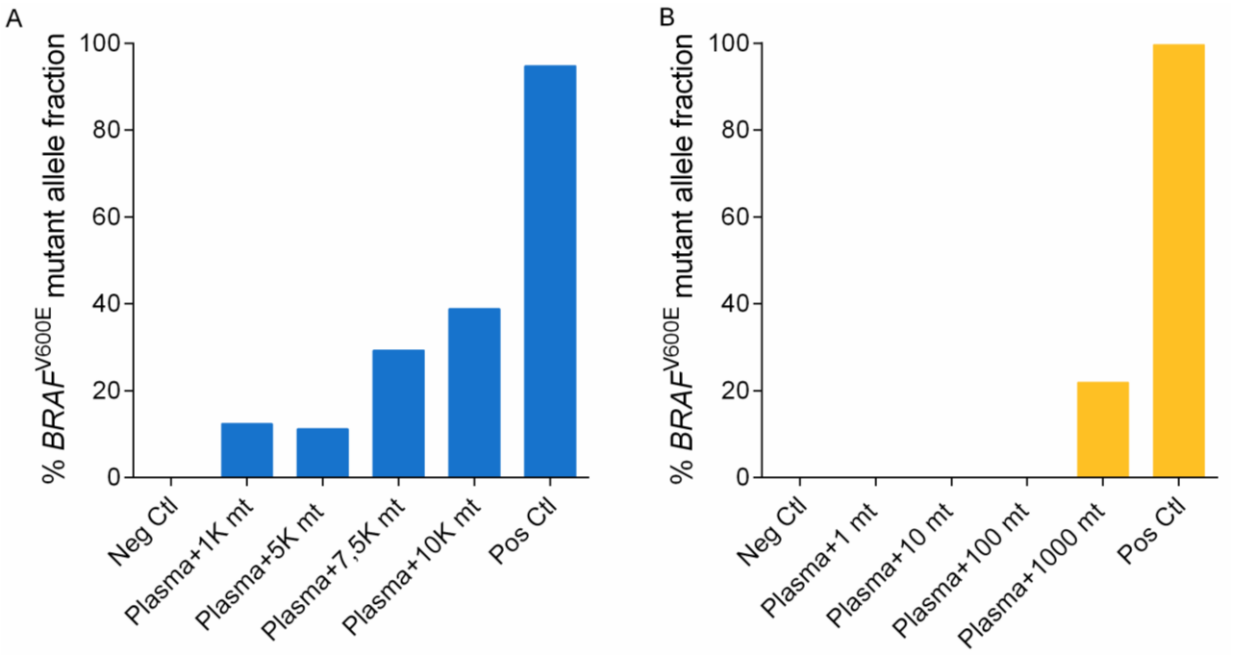

Figure 4.1 Validation of the ctDNA amplicon-based NGS assay sensitivity

A. Increasing numbers of *BRAF*^{V600E}-positive melanoma cells (1,000 up to 10,000 Ma-Mel-007 cells) were spiked into an unknown background of wt *BRAF* plasma (1 ml). **B.** *BRAF*^{V600E} gene copies ranging from 1 copy up to 1,000 copies (gDNA from Ma-Mel-007 cells) were spiked into a background of 10,000 wt *BRAF* copies (cfDNA from healthy donor). Neg Ctl: negative control (cfDNA from healthy donor), Pos Ctl: Ma-Mel-007 gDNA in both experiments.

4.1.2. Validation of the ctDNA TA-NGS protocol in patient derived plasma samples

Next, a test set of plasma samples from advanced stage melanoma patients with active tumor load was collected. Plasma aliquots were obtained from 13 melanoma patients with known oncogenic mutations in the *BRAF*, *NRAS*, *GNAQ*, *GNA11*, *MAP2K1* genes, and in the *TERT* promoter region and libraries were prepared. Patient characteristics and tumor tissue genotypes are shown in **Table 4.1**.

Table 4.1 Characteristics of patient derived plasma samples for TA-NGS analyses

Patient ID	Mutation	Stage*	Tumor load**	Treatment
ES021075	wt	IV	Lung, brain, lymph node	dabrafenib
ES022674	wt, *TERT*^{CC242TT}	IV	Lung, liver, peritoneal	ipilimumab plus nivolumab
ES022736	*BRAF*^{V600E}	IV	Lung, kidney	vemurafenib
ES017337	*BRAF*^{V600E}	IV	Spleen, kidney	pembrolizumab
ES023039	*BRAF*^{V600E}	IV	In-transit skin (leg)	dabrafenib plus trametinib
ES023330	*BRAF*^{V600E}, *TERT*^{C250T}	IV	Lung, liver	baseline
ES022362	*NRAS*^{Q61R}, *TERT*^{C250T}	IV	Lung, liver	baseline
ES021760	*NRAS*^{Q61R}	IV	Brain	baseline
ES022553	*GNAQ*^{Q209L}	IIIC	Lymph node	baseline
ES023493	*GNAQ*^{Q209P}	IV	Liver	baseline
ES022861	*GNA11*^{R148C}, *TERT*^{CC228TT}	IV	Lung	baseline
ES021057	*GNA11*^{Q209L}	IIIC	Lymph node	baseline
ES023616	*MAP2K1*^{E203}, *TERT*^{CC242TT}	IV	Lymph node	baseline

ID: identification, * according to AJCC 2009, ** as assessed by CT/MRI scans

The analysis revealed that of the 12 plasma samples only 4 were positive for the expected mutational state: the *BRAF*^{V600E} mutation was detected in plasma samples from patients ES022736, ES017337 and ES023330 with 49.6%, 11.8%, and 5.5% mutant allele frequency, respectively. Patient ES022362 carried the *NRAS*^{Q61R} mutation in the tested plasma aliquot with 10% mutant allele frequency. The other 8 plasma samples were negative for the mutations determined before in the respective melanoma tissues (**Figure 4.2**, see blue color bars). In 2 out of 5 patients (ES022362 and ES022861) *TERT*^{prom} mutations were detected in plasma, however at different

locations as determined before in tissue using the same TA-NGS assay (**Figure 4.2**, see yellow color bars).

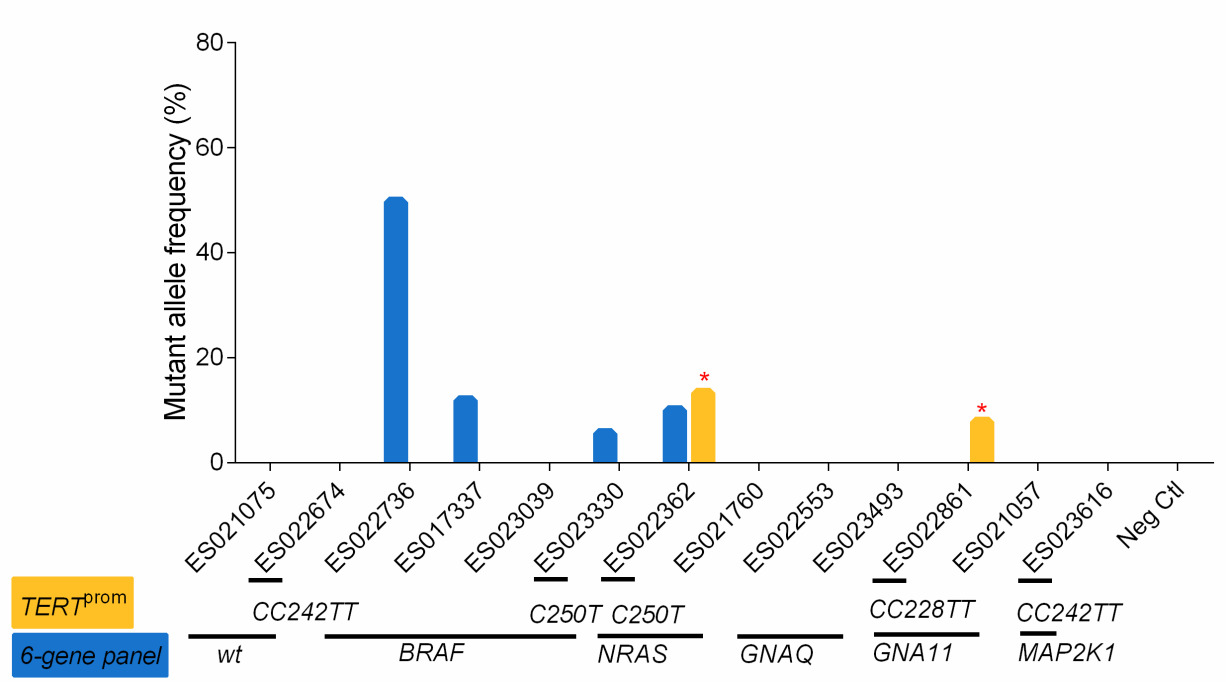

Figure 4.2 Detectable mutations in ctDNA with TA-NGS

Libraries were prepared from ctDNA isolated from 1 ml plasma aliquots of patients with metastatic melanoma carrying mutations in the *BRAF*, *NRAS*, *GNAQ*, *GNA11*, *MAP2K1* oncogenes, and in the *TERT* promoter region. Detectable mutations using the 6-gene panel multiplex library are shown in blue bars. Amplification of the promoter region of *TERT* was carried out in a separate PCR reaction, then pooled together with multiplex PCR products. *TERT*^{prom} mutations are shown in yellow bars. Wt: Wild-type. Neg Ctl: negative control (cfDNA from healthy donor). Red asterisks indicate cases with discordance between plasma and tumor tissue genotype of the *TERT*^{prom}.

In sum, the degree of inter-rater agreement in the mutations detected in plasma and the mutations detected before in tissue samples was poor for the applied TA-NGS assay (Cohen's inter-rater agreement: 38.89%, Kappa=0.182, 95% CI -0.006 to +0.370). Based on these results, I hypothesized that the mutant allele frequencies of the selected genes are very low in the isolated ctDNA samples and the applied TA-NGS was not sensitive enough to detect low mutant allele fractions. Therefore, I sought for additional optimization to achieve a higher degree of inter-rater agreement with the tissue mutational states.

4.1.3. Optimization of the ctDNA TA-NGS protocol in patient derived plasma samples

To achieve better concordance between plasma and tumor tissue genotypes for the ctDNA TA-NGS assay, new plasma aliquots were acquired from 5 of the 13 patients (**Table 4.1**). This time, 2 ml plasma aliquots were used for ctDNA isolation in order to increase the starting DNA quantity. Additionally, I adjusted the analytic thresholds in the Biomedical Genomics Workbench software (Qiagen®) used for NGS evaluation in our department. The new threshold for the minimum count was set at 2 counts (before it was 5), while the threshold for the mutant allele frequency was decreased from 5% to 1.5%.

This time, TA-NGS revealed that out of the 5 plasma samples analyzed, 4 samples were positive for the matching mutational state in tissue: the *BRAF*^{V600E} mutation was detected in the plasma sample from ES023330 with 5.5 % frequency. Patient ES022362 carried the *NRAS*^{Q61R} mutation in the tested plasma aliquot with 4.9 % mutant allele frequency. Patient ES023616 carried the *MAP2K1*^{E203K} variant with 2.9% mutant allele frequency, which was not seen in the previous analyses settings (**Figure 4.3**, blue color bars). *TERT*^{prom} mutations in plasma matched the mutational state of the respective melanoma tissues in 2 out of 5 patients (ES022362 and ES022861) with 7.1% and 1.7% mutant allele frequency; however, in 2 samples (ES022674, ES023616), *TERT* promoter mutations were detected at separate locations as compared to tissue. In one patient (ES023330), still no *TERT*^{prom} mutation was detected at all (**Figure 4.3**, yellow color bars).

So far, an improved, but still insufficient concordance between plasma vs. tissue mutation detection was achieved (68.75 % Cohen's inter-rater agreement, Kappa=0.394, 95% CI -0.019 to +0.807). Thus, technical issues in mutational calling were assumed. For example, in the analysis of another plasma aliquot (ES0414474), mutations were called in genomic regions, which were not included in the applied 6-gene TA-NGS panel. The supposedly falsely detected mutations occurred in genes (e.g. *CDK4* or *TP53*) that are part of a 30-gene TA-NGS protocol, which is routinely used in our department to assess the mutational profiles of melanoma tissue samples. Because the 'plasma 6-gene TA-NGS panel' is part of the 'tissue 30-gene TA-NGS panel', the same bed file was used for mutation calling, which might have played a role in the detection of the false mutations.

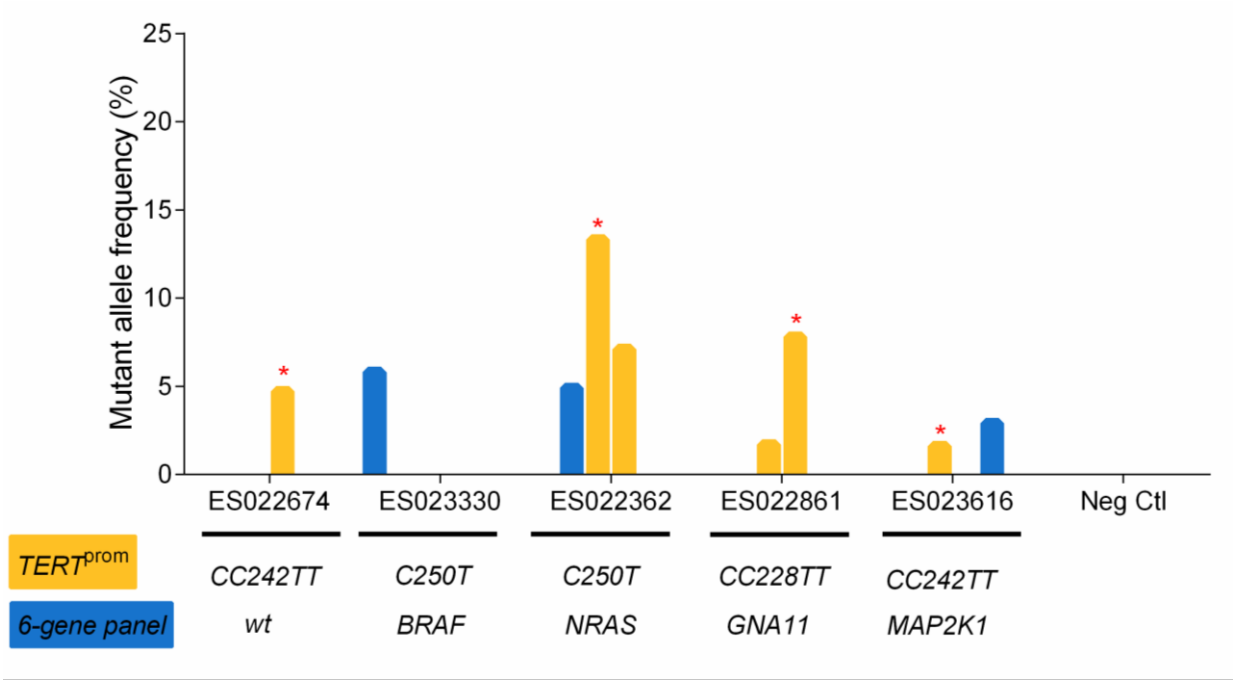

Figure 4.3 Detectable mutations in ctDNA with TA-NGS using the optimized settings

Libraries were prepared from ctDNA isolated from 2 ml plasma aliquots of patients with metastatic melanoma carrying mutations in the *BRAF*, *NRAS*, *GNA11*, *MAP2K1* oncogenes, and in the *TERT* promoter region. Detectable mutations using the 6-gene panel multiplex library are shown in blue bars. Amplification of the promoter region of *TERT* was carried out in a separate PCR reaction, then pooled together with multiplex PCR products. *TERT*^{prom} mutations are shown in yellow bars. Wt: Wild-type. Neg Ctl: negative control (cfDNA from healthy donor). Red asterisks indicate cases with discordance between plasma and tumor tissue genotype of the *TERT*^{prom}.

To find out whether the false mutations were caused by errors in mutational calling or contamination from libraries prepared from tissues, I first analyzed the median coverage of genes from the 6-gene TA-NGS panel as compared to falsely detected genes. In fact, the evaluation of the median coverage revealed that false mutations had a 6-fold lower median coverage, suggesting that the corresponding genomic regions were not amplified in the ctDNA libraries. Next, I tested the backup control libraries by qPCR with primers flanking the regions of falsely detected mutations and a control region that should be abundantly present in all samples analyzed (see **Table 3.8**). Indeed, the supposedly falsely detected gene sequences, for example from *CDK4* and *TP53*, could be only amplified by qPCR in control gDNA samples and

not in the ctDNA libraries, while the control DNA region could be amplified in all samples with low Ct values (**Figure 4.4**). So, I concluded that a contamination of the plasma libraries was unlikely, and errors in mutational calling were the reason for the discrepancies seen in the TA-NGS data.

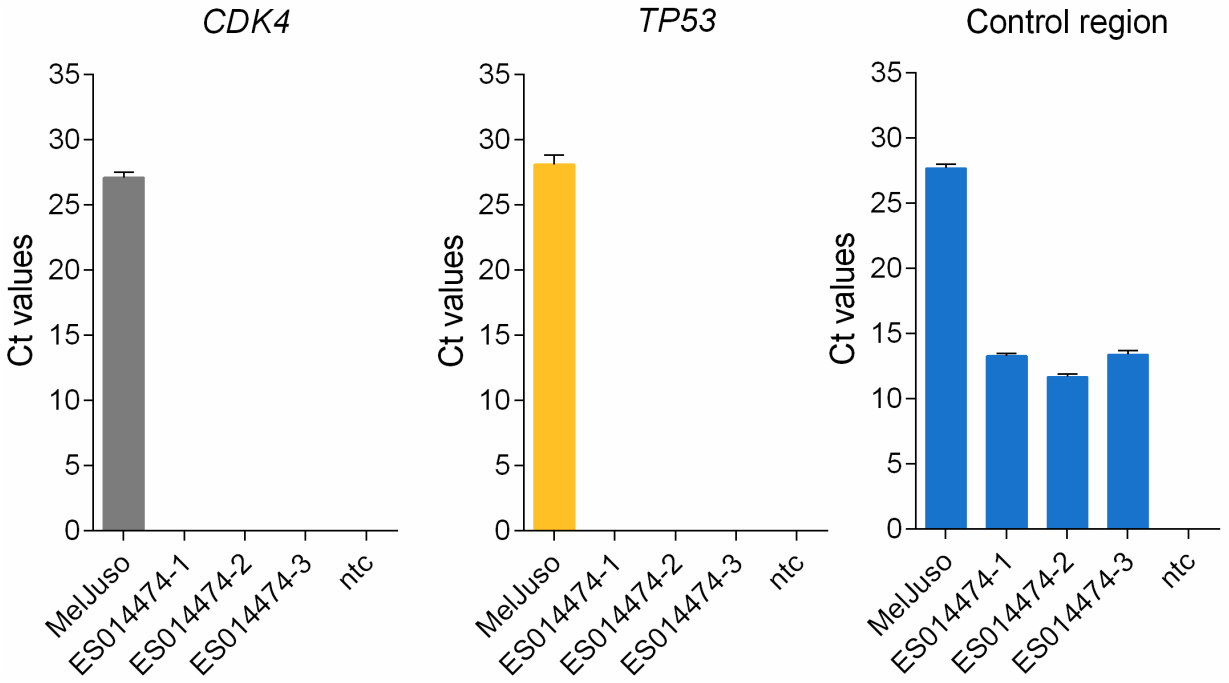

Figure 4.4 qPCR analysis of genes supposedly falsely detected by TA-NGS

Purified libraries from patient ES014474 were diluted to 500 pg/µl and tested with primers designed to cover the target amplicons in the *CDK4* and *TP53* genes and a control genomic region. Control gDNA from MelJuso cells was included as a positive control. Data represent mean±sd from triplicate wells of qPCR experiment. ntc: PCR grade water (no template control).

In sum, the proposed 6-gene TA-NGS approach could neither reliably nor reproducibly detect ctDNA in plasma samples of melanoma patients based on the available Illumina® Miseq® platform. I concluded that ctDNA measurement requires a more robust, more sensitive (also more cost effective) technology to guarantee valid interpretations for disease monitoring. Hence, the focus of the project shifted to the establishment and validation of ddPCR assays as an alternative method.

4.2. Application of ddPCR for monitoring therapy responses in metastatic melanoma patients

4.2.1. Selection and validation of ctDNA assays

4.2.1.1. Selection of candidate mutations

Candidate mutations for ctDNA monitoring were selected based on the most frequently occurring genomic alterations in melanoma, so that the tumor burden of a high number of patients could be assessed by the ddPCR assay. According to the literature, mutations in the V600 codon of *BRAF* affect ~50% of melanomas. Mutations in the Q61 codon in *NRAS* are found in ~23% and mutations in the promoter region of the *TERT* gene in ~74% of melanomas (102,107). In particular, mutations in the *NRAS* gene are known to be involved in genetic escape of melanoma cells from MAPK-targeted drugs and, thus, additionally represent a promising marker for therapy resistance (108). Based on an exploratory analysis of 151 FFPE melanoma tissues archived at the Essen SCABIO biobank and analyzed by TA-NGS for their mutational states, the combination of hotspot genetic alterations in these 3 genes in a ddPCR approach is expected to cover around 80% of all melanoma patients (**Figure 4.5**). Similar frequencies of *BRAF*^{V600E}, *NRAS*^{Q61} hotspot and *TERT*^{C228T}, *TERT*^{C250T} promoter mutations were reported in the literature (106).

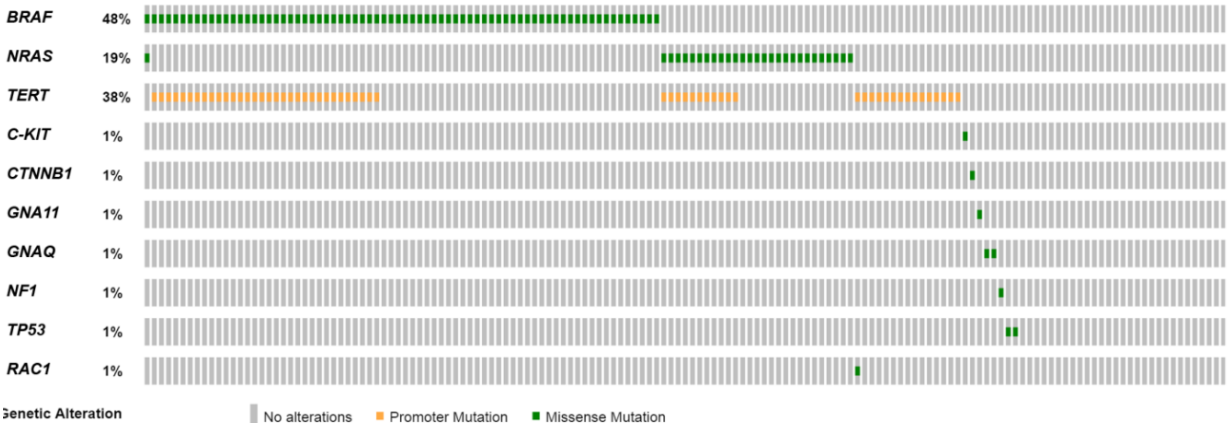

Figure 4.5 Frequency of somatic mutations in melanomas

151 FFPE melanoma tissue samples were analyzed by TA-NGS. Each column represents one sample. The percentage of samples with detected gene alterations is indicated on the left side. From 72 *BRAF* mutations, 69 occurred at the V600 codon and from 28 *NRAS* mutations, 24 were at the Q61 codon. *TERT*^{C228T} and *TERT*^{C250T} mutations accounted for 53 out of the 58 *TERT* promoter mutations [map was created with OncoPrinter tool (37,38)].

4.2.1.2. Analytical sensitivity of $BRAF^{V600E}$ and $NRAS^{Q61}$ ddPCR assays

For determination of the *BRAF*^{V600E} and *NRAS*^{Q61} assay sensitivity, increasing amounts of gDNA from homozygous mutant melanoma cell lines (ranging from 1 to 1,000 gene copies) were mixed into a background of 10,000 copies of wt gDNA to create mutant concentrations ranging from 0.01% to 10%. (**Figure 4.6A, B**). An analytical sensitivity of 0.01% was achieved for both the *BRAF*^{V600E} and *NRAS*^{Q61} mutation detection assays (detection of 1 mutant copy in a background of 10,000 wt copies, **Figure 4.6C, D**). Both assays showed high reproducibility in six technical replicates from two independent experiments.

4.2.1.3. Lowest limit of detection of $TERT^{prom}$ assays

For the *TERT*^{C228T} and *TERT*^{C250T} assays, instead of technical sensitivity, the absolute limit of detection was assessed, i.e. the lowest target copy number that can be detected, because all available cell lines were heterozygous for the respective mutations. For both assays, increasing amounts of gDNA from heterozygous mutant melanoma cell lines (ranging from 1 to 10,000 gene copies) were tested in a 20 µl reaction volume (**Figure 4.7A,B**) revealing a limit of detection of 1 *TERT*^{C250T} and 10 *TERT*^{C228T} copies per reaction (**Figure 4.7C,D**). Both assays showed high reproducibility in six technical replicates from two independent experiments.

4.2.1.1. Assessment of false positive rate

The false positive rate of all mutation-specific probes used for ddPCR (*BRAF*^{V600E}, *NRAS*^{Q61}, *TERT*^{C228T}, *TERT*^{C250T}) was determined using the respective wt gDNA. Increasing amounts of wt gDNA were tested in triplicate reactions and the detected wt events proportionally increased to the amount of the gDNA input. All assays reliably distinguished mutant from wt droplets with zero false positives (**Figure 4.8A-D**).

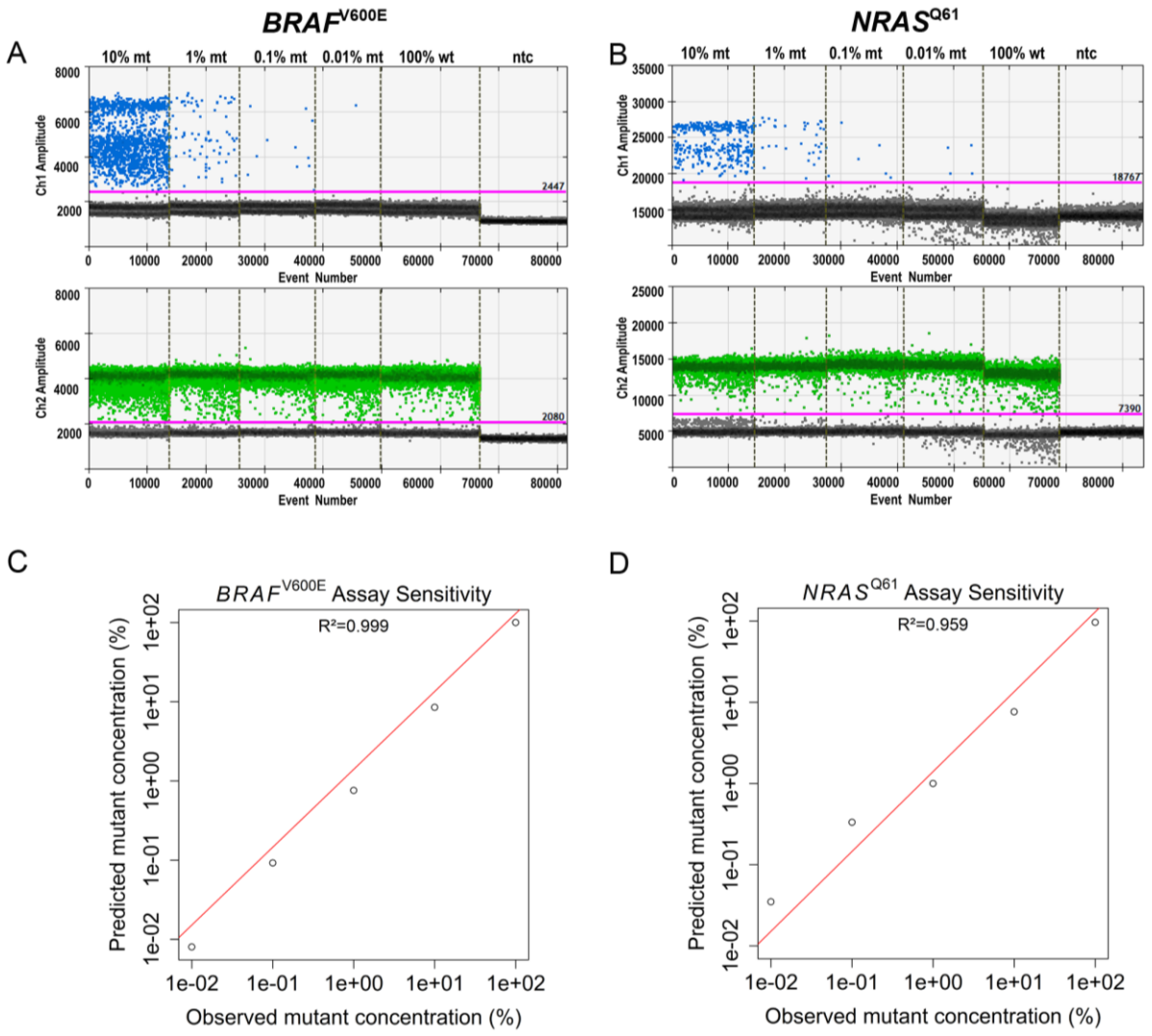

Figure 4.6 Technical validation of *BRAF*^{V600E} and *NRAS*^{Q61} mutation detection with ddPCR

A-B. One-dimensional scatter plots of fluorescent amplitudes showing total detected droplets corresponding to mutant concentrations ranging from 0.01% to 10%. Blue dots represent mutation (mt) positive droplets; green dots represent wild-type (wt) droplets. Negative droplets are shown in gray color. **C-D.** Analytical sensitivity. R^2 was calculated for linear regression (plotted in red). For the validation of the *BRAF*^{V600E} assay, gDNA from the *BRAF*^{V600E}-mutant Ma-Mel-007 (homozygous mutant) and the wt *BRAF* MelJuso cells were used. For the validation of the *NRAS*^{Q61} assay, gDNA from UKE-Mel-039a (homozygous *NRAS*^{Q61L}) and the wt *NRAS* MeWo cells were used.

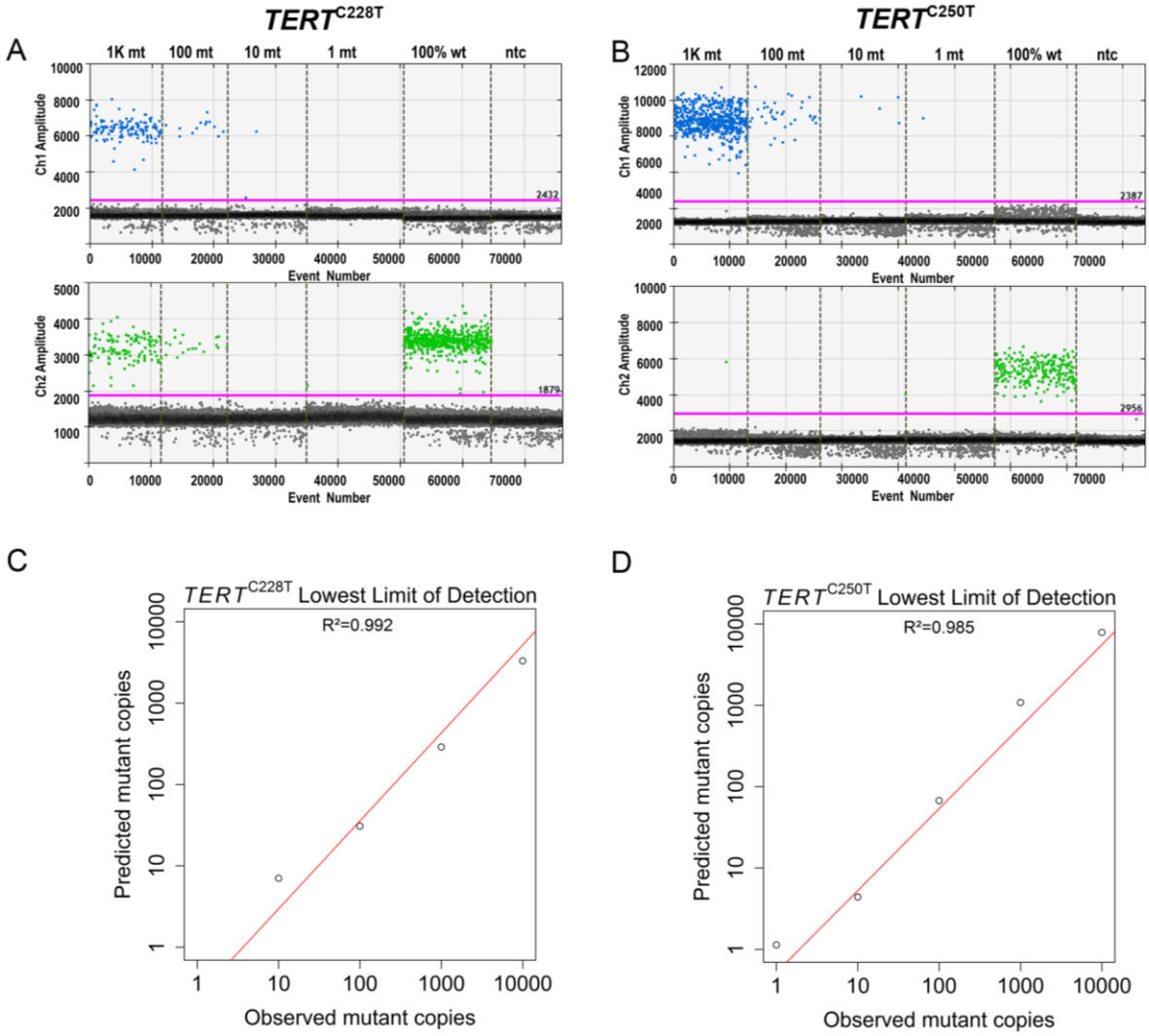

Figure 4.7 Technical validation of *TERT*^{prom} mutation detection using ddPCR

A-B. One-dimensional scatter plots of fluorescent amplitudes showing total detected droplets corresponding to mutant concentrations ranging from 1 to 10,000 copies per 20 µl reactions. Blue dots represent mutation (mt) positive droplets; green dots represent wild-type (wt) droplets. Negative droplets are shown in gray color. **C-D.** Lowest limit of detection. R^2 was calculated for linear regression (plotted in red). The *TERT*^{C228T} assay was validated using 451-Lu-BR cells (heterozygous for *TERT*^{C228T}, wt for *TERT*^{C250T}) as a mutation control and WM3734 cells (wt for *TERT*^{C228T}, heterozygous for *TERT*^{C250T}) as a wild-type control. The *TERT*^{C250T} assay was validated using gDNA from WM3734 cells (heterozygous for *TERT*^{C250T}, wt for *TERT*^{C228T}) as a mutation control and gDNA from 451-Lu-BR cells (wt for *TERT*^{C250T}, heterozygous for *TERT*^{C228T}) as wild-type control.

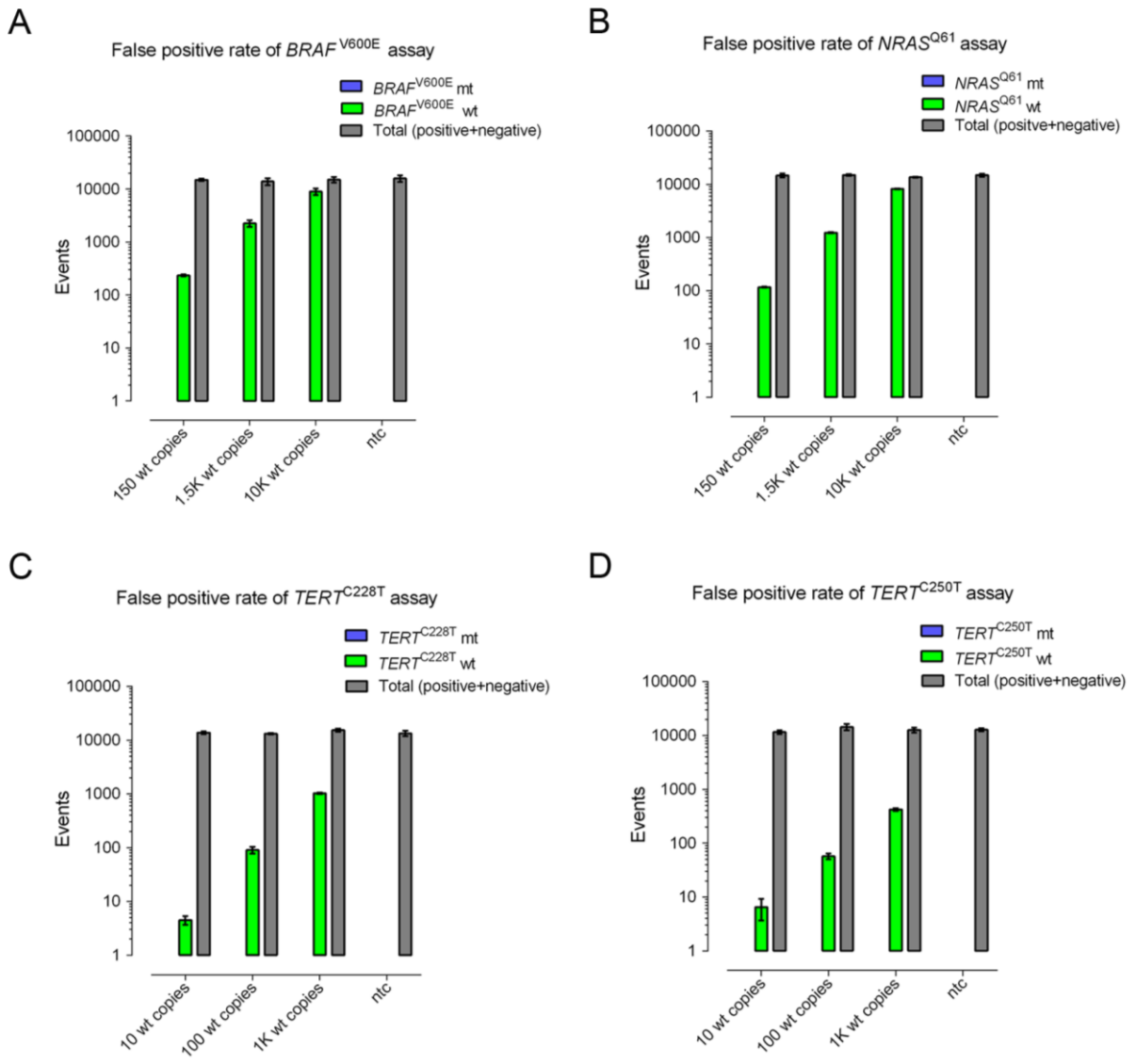

Figure 4.8 False positive detection rate of ddPCR assays

A-D. Known quantities of wild-type (wt) gDNA were tested against wild-type and mutant-specific probes to test false positivity of the respective mutation detection assay. Blue bars represent positive mutation (mt) detection events (bars not visible because of lack of events); green bars represent wt detection events. Total events of the mutation detection assays (negative plus positive droplets) are shown in gray color. Data are representative of at least two independent experiments; bars depict the mean±sd from three technical replicates. ntc: no template control.

4.2.2. Patient characteristics and cohort summary

4.2.2.1. Training cohort

The training cohort consisted of 96 patients (58/96 male and 38/96 female) with advanced metastatic melanoma (5% stage IIIB, 20% stage IIIC, and 75% stage IV according to the AJCC 2009 classification) identified in the biobank of the Essen Department of Dermatology in agreement with the study's eligibility criteria (see Methods, **Figure 4.9**).

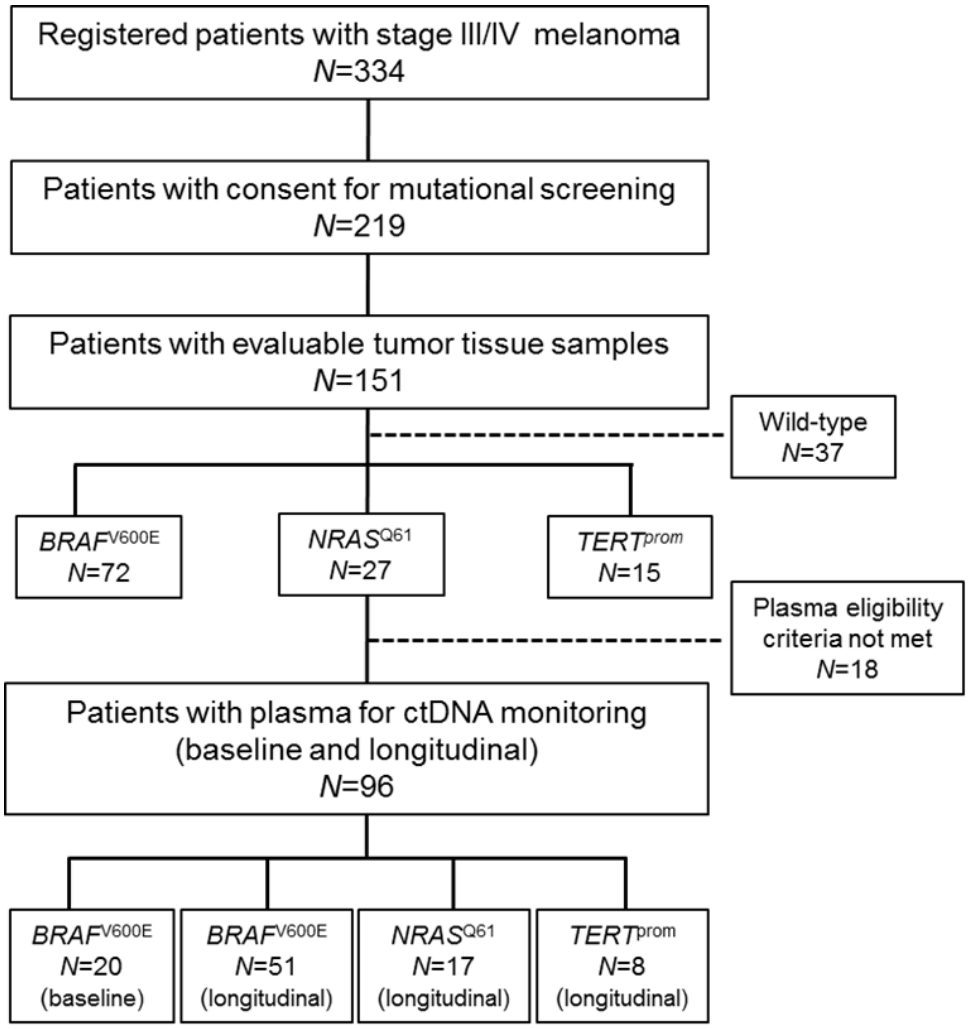

Figure 4.9 Patient enrollment in the training cohort

Overview of patient enrollment and plasma sample collection for ctDNA monitoring by ddPCR.

Patients received tumor mutational testing, longitudinal blood sampling, and treatment as part of standard care or within clinical trials. Amplicon-based next generation sequencing of tumor tissues was used to determine actionable oncogenic mutations of the melanomas. 71 *BRAF*^{V600E}-positive patients were included with available plasma samples archived before therapy start (baseline). In 51 of these patients (patient IDs E1-E51, **Figure 4.10A**)

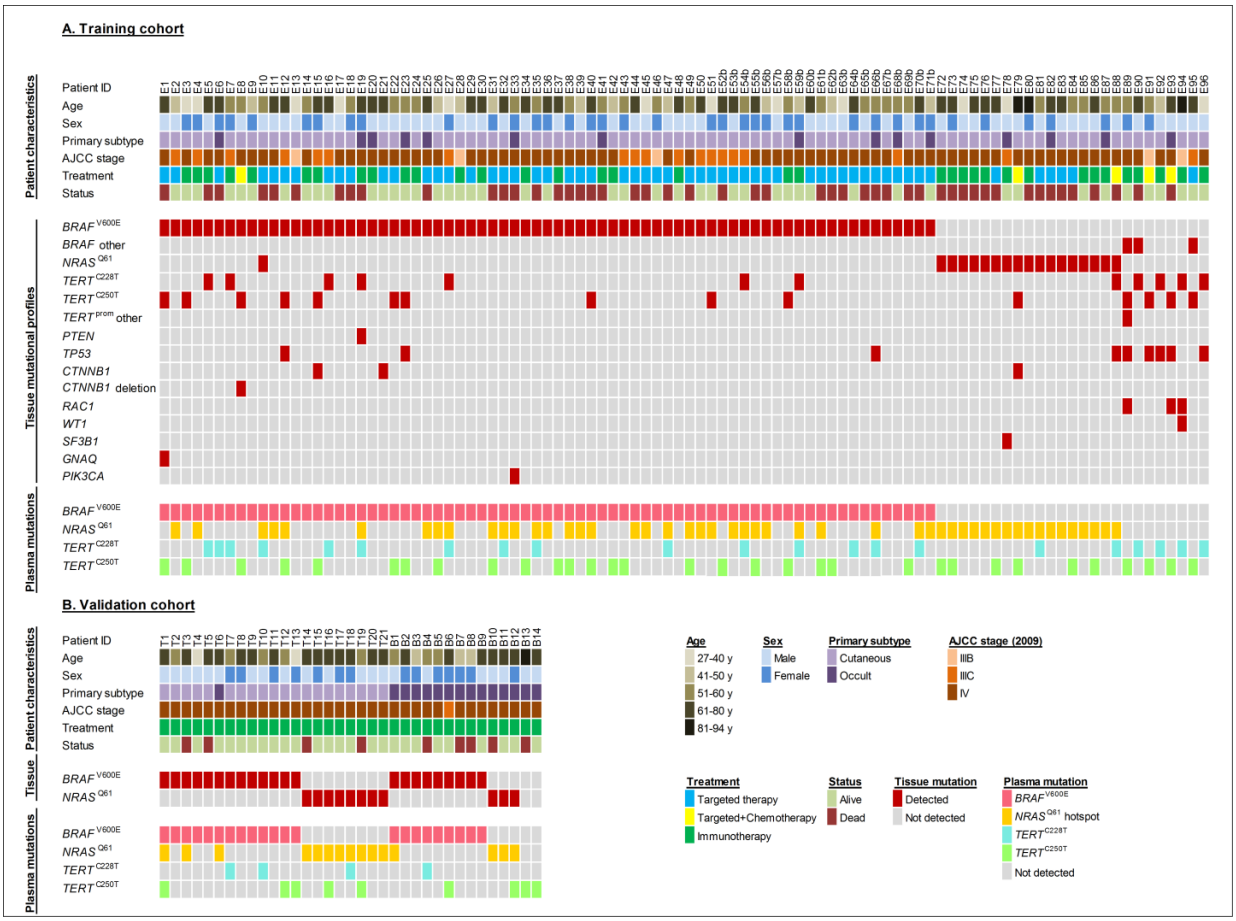

Figure 4.10 Basic characteristics of melanoma patients with *BRAF*^{V600E}, *NRAS*^{Q61} and *TERT*^{prom} mutations

Overview of the **A.** training cohort (96 stage III and IV patients) and **B.** validation cohort (35 stage III and IV patients). In the upper panels, the demographic and tumor characteristics are represented. The middle panels show mutations detected by TA-NGS in respective tumor samples. The lower panels correspond to respective plasma samples analyzed with ddPCR. Patient IDs marked with 'b' represent patients with only baseline plasma samples.

3 additional plasma samples were archived at 6-8 weekly intervals under therapy and one sample after therapy or in case of progressive disease, at the time point, when the tumor relapsed (i.e. baseline, week 4, week 10, week 18, week 35). Another 17 patients had melanomas with *NRAS*^{Q61} hotspot mutations and 8 had mutations in the *TERT* promoter (*TERT*^{C250T} and*TERT*^{C228T}) region. Also from those patients longitudinal plasma samples were available. *TERT*^{prom} mutations co-occurred with the *BRAF*^{V600E} and *NRAS*^{Q61} mutations in 19 patients, from which 14 were included in longitudinal analysis. Altogether, 22 patients were monitored for the *TERT*^{prom} mutations. The majority of the included melanomas were classified as cutaneous (81/96). 15 melanomas were nodal and had an unknown primary tumor. The median age of the patients was 58 years (range 27-83 years). In total, the training dataset was comprised of 560 plasma samples. 60.5% (58/96) of the patients received MAPK-signaling pathway targeted treatment and 34.5% (33/96) CTLA-4 or PD-1 immune checkpoint inhibition. 5% (5/96) received VEGF pathway signaling-targeted therapy in combination with chemotherapy. Patients with the *BRAF*^{V600E} mutation were treated with BRAF and MEK inhibitors or immune checkpoint inhibitors. *BRAF*^{V600E}-negative (*NRAS*^{Q61}- or mutant *TERT*^{prom} positive) patients received immune checkpoint inhibitors or tyrosine kinase inhibitors (e.g. pazopanib, nintedanib). From the 51 serially monitored *BRAF*^{V600E} patients, 18 were classified by recorded MRI/CT results as therapy responders (CR/PR) and 33 of them were classified as progressing (SD/PD). Among the *NRAS*^{Q61}- and *TERT*^{prom}-mutated patients, 2 and 5, respectively, responded to therapies, while 15 and 17, respectively, progressed. The median follow-up was 24 months (range 9-39 months) after treatment initiation. In addition, patients were serially monitored for serum LDH and S100 levels.

4.2.2.1. Independent validation cohort

35 patients (21/35 male and 14/35 female) with advanced metastatic melanoma (3% stage IIIC, and 97% stage IV according to the AJCC 2009 classification) were identified in biobanks of the Department of Dermatology, Tübingen University Medical Center and Department of Medical Oncology of the Universitair Ziekenhuis in Brussels (**Figure 4.10B**).

Sampling was done prospectively within pharmaceutical trials, early access, or biobanking programs. 22 *BRAF*^{V600E}-positive patients were included with available

plasma samples from baseline plus 2 additional time points (week 6, week 12). Another 11 patients had melanomas with *NRAS*^{Q61} hotspot mutations and 2 had the *TERT*^{C250T} mutation. Also from those patients, longitudinal plasma samples were available. *TERT*^{prom} mutations co-occurred with the *BRAF*^{V600E} and *NRAS*^{Q61} mutations in 11 patients. The majority of the included melanomas were classified as cutaneous (20/35), and 15 had an unknown primary tumor. The median age of the patients was 66 years (range 39-94 years). In total, the validation dataset was comprised of 104 plasma samples. Patients in this cohort were treated with CTLA-4 or with CTLA-4 plus PD-1 immune checkpoint inhibition. From the 22 serially monitored *BRAF*^{V600E} patients, 9 were classified by recorded MRI/CT results as therapy responders (CR/PR) and 13 of them were classified as progressing (SD/PD). Among the 11 *NRAS*^{Q61} and 2 *TERT*^{prom}-mutated patients, 4 and 1, respectively, responded to therapies, while 7 and 1, respectively, progressed. The median follow-up was 21 months (range 4-41 months) after treatment initiation. Patients were additionally serially monitored for serum LDH levels.

4.2.3. Background levels of mutant-specific ctDNA in healthy donors

To determine the 'physiological' background noise of the selected ctDNAs for better assessment of assay reliability, plasma samples of 96 healthy donors were acquired with no known history of malignant disease (see Methods). 53 of those healthy samples were tested for *BRAF*^{V600E} ctDNA in comparison to baseline plasma samples from 51 *BRAF*^{V600E}-positive patients of the training cohort with known active metastatic disease. In addition, 18 of the healthy samples were tested for *NRAS*^{Q61} ctDNA and compared to plasma from 17 *NRAS*^{Q61}-positive melanoma patients and 25 samples for *TERT*^{prom} mutations compared to plasma from 22 *TERT*^{prom}-positive melanoma patients. *BRAF*^{V600E} ctDNA was found in healthy donors with a mean detection rate of 1.19 copies/ml of plasma (range 0-10 copies). *NRAS*^{Q61} ctDNA was found at a mean detection rate of 1.77 copies/ml (range 0-8 copies) and *TERT*^{prom} mutated ctDNAs (*TERT*^{C250T} or *TERT*^{C228T}) at a mean detection rate of 1.86 copies/ml (range 0-12 copies). In total, the plasma ctDNA levels from metastatic melanoma patients were 933-fold higher (ranging from 6 to 36,400 copies/ml, $P<0.0001$, **Figure 4.11A-C**). With the data, receiver operating characteristics curves (ROC) showed an area under the curve (AUC) of 97.02 for *BRAF*^{V600E}, 98.84 for *NRAS*^{Q61}, and 92.24 for the *TERT*^{prom} assays to distinguish healthy people from advanced melanoma patients (**Figure 4.11D-F**). All assays reached high sensitivity, specificity, and positive

predictive values (**Appendix 1**). Furthermore, ROC analysis allowed determination of thresholds, which were subsequently used to evaluate the predictive impact of ctDNAs at baseline.

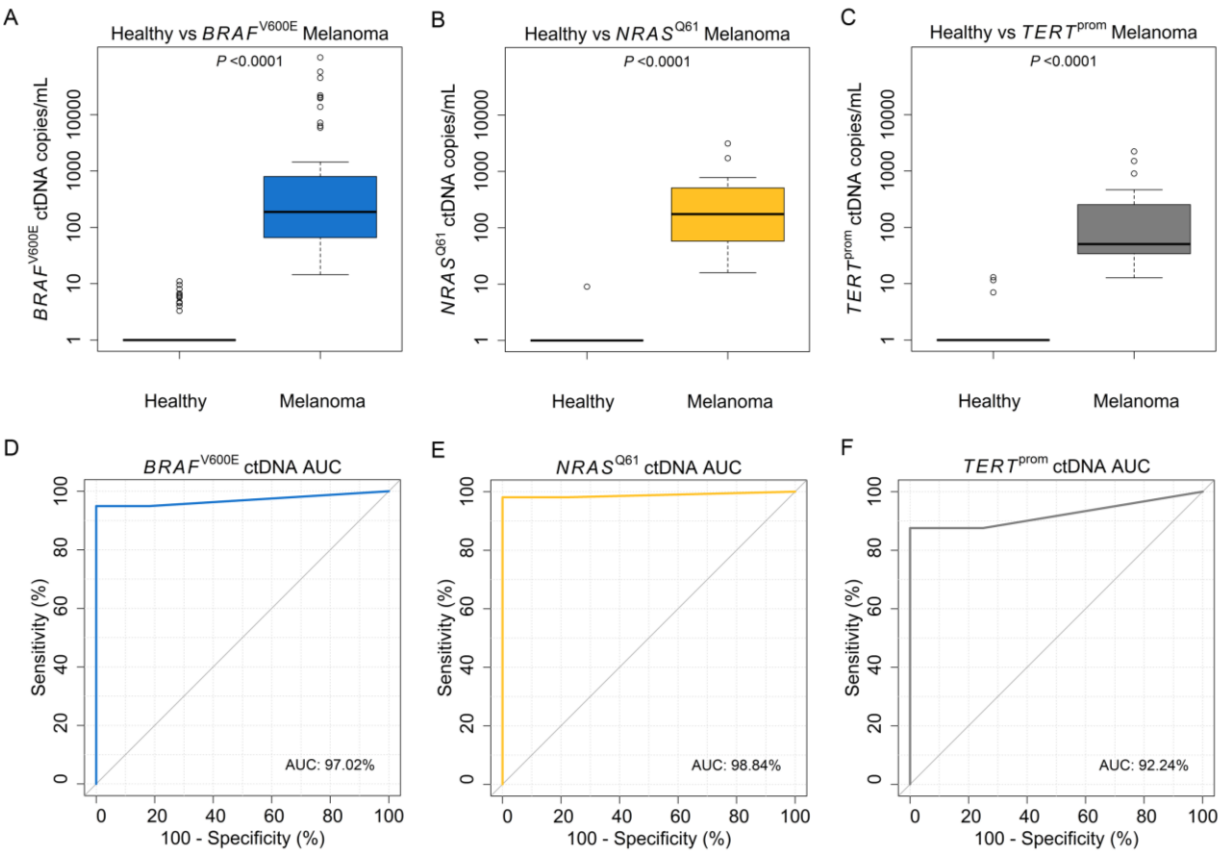

Figure 4.11 Detection of melanoma specific ctDNA using ddPCR

A-C. Box-and-whisker plots showing ctDNA detection levels in baseline plasma samples of the training cohort vs. healthy donors. **A.** Plasma samples from *BRAF*^{V600E}-positive melanoma patients (*N*=51) vs. healthy donors (*N*=53). **B.** *NRAS*^{Q61}-positive melanoma patients (*N*=17) vs. healthy donors (*N*=18). **C.** *TERT*^{prom} mutant melanoma patients (*N*=22) vs. healthy donors (*N*=25). Significance was assessed by Mann-Whitney U test. Box-and-whisker plots represent median values and interquartile ranges. For graphical presentation and statistical analyses, samples with no detectable ctDNA levels were given a value of 1 copy per ml. **D-F**. ROC analysis plots of ctDNA levels of individuals classified either as "healthy" or "melanoma". The diagonal line indicates a hypothetical test with non-discriminatory value. ROC curves were computed without smoothing.

4.2.4. The ctDNA level correlates with melanoma tumor burden and is a risk factor for disease progression at baseline

Previous reports suggested a correlation between ctDNA levels and tumor burden in melanoma patients (75,78,82,85,86,109). To confirm this also for the ddPCR assays used in our lab, I tested the baseline plasma samples from all 96 patients of the training cohort for ctDNAs matching the NGS-determined mutational state of the respective melanoma tissues. ctDNA was seen in 99% (84/85) of the cases when patients had a radiologically detectable tumor burden in lymph nodes or organs (ranging from 17-103,377 copies/ml). As expected, the baseline (i.e. before therapy start) ctDNA levels for all assays showed a significant correlation with increasing tumor stage (P<0.05, Welch's t-test) (**Figure 4.12A-D**). The routinely used tumor monitoring marker LDH showed a weak, serum S100 no association with tumor stage (**Figure 4.12E**). The rank correlation between ctDNA and serum LDH levels (rho=0.43, rho=0.27, and rho=0.18 in the *BRAF*^{V600E}, *NRAS*^{Q61}, and *TERT*^{prom} datasets, respectively, **Figure 4.13A-C**) and the correlation with serum S100 levels (rho=0.38, rho=0.27, and rho=0.12, **Figure 4.13D-F**) was weak. Therefore, ctDNA is a better candidate of tumor stage assessment tool than the currently used serum tumor load markers.

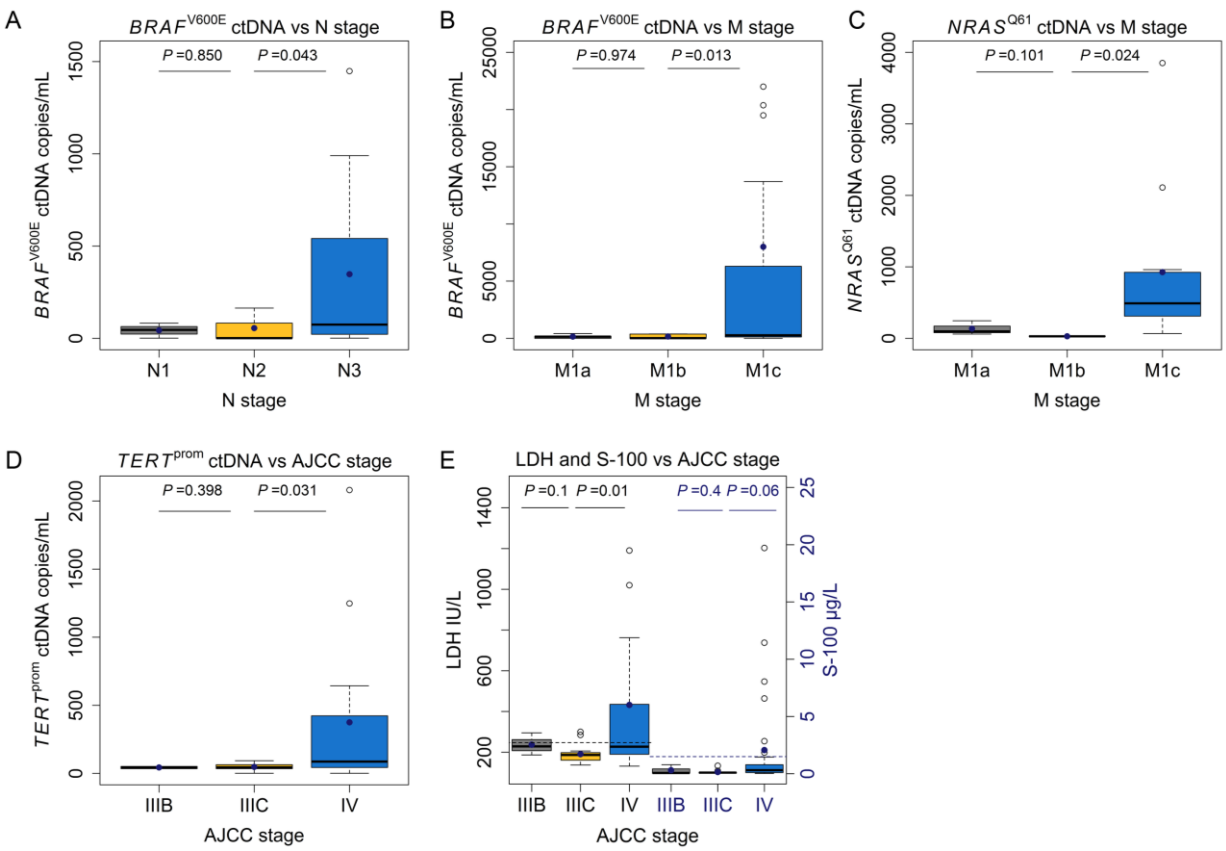

Figure 4.12 Correlation of baseline ctDNA levels with metastatic stage in the training cohort

Correlation of baseline *BRAF*^{V600E} ctDNA levels with increasing metastatic tumor load in **A.** lymph nodes (N1, *N*=3; N2, *N*=3; and N3, *N*=14) and **B.** organs (M1a, *N*=5; M1b, *N*=5; M1c, *N*=41). **C.** Correlation of *NRAS*^{Q61} ctDNA levels with organ metastasis (M1a, *N*=3; M1b, *N*=2; M1c, *N*=11) **D.** Correlation of mutant *TERT*^{prom} ctDNA levels with metastatic progression from loco-regional (stage IIIB, *N*=2, or IIIC, *N*=6) to systemic disease (stage IV, *N*=14) in patients with *TERT*^{prom}-mutated melanomas. **E.** Correlation of baseline serum LDH and S100 levels with metastatic progression in *BRAF*^{V600E}-positive patients (dotted line, ULN, see Methods). Box-and-whisker plots represent median values and interquartile range; the mean values are plotted as blue dots. Welch's t-test was used to calculate statistical significance.

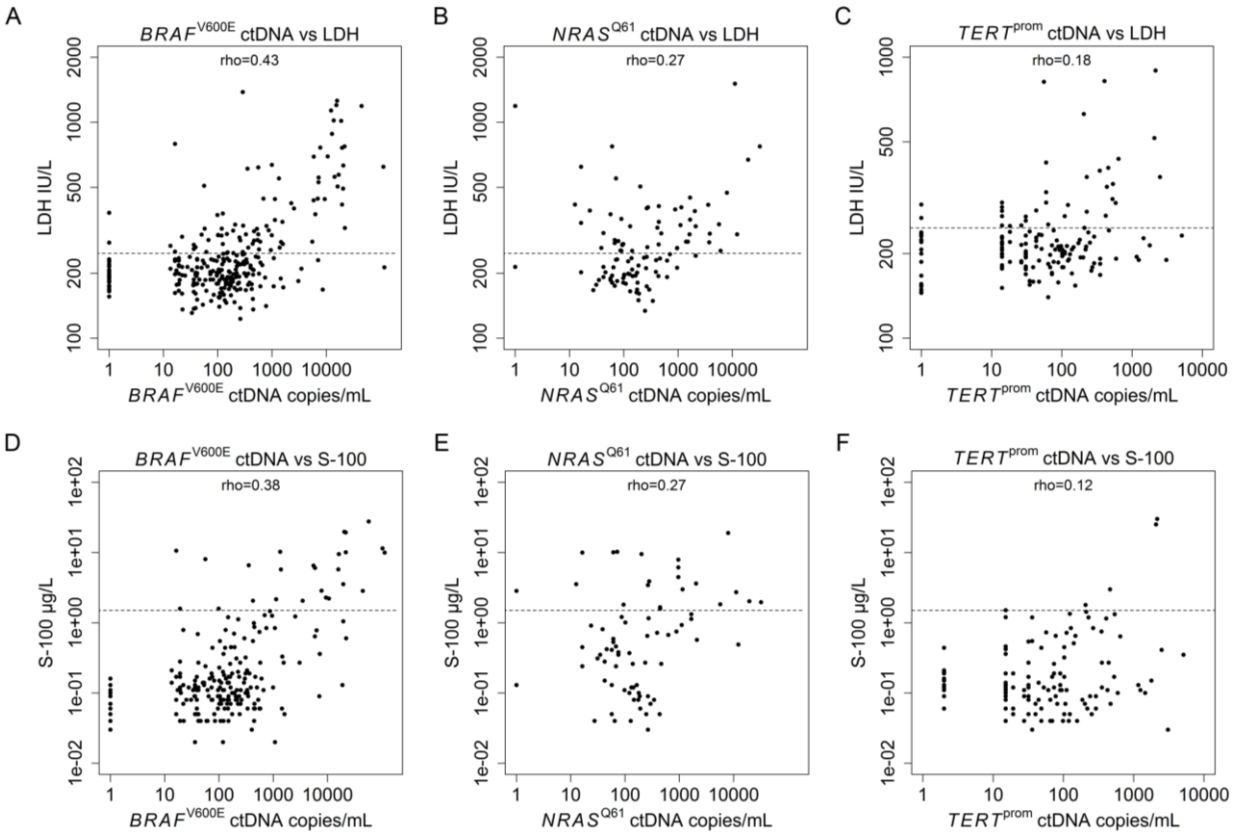

Figure 4.13 Correlation of ctDNA levels with routine serum markers in the training cohort.

Correlation of serum LDH levels with **A.** *BRAF*^{V600E} (*N*=274) **B.** *NRAS*^{Q61} (*N*=97) and **C.** mutant *TERT*^{prom} (*N*=152) ctDNA levels in the training cohort. Correlation of serum S100 levels with **D.** *BRAF*^{V600E} (*N*=216) **E.** *NRAS*^{Q61} (*N*=67), and **F.** mutant *TERT*^{prom} (*N*=124) ctDNA levels in the training cohort. Sample pairs were analyzed for the Spearman's correlation coefficient (rho). The ULN (dotted line) for LDH is 247 IU/L and for S100 is 1.5 µg/L.

To assess the clinical utility of the ctDNA thresholds, baseline plasma samples were analyzed in Cox regression analyses (see Methods). I found that, a ctDNA level above the thresholds identified in ROC analysis (**Figure 4.11D-F**, **Appendix 1**) was a significant risk factor for disease progression in univariable analysis (HR 8.48, 95% CI 1.16-62.05, *P*=0.03, log rank test). Also elevated LDH (HR 1.79, 95%CI 1.08-2.98, *P*=0.02) but not S100 (HR 1.30, 95%CI 0.78-2.18, *P*=0.31, log rank test) represented a significant predictor of progression in univariable analysis. However, in multivariable analysis only the ctDNA level significantly correlated with disease progression (HR 7.47, 95% CI 1.01-55.52, *P*=0.05, log rank test) (**Table 4.2**).

Table 4.2 Elevated baseline ctDNA is a risk factor for disease progression

Plasma samples above the ctDNA threshold determined by ROC analyses (see Appendix 1) were classified as elevated. The ULN for S100 is 0.15 µg/L and for LDH is 247 IU/L. HR with 95% CI is listed for the binary variable option indicated, with the second option being HR=1.

	Univariable analysis			Multivariable analysis		
Heading risk factors	**HR**	**95% CI**	***P***	**HR**	**95% CI**	***P***
elevated ctDNA	8.48	1.16-62.05	0.035	7.43	1.01-55.19	0.049
elevated S100	1.30	0.78-2.18	0.309	1.08	0.56-1.96	0.781
elevated LDH	1.79	1.08-2.98	0.022	1.51	0.85-2.70	0.161

HR: Hazard Ratio, CI: Confidence Interval, *P*: log rank test

4.2.5. The ctDNA profiles of melanoma patients correlate with radiologic response and tumor progression under therapy

To further validate the previous findings, ROC curves were computed for longitudinally assessed *BRAF*^{V600E}, *NRAS*^{Q61}, and *TERT*^{prom} ctDNA as well as LDH (*N*=274, *N* =97, *N*=152 in the *BRAF*^{V600E}, *NRAS*^{Q61}, and *TERT*^{prom} datasets, respectively) and S100 levels (*N*=216, *N*=67, *N*=124 in the *BRAF*^{V600E}, *NRAS*^{Q61}, and *TERT*^{prom} datasets, respectively) based on timely matching CT/MRI results (categorized into presence or absence of tumor burden). The AUCs of all ctDNA assays were superior to serum LDH and S100 (**Figure 4.14A-C**). For example, the AUC area difference between *BRAF*^{V600E} ctDNA and LDH was 23.6% (*P*<0.0001, Delong's test) and between *BRAF*^{V600E} and was S100 20.7% (*P*=0.0003, Delong's test) (**Appendix 2**). The ROC analysis furthermore allowed determination of ctDNA thresholds, which were subsequently used to evaluate the predictive impact of ctDNAs during therapy (**Appendix 2**, threshold at 35.85 copies/ml for *BRAF*^{V600E} ctDNA, 51.5 copies/ml for *NRAS*^{Q61}, and 32.83 copies/ml for *TERT*^{prom}).

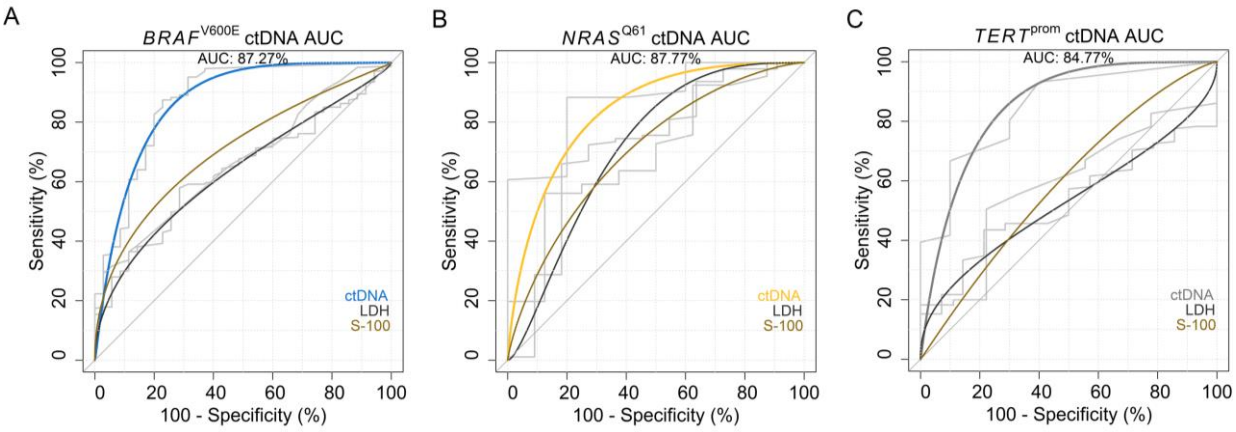

Figure 4.14 ctDNA as a marker of tumor load and its predictive value for occurrence of radiologic tumor burden in melanoma patients

A-C. AUCs ctDNA vs. LDH (*N*=274, *N*=97, *N*=152 in the *BRAF*^{V600E}, *NRAS*^{Q61}, and *TERT*^{prom} datasets, respectively) and S100 (*N*=216, *N*=67, *N*=124 in the *BRAF*^{V600E}, *NRAS*^{Q61}, and *TERT*^{prom} datasets, respectively). AUCs were calculated by ROC analysis based on CT/MRI radiologic results (presence or absence of detectable tumor load). The diagonal line indicates a hypothetical test with non-discriminatory value. ROC curves are visualized in gray without smoothing; additionally, each ROC curve is represented with smoothing using binormal function. Detailed ROC parameters are shown in Appendix 2.

To assess ctDNA levels under targeted and immune checkpoint inhibition (for drug types, see Methods), in total 540 plasma samples of 76 patients were analyzed by ddPCR and compared to radiologic staging results (training cohort: 51 *BRAF*^{V600E}, 17 *NRAS*^{Q61}, and 22 *TERT*^{prom} mutant patients). Plasma samples were available at baseline before therapy and at 4 consecutive time points (see Methods). CT/MRI scans were done every 6-12 weeks. As expected, patients with radiologic evidence of response showed a statistically significant decreasing course of ctDNA irrespective of the ctDNA mutation type or the drug type. Non-responders had rising ctDNA levels (**Figure 4.15A-B** and **Figure 4.16A-D**). Targeted therapies seemed to decrease the ctDNA copy number faster than immune checkpoint inhibitors (mean decrease of 31% vs. 15% at week 4, *P*<0.0001; combined analysis of data from **Figure 4.15A-B** and **Figure 4.16A-D**, where differences remained significant with *P*<0.0001 for all time points; unpaired t-test).

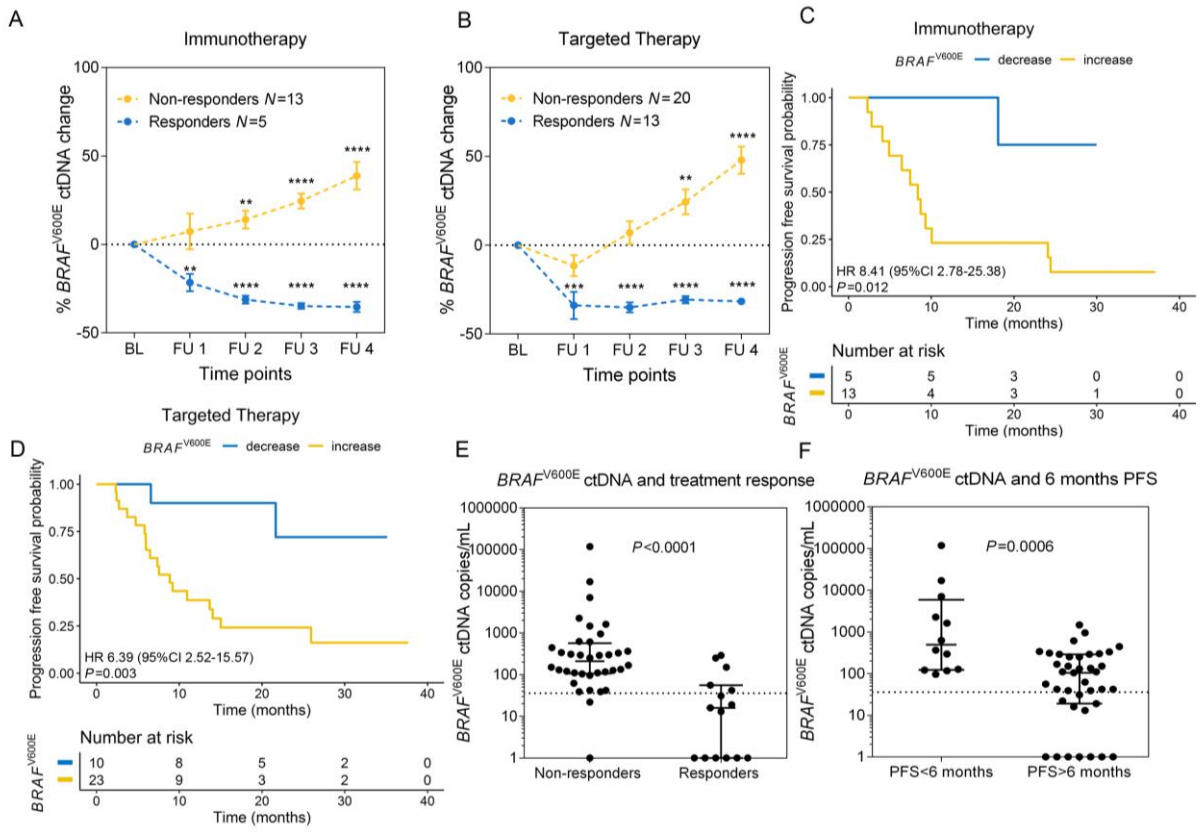

Figure 4.15 Changes of the *BRAF*^{V600E} ctDNA levels correlate with therapy response and progression free survival

Changes in mean *BRAF*^{V600E} ctDNA levels after therapy initiation relative to baseline (BL) from patients who received **A.** immune checkpoint inhibition (*N*=18 patients) and **B.** signaling targeted therapy (*N*=33). Follow-up sampling (FU 1-4) was done every 4-6 weeks. Asterisks indicate *P* values (* *P*<0.05, ** *P*<0.01, *** *P*<0.001 and **** *P*<0.0001) from unpaired t-test. The data represent mean±SEM. Kaplan-Meier plots for PFS of the same melanoma patients as assessed by routine radiologic scans. **C.** Immune checkpoint inhibition (patients with ctDNA decrease *N*=5 vs. increase *N*=13) and **D.** signaling targeted therapy (patients with ctDNA decrease *N*=10 vs. increase *N*=23). Categorization into 'decrease' vs. 'increase' was based on average ctDNA changes over 4 sampling time points relative to the baseline. HR is indicated for ctDNA increase. The *P* value was determined by the log rank test. **E, F.** Scatter dot plots of *BRAF*^{V600E} ctDNA levels of responders vs. non-responders grouped according to **E.** radiologic response 10 weeks after receiving any therapy or **F.** radiologic PFS at 6 months of therapy (Mann-Whitney U test). Points represent individual patients; median with interquartile range is indicated for each plot. Dotted lines indicate ctDNA thresholds as determined by ROC analyses (see Appendix 2).

Furthermore, I found that the detected changes in ctDNA levels correlated with the duration of PFS under therapy. For example, in the *BRAF*^{V600E} dataset, the dynamic increase in ctDNA (averaged over 4 sampling time points) relative to the baseline measurement was significantly associated with decreased PFS irrespective of the treatment type given (immunotherapy: HR 8.41 95%CI 2.78-25.38, *P*=0.01, log rank test, **Figure 4.15C** and targeted therapy: HR 6.39 95% CI 2.52-15.57 *P*=0.003, **Figure 4.15D**).

Regarding absolute copy numbers of *BRAF*^{V600E} ctDNA across all patients treated (targeted and immunotherapy), the median value of non-responders was 209.5 copies/ml at 10 weeks of treatment, significantly higher than in responders (16 copies/ml, *P*<0.0001, Mann-Whitney U test, **Figure 4.15E**), and well above the threshold defined by ROC analysis (35.85 copies/ml, **Appendix 2**). Accordingly, the median was 494.5 copies/ml in patients with a PFS below 6 months, significantly higher than in patients with a PFS above 6 months (*P*=0.0006, Mann-Whitney U test, **Figure 4.15F**). Fisher's exact test confirmed the statistically significant association of the ROC-determined ctDNA threshold and treatment response (*P*<0.0001, for 6 months PFS *P*=0.05, **Appendix 3-4**).

Similarly, *NRAS*^{Q61} and *TERT*^{prom} patients with a PFS above 6 months had significantly lower ctDNA copies when compared to patients with shorter PFS (*P*=0.0003; *P*=0.01 respectively, Mann-Whitney U test, **Figure 4.16E,F**). Also, here the ROC-determined ctDNA thresholds (*NRAS*^{Q61}: 51.5 copies/ml; *TERT*^{prom}: 32.83 copies/ml) significantly discriminated between a PFS >6 months or <6 months (*P*=0.03; *P*=0.03 respectively, Fisher's exact test, **Appendix 5-6**). Patients in the *NRAS*^{Q61} and *TERT*^{prom} datasets who responded to treatment also had lower absolute ctDNA copy numbers than non-responders (*P*=0.06 and *P*=0.008, respectively, Mann-Whitney U test, **Figure 4.16G,H**). Again, the ctDNA threshold significantly discriminated between responders and non-responders (*P*=0.02 and *P*=0.005, respectively, Fisher's exact test, **Appendix 7-8**).

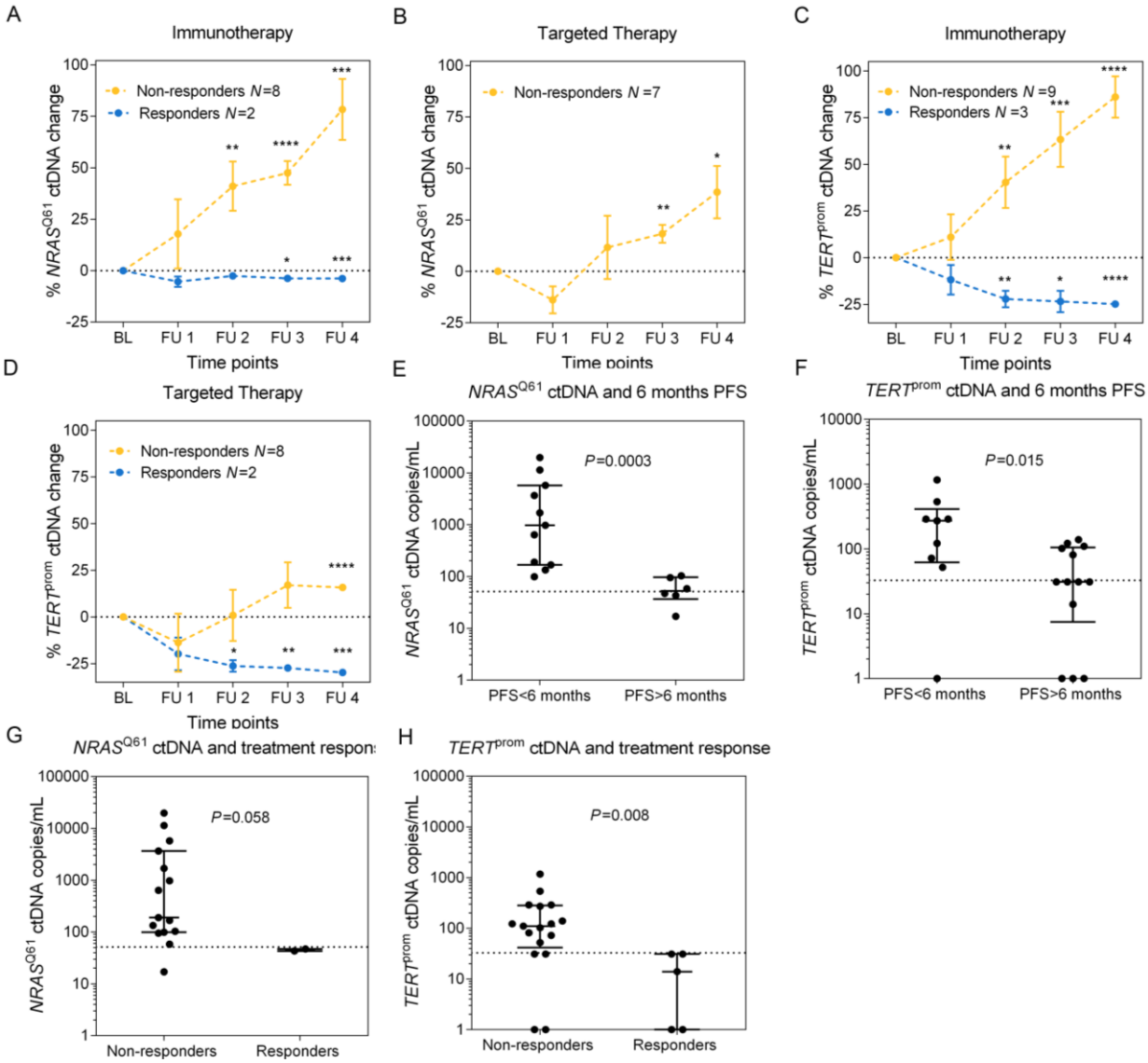

Figure 4.16 Changes of *NRAS*^{Q61} and *TERT*^{prom} ctDNA levels correlate with therapy response and progression free survival.

A, B. Changes in mean *NRAS*^{Q61} and **C, D**. *TERT*^{prom} ctDNA levels after therapy initiation relative to baseline (BL) from patients who received **A, C.** immune checkpoint inhibition (*N*=10 and *N*=13 patients) and **B, D.** signaling targeted therapy (*N*=7 and *N*=10). Follow-up sampling (FU 1-4) was done every 4-6 weeks. Asterisks indicate *P* values, where * *P*<0.05, ** *P*<0.01, *** *P*<0.001 and **** *P*<0.0001 from unpaired t-test. The data represent mean±SEM. **E-H.** Scatter dot plots of *NRAS*^{Q61} and *TERT*^{prom} ctDNA levels of responders vs. non-responders grouped according to **E,F.** radiologic PFS at 6 months of therapy **G,H.** radiologic response 10 weeks after receiving any therapy (Mann-Whitney U test). Points represent individual patients; median with interquartile range is indicated for each plot. Dotted lines indicate ctDNA thresholds as determined by ROC analyses (see Appendix 2).

In order to interpret these findings in a clinical setting, I next evaluated how the change in ctDNA copy numbers relative to previous measurements correlates with PFS. This way of seeing ctDNA data is closer to the clinical reality where therapeutic decisions have to be made in real-time based on the present ctDNA course (or in case that baseline information is not available). For example, in the *BRAF* dataset, an average ctDNA fall of 11% per week was significantly associated with high PFS (20.05 months, 95% CI 16.60-26.40), while an average ctDNA increase of 40% per week was associated with low PFS (8.55 months, 95% CI 7.05-13.97, *P*=0.0005, Mann-Whitney U test, **Table 4.3**).

Similar results were seen for the *NRAS*^{Q61} and *TERT*^{prom} datasets (*P*=0.03; *P*=0.01, respectively, **Table 4.3**).

Table 4.3 Changes in ctDNA levels identify therapy responders and non-responders

Differences in PFS of patients with decreasing or stable levels compared to patients with increasing plasma ctDNA levels.

ctDNA response	Mean ctDNA change/week (%)	Median PFS (months)	95% CI	*P*	Patients (*N*)
***BRAF*^{V600E} patients**					
Decreasing or stable ctDNA	-11	20.05	16.60-26.40	0.0005	15
Increasing ctDNA	+40	8.55	7.05-13.97		36
***NRAS*^{Q61} patients**					
Decreasing or stable ctDNA	-5	17.39	13.28-21.50	0.029	2
Increasing ctDNA	+47	4.01	2.81-7.47		15
***TERT*^{prom} patients**					
Decreasing or stable ctDNA	-17	18.08	11.80-24.98	0.012	5
Increasing ctDNA	+26	5.98	4.56-11.24		17

PFS: Progression Free Survival, CI: Confidence Interval, *P*: Mann-Whitney U test, *N*: number

Alternatively, a ctDNA increase from the 25th percentile (reflects a mean ctDNA change per week above 3.7 %) to the 75th percentile (mean ctDNA change per week above 21.1 %) was significantly associated with an increased risk of disease progression (25th percentile: HR 3.82 95% CI 1.78-8.21, *P*=0.0002; 75th percentile: HR 7.55 95% CI 3.23-17.66, *P*<0.0001, log rank test, **Figure 4.17**).

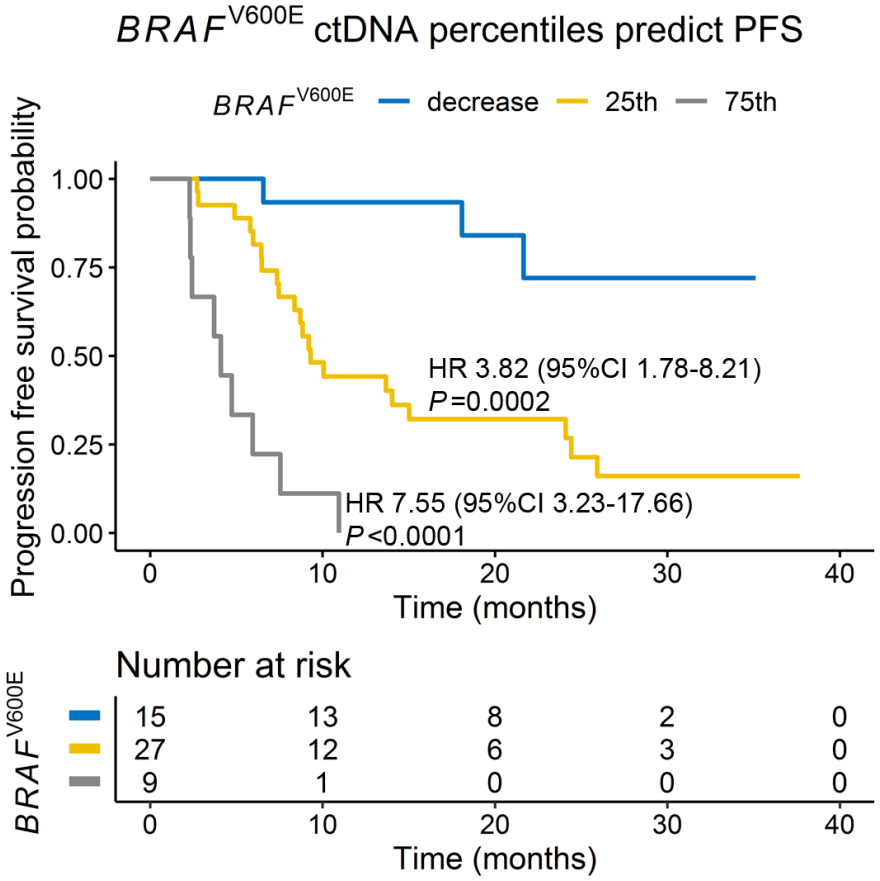

Figure 4.17 *BRAF*^{V600E} ctDNA percentiles predict PFS

Kaplan-Meier plot of radiologic PFS of *BRAF*^{V600E} melanoma patien0074s with different ctDNA percentiles. HR for the 25th and 75th percentiles was calculated relative of ctDNA decrease. *P* values were determined by the log rank test.

4.2.6. Changes in the ctDNA profile indicate therapy response and failure earlier than radiologic scans

To assess the temporal relationship between ctDNA changes and therapy response or disease progression, lead-time was calculated for ctDNA detection starting from the moment of radiologic detection of decreased or increased tumor burden. With the *BRAF*^{V600E} assay in the training cohort, a ctDNA decrease compared to the previous sampling time point preceded radiologic detection of response in 12 of 15 (80%) of responders with an average lead-time window of 1.5 months (range 0.023-3.45 months, *P*=0.003, Wilcoxon signed rank test, **Figure 4.18A**, for calculation, see Methods). In 31 of 36 (86%) of the non-responders, ctDNA increase preceded radiological progression with an average lead-time window of 3.5 months (range 0.23-18.86, *P*<0.0001, Wilcoxon signed rank test, **Figure 4.18B**). Similarly, an *NRAS*^{Q61} ctDNA increase preceded radiologic progression in 14 of 16 patients (87.5%) and an increase in mutant *TERT*^{prom} promoter ctDNA in 14 of 17 patients (82%) with average lead-time windows of 3 months (range 0.03-16.63, *P*=0.0001, Wilcoxon signed rank test) and 4 months (range 0.49-13.80 months, *P*=0.0001, Wilcoxon signed rank test), respectively (**Figure 4.18C,D**).

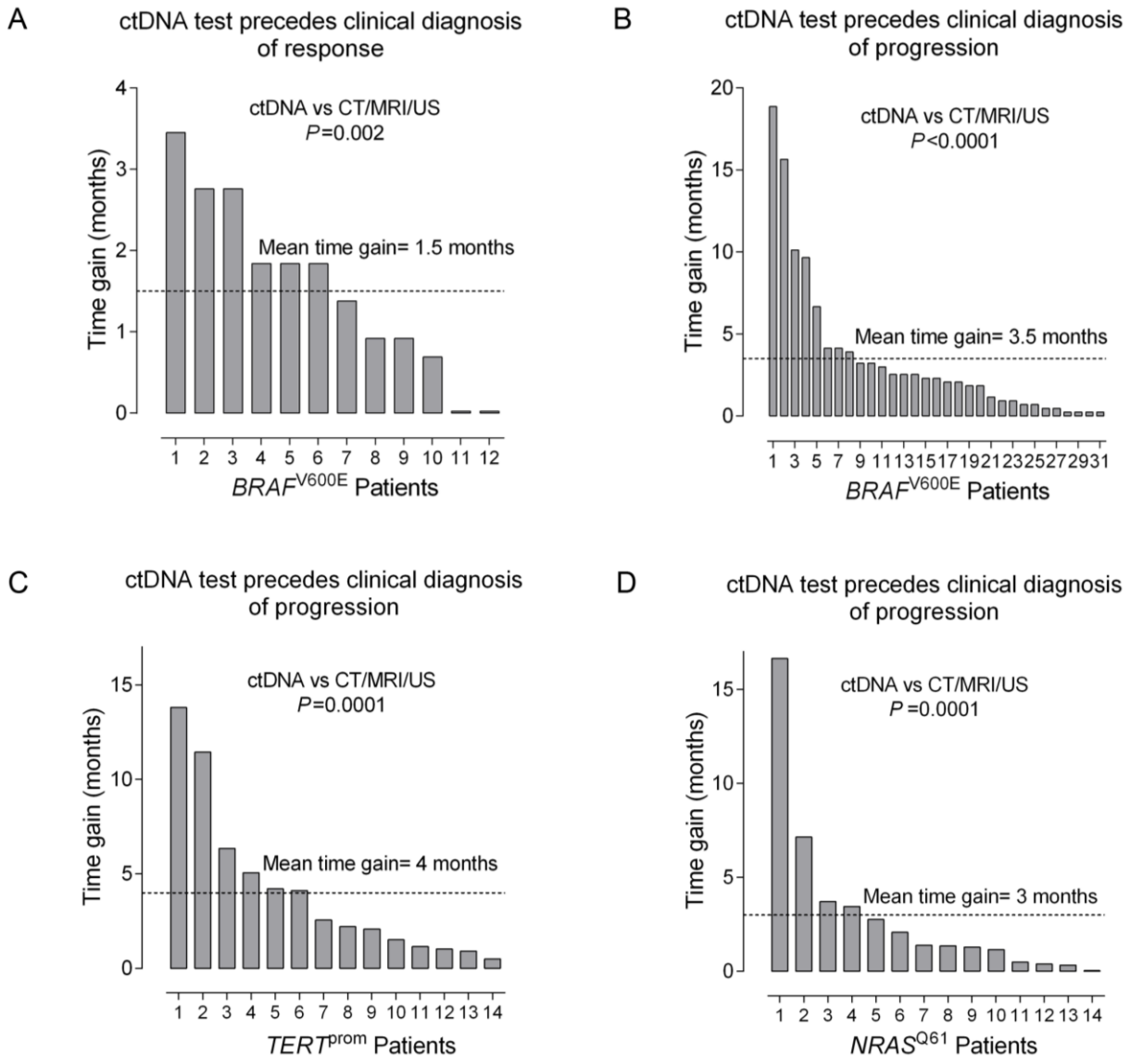

Figure 4.18 Time gain in assessment of disease progression in the training cohort

ctDNA as an early predictive parameter for therapy response and failure **A.** Decreasing *BRAF*^{V600E} ctDNA levels (as compared to the last sampling time point) preceded radiological detection of response in 12 of 15 responders with an average lead-time window of 1.5 months (range 0.023–3.45 months). **B.** Increasing *BRAF*^{V600E} ctDNA levels preceded radiological progression in 31 of 36 non-responders with an average lead-time window of 3.5 months (range 0.23–18.86 months). **C.** Increasing *NRAS*^{Q61} ctDNA preceded radiological detection of progression in 14 of 15 patients with an average lead-time window of 3 months (range 0.03–16.63 months). **D.** Increasing *TERT*^{prom} ctDNA preceded radiological progression in 14 of 17 patients with an average lead-time window of 4 months (range 0.49–13.80 months). *P* values indicate Wilcoxon signed rank test. Due to small number of *NRAS*^{Q61} and *TERT*^{prom} responders, time gain was not assessed in those patients.

4.2.7. ctDNA dynamics in the validation cohort

To validate the findings presented above, 35 additional patients were added to my study who received immune checkpoint inhibition (for drug types, see Methods) at the University Medical Center Tübingen and at the Universitair Ziekenhuis in Brussels. This independent cohort of patients was used to validate the clinical utility of ctDNA monitoring by ddPCR in predicting treatment response and progression free survival.

I assessed the dynamic changes of ctDNA, and as expected, patients with radiologic evidence of response showed a statistically significant decreasing course of ctDNA irrespective of the ctDNA or the drug type. Non-responders had rising ctDNA levels (**Figure 4.19A**, pooled data of all 35 patients with *BRAF*^{V600E}, *NRAS*^{Q61} and *TERT*^{prom} mutations).

I confirmed that the increase in ctDNA (averaged over 2 sampling time points) relative to the baseline measurement was significantly associated with decreased PFS (HR 8.44 95%CI 3.54-20.12, *P*<0.0001, log rank test, **Figure 4.19B**).

Regarding absolute copy numbers of ctDNA across all patients treated, the median ctDNA value of non-responders was 144 copies/ml at 12 weeks of treatment, significantly higher than in responders (12 copies/ml, *P*<0.0001, Mann-Whitney U test, **Figure 4.19C**, pooled data of all 35 patients with *BRAF*^{V600E}, *NRAS*^{Q61} and *TERT*^{prom} mutations) and well above the threshold defined by ROC analysis in the training cohort (**Appendix 2**).

The median was 127 copies/ml in patients with a PFS below 6 months, significantly higher than in patients with a PFS above 6 months (14 copies/ml, *P*=0.003, Mann-Whitney U test, **Figure 4.19D**, pooled data of all 35 patients with *BRAF*^{V600E}, *NRAS*^{Q61} and *TERT*^{prom} mutations). Fisher's exact test confirmed a significant association of the ROC-determined ctDNA threshold (see **Appendix 2**) with treatment response (*P*<0.0001) or 6 months PFS (*P*=0.002) (**Appendix 9-10**).

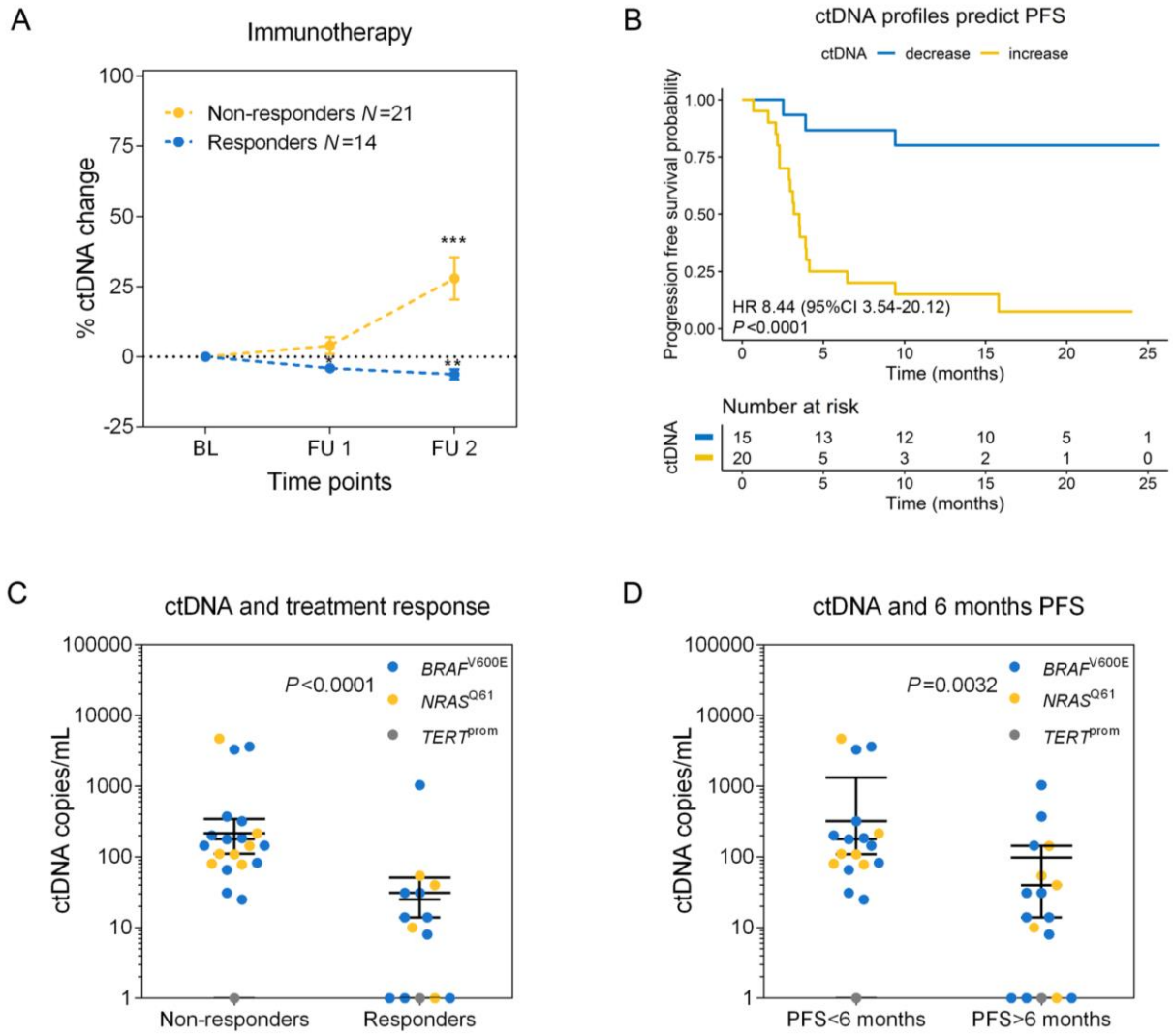

Figure 4.19 Independent validation cohort

A-D. ctDNA dynamics correlate with clinical outcome in the validation cohort. **A.** Changes in mean ctDNA levels after therapy initiation relative to baseline (BL) from patients who received immune checkpoint inhibition (*N*=35 patients). Follow-up sampling (FU 1-2) was done every 6 weeks. Asterisks indicate *P* values (* *P*<0.05, ** *P*<0.01, *** *P*<0.001) from unpaired t-test. The data represent mean±SEM. **B.** Kaplan-Meier plot for PFS of the same melanoma patients as assessed by routine radiologic scans (patients with ctDNA decrease *N*=15 vs. increase *N*=20). Categorization into 'decrease' vs. 'increase' was based on average ctDNA changes over 2 sampling time points relative to the baseline. HR is indicated for ctDNA increase. The *P* value was determined by the log rank test. Scatter dot plots of *BRAF*^{V600E} ctDNA levels of responders vs. non-responders grouped according to **C.** radiologic response 12 weeks after receiving any therapy or **D.** radiologic PFS at 6 months of therapy (Mann-Whitney U test). Points represent individual patients; median with interquartile range is indicated for each dataset.

4.2.8. Baseline NRAS^{Q61} ctDNA is an independent predictor of progressive disease and overall survival in MAPKi-treated patients

Mutations in *NRAS*^{Q61} have been reported in patients who developed resistance to *BRAF* inhibitors (108,110). Thus, I tested the presence of *NRAS*^{Q61} ctDNA in longitudinal plasma samples from patients with positive *BRAF*^{V600E} tumor status under MAPK-targeted therapy (*N*=33). Unexpectedly, I detected *NRAS*^{Q61} ctDNA in 21 of the 33 patients already at baseline before treatment.

In contrast to the common dogma of mutual exclusivity, *NRAS*^{Q61} ctDNA clearly co-occurred with *BRAF*^{V600E} ctDNA, however, in the majority of the cases at lower levels (16/21 cases). Moreover, I found that the presence of plasma *NRAS*^{Q61} ctDNA in baseline samples of the 33 *BRAF*^{V600E} patients significantly correlated with shorter PFS (HR 3.18 95% CI 1.31-7.68, *P*=0.03, log rank test) (**Figure 4.20A**) and shorter OS (HR 4.08 95%CI 1.57-10.58, *P*=0.01, log rank test) (**Figure 4.20B**) under MAPKi treatment.

To test whether this observation is true for all MAPKi treated *BRAF*^{V600E} patients; I analyzed additional 20 patients who had available plasma samples at baseline. I found that the detection of *NRAS*^{Q61} mutation at baseline in all MAPKi treated *BRAF*^{V600E} patients (*N*=53) was significantly associated with disease progression in univariable analysis (HR 2.95, 95% CI 1.35-6.44, *P*=0.006, log rank test). Elevated LDH (HR 2.31, 95%CI 1.12-4.75, *P*=0.02) but not S100 (HR 2.04, 95%CI 0.99-4.22, *P*=0.51, log rank test) represented a significant risk factor for progression in univariate analysis, too. However, in multivariable analysis, only elevated *NRAS*^{Q61} ctDNA significantly predicted disease progression (HR 2.69, 95% CI 1.17-6.16, *P*=0.02, log rank test, **Table 4.4**).

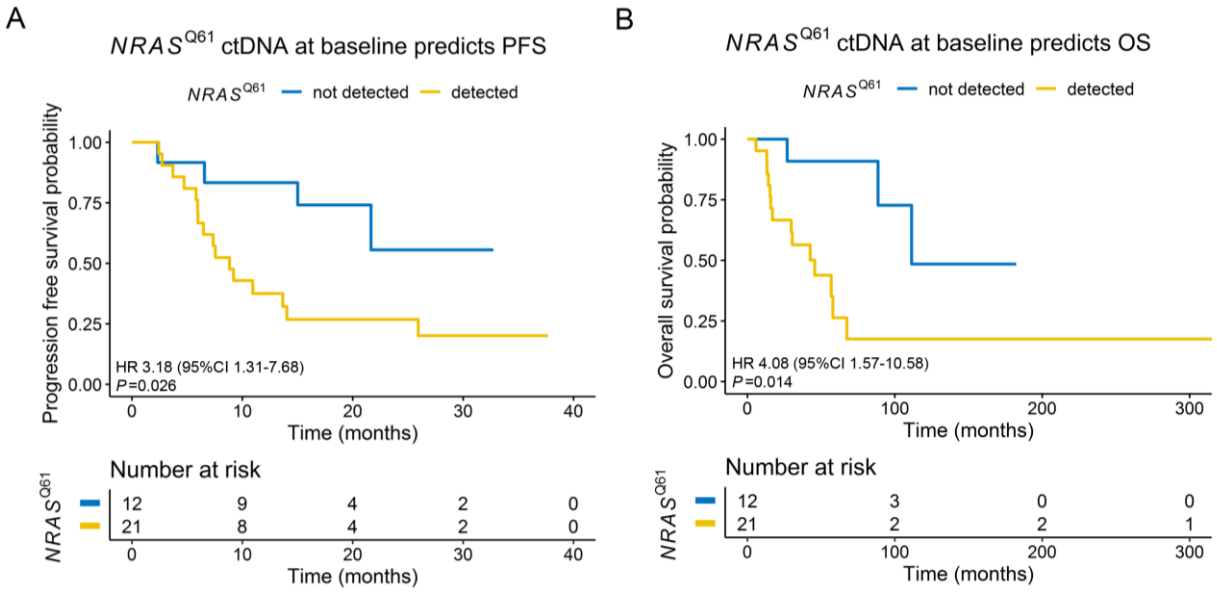

Figure 4.20 Detection of *NRAS*^{Q61} at baseline is a predictor of worse clinical outcome in MAPKi-treated patients

Kaplan-Meier plots for **A.** radiologic PFS and **B.** OS of patients with *BRAF*^{V600E}-positive tumors who received MAPK signaling targeted therapy (*N*=21 with positive *NRAS*^{Q61} detection in baseline plasma vs. *N*=12 without detection). HR is listed for ctDNA detected. *P* values were determined by the log rank test.

Table 4.4 *NRAS*^{Q61} baseline ctDNA is a risk factor for disease progression

The ULN for S100 is 0.15 µg/L and for LDH is 247 IU/L. HR with 95% CI is listed for the binary variable option indicated, with the second option being HR=1.

	Univariable analysis			Multivariable analysis		
Heading risk factors	**HR**	**95% CI**	***P***	**HR**	**95% CI**	***P***
NRAS^{Q61} detected	2.95	1.35-6.44	0.006	2.69	1.17-6.16	0.019
elevated S100	2.04	0.99-4.22	0.510	1.59	0.68-3.68	0.276
elevated LDH	2.31	1.12-4.75	0.022	1.62	0.69-3.78	0.260

HR: Hazard Ratio, CI: Confidence Interval, *P*: log rank test

Since ddPCR has shown great sensitivity, even in the context of very low frequency variants, I proposed to analyze plasma and tissue genotypes using ddPCR and compare results to the existing TA-NGS determined tumor tissue genotypes. To test if potential differences in the assay sensitivities of NGS vs. ddPCR may account for the observed discrepancies of the patients' *NRAS*^{Q61} mutational states, I obtained genomic DNA isolated from 51 melanoma tissue samples that previously underwent TA-NGS and re-analyzed them on the ddPCR platform. Indeed, of 12 *BRAF*^{V600E} patients whose plasma samples were positive for *NRAS*^{Q61} ctDNA at baseline, but with negative *NRAS*^{Q61} tumor tissue according to TA-NGS, 8 were also positive in tissue, when tested with the ddPCR assay (**Figure 4.21**). However, in another 4 cases, only plasma ddPCR could detect the positive mutational *NRAS*^{Q61} state, while the tumor sample remained negative also with ddPCR. The opposite scenario, i.e. positive *NRAS*^{Q61} state in tissue and negative in plasma, was only found in two cases.

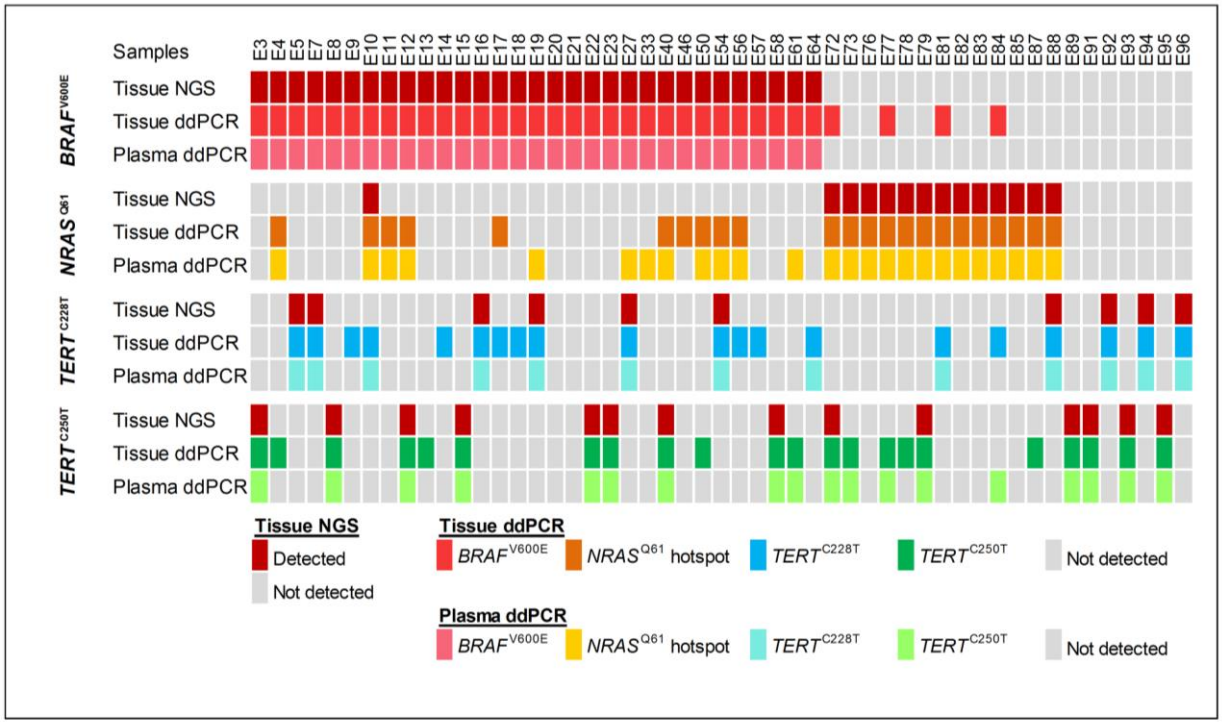

Figure 4.21 Overview of matched tumor tissue and plasma genotypes

Overview of 51 *BRAF*^{V600E}, *NRAS*^{Q61} and *TERT*^{prom} matched tumor tissue and plasma samples of patients who had available tumor biopsy at therapy baseline. Tumor samples were routinely analyzed for *BRAF*^{V600E}, *NRAS*^{Q61} and *TERT*^{prom} mutations with amplicon-based next generation sequencing (see also Figure 4.10) and afterwards re-analyzed by ddPCR. Plasma was sampled at baseline, i.e. prior to systemic therapy initiation, and analyzed for ctDNAs by ddPCR.

Thus, the presence of baseline *NRAS*^{Q61} ctDNA significantly correlated with progressive disease in patients receiving MAPK inhibition suggesting performance of plasma ctDNA screening with sensitive assays already at baseline for therapeutic decision making.

Taken together, my results support the value of ddPCR-assessed ctDNA as a sensitive and robust biomarker of disease progression and therapy response in melanoma. I demonstrated that ctDNA profiles and changes in absolute ctDNA copies early after therapy initiation are predictive of PFS in a large training dataset and confirmed this in an independent validation dataset. Monitoring of ctDNA by ddPCR is capable of detecting changes in the tumor burden earlier than standard radiologic CT or MRI imaging. ctDNA profiling at baseline, e.g. of *NRAS*^{Q61}, could add valuable information to clinical routine even for initial therapeutic decision making.

5. Discussion

In order to make precision oncology a reality, there is a great need to identify highly predictive, non-invasive monitoring technologies. Melanoma has been shown to be a genetically heterogeneous systemic disease (18,64) and the emergence of therapy-surviving tumor clones is known to predict secondary mutation-driven resistance (108,110–114). The application of ctDNA assays to metastatic melanoma has been recently reported to be a promising tool in terms of detecting tumor-derived mutant DNA over time (74–88,115,116).

The current technologies that are commonly used for detection of DNA alterations in ctDNA include mainly PCR- or NGS-based assays. Recent advances in PCR-based genomic methodologies allowed increasingly sensitive detection of rare gene copies (117). Technologies like BEAMing (beads, emulsion, amplification and magnetics) (118), PAP [pyrophosphorolysis activated polymerization (119)], and droplet ddPCR are by far the most sensitive technologies down to 0.01% or lower sensitivity levels (117,120). NGS is less sensitive [(1% sensitivity, (121)], but has the advantage of assessing a broader range of genes including sequence information.

5.1. Targeted amplicon based next generation sequencing of ctDNA samples

TA-NGS is a highly powerful and well-established technology for the discovery and screening of genetic variants in human cancers. An important advantage of TA-NGS gene panels is that it can give a broad view on driver and non-driver mutations as well as gene rearrangements at the same time, which is critical for clinical decision making or disease monitoring. Recently, it has been shown for various cancers that NGS can be applied to monitor cancer specific variants in plasma (122–127). In order to comprehensively characterize the evolution of tumor progression, and to identify the time point of resistance, the use of NGS gene panels could provide a practical approach. For example, Girotti *et al* showed the utility of 10-gene panel NGS platform in longitudinal monitoring of metastatic melanoma patients (76). The study suggested that monitoring of the driver mutations in *BRAF* and *NRAS* could be used to prospectively evaluate response to targeted and immunotherapies. The ctDNA results showed a clear correlation with radiologic imaging and LDH measurements.

My project aimed to establish a TA-NGS suitable for monitoring variants in frequently mutated melanoma genes like *BRAF*, *NRAS*, *MAP2K1*, *MAP2K2*, *GNA11* and *GNAQ* and in the promoter region of *TERT* gene (102,106,107). Reports by other groups estimate a TA-NGS assay sensitivity of 1-2% (117,121). However, in the dilution series of my study using cell line-derived DNA, a considerably lower sensitivity was achieved, where the lowest limit of detection was 1,000 mutant copies in the background of 10,000 wt copies (reflecting a mutant allele frequency of 10%). The degree of agreement between the tissue mutational state of the assessed 6 genes plus the *TERT* promoter region and the ctDNA state in my test set of human plasma samples was only 39%. The strongest discrepancies in the detected genotypes were observed for the promoter region of *TERT*. The *TERT* promoter region is a challenging target, as it is GC-rich (above 70%) and contains many repetitive elements. Moreover, the mutations are located in close proximity to each other. Thus, assays designed for *TERT*^{prom} PCR amplifications, including TA-NGS, require a thorough experimental design (e.g. of primers) and careful data evaluation. For technical optimization, I increased the starting DNA quantity and additionally adjusted count and frequency thresholds in the NGS analysis software to achieve better detection rates. Thereafter, TA-NGS-based ctDNA detection improved with regard to detection of lower frequency variants. However, there were still insuperable discrepancies between the plasma and tissue mutational states of several samples, especially in case of the *TERT*^{prom} mutations.

My observations also indicated that the sequencing coverage of the Illumina® Miseq® used here may not be sufficient for detection of low mutant allelic fractions, particularly for subclonal variants. The content of cfDNA in plasma is indeed relatively low with an average concentration of 30 ng/ml (128). Thus, it is possible that a higher coverage depth (by using different sequencing instruments) could have uncovered low mutant frequencies also in our plasma samples. In this regard, Shu *et al* demonstrated that increasing the coverage depth to 300-500x indeed can result in significant improvement of tissue-plasma mutation concordance (124). However, next to purely technological considerations, there are several other possibilities which can influence the number of discordant cases, e.g. the time frame between the two biopsy modalities (tissue vs. blood), different treatment effects, differences in the biopsy techniques, or the sites of the metastatic organ (low vs. high ctDNA releasing sites) (129–131).

While many groups demonstrated promising results for the utility of NGS panels for ctDNA measurement, several reports also discuss potential difficulties of this technique, especially issues regarding to reproducibility and reliability (75,76,122–127,129–131). Besides, NGS analysis is rather time consuming, relatively costly, and less sensitive than other modern genomic technologies. Also, the results of my research project suggested that there is a high need for significant improvements in order to introduce TA-NGS-based approaches into the clinical practice. In the context of personalized medicine, NGS analysis of liquid biopsies could still be a promising approach, particularly in the discovery of novel cancer biomarkers. Hence, highly sophisticated NGS-based liquid biopsy projects are currently ongoing worldwide including also collaborative research efforts within the MELGEN consortium to which our group is intending to contribute in future, too.

5.2. Application of ddPCR for monitoring therapy responses in metastatic melanoma patients

Single tumor biopsies mostly fail to reflect the full biological diversity of tumors, and in particular, the dynamics in disease progression and development of drug resistance. The use of ctDNA for ddPCR-guided liquid biopsies could be a promising real-time monitoring application for therapeutic decision making. Unlike NGS gene panels, ddPCR is limited in multiplexing; however, it is fast, cost effective, and highly sensitive in detecting low frequency mutations. Specifically, quantification of the absolute gene copy number, which can be done by ddPCR, but not by NGS, is important for longitudinal disease monitoring, where fluctuations of the physiological backgrounds (i.e. wt cfDNA) can occur and influence result interpretations.

One of the first studies that employed ddPCR for monitoring melanoma progression was published by Sanmamed *et al* (86). The authors evaluated *BRAF*^{V600E} ctDNA in plasma samples of 20 patients who have received BRAFi (vemurafenib, dabrafenib) and correlated the *BRAF*^{V600E} levels with tumor burden and survival. They found that lower baseline *BRAF*^{V600E} (<216 copies/ml) significantly correlated with longer PFS and OS. Lee *et al* demonstrated that mutant ctDNA can be used to predict responses to anti PD-1 therapy in 76 metastatic patients with mutations in *BRAF*, *NRAS* and *KIT*. The authors also showed that ctDNA evaluation within the first 12 weeks of therapy provides more accurate response assessment than current monitoring tools (78).

My study was designed to establish and validate plasma-based assays that allow the dynamic quantitative detection of ctDNA as a clinically applicable biomarker for tumor load, disease prognosis, and prediction of therapy response. To my knowledge, this is the largest longitudinal study on melanoma ctDNA to date, including assessment of *BRAF*^{V600E}, 5 mutations in the *NRAS*^{Q61} codon, and 2 mutations in the promoter region of the *TERT* gene in 131 individuals. According to published genetic melanoma landscaping analyses, the combination of these assays covers about 80% of all melanomas (106). In addition, my findings were validated by an independent cohort of samples, which were prospectively collected at different clinical centers.

5.2.1. ddPCR is a sensitive tool to detect low frequency mutations

An important first consideration of my study was to reliably distinguish between the tumor-derived ctDNA and the wt cfDNA fraction. Wild-type cfDNA is released from normal cells throughout the body. Thus, the proportion of tumor-specific genetic information can be very low and it needs highly sensitive methods for its detection. In dilution series using cell line-derived DNA, I could ensure that the ddPCR assays applied here are reproducible and able to detect 1 mutant gene copy (in the background of 10,000 wt DNA copies or in a reaction volume of 20 µl) where assay linearity was maintained. The reported sensitivities in this study are similar to previously published results for *BRAF*^{V600E} and *NRAS*^{Q61} (87). Importantly, the *TERT*^{prom} ddPCR assays were highly specific to their respective mutations, without false positive results in the nearby *TERT*^{prom} mutations.

I reported ddPCR results as copies/ml instead of mutant fraction relative to wild-type, which is increasingly considered as a precise measure in the field of ctDNA research (75,77,78,82,86,88,132–134). Fluctuations in the absolute mutated copies are able to accurately reflect changes in the tumor. Diaz *et al* demonstrated via mathematical modeling on data from *KRAS* mutant ctDNA of colorectal cancer patients, that it needs the DNA release of 44 million tumors cells into the bloodstream to reach a detection rate of 1 mutant copy per milliliter of blood (134). This observation is intriguing, given that current imaging techniques are able to detect tumor masses of 7-10 mm in size, equivalent to 1 billion cancer cells (135). Therefore, monitoring ctDNA changes on the absolute copy level is crucial for reliable interpretations of tumor burden and for interpretation of tumor evolutionary processes, especially in the clonal expansion of resistant cells.

5.2.2. Impact of sample processing and storage conditions on mutation detection

Although previous reports recommend standardized protocols for blood collection and ctDNA isolation (136), ctDNA was reliably detected in my study also in patient samples that were isolated from plasma following different collection procedures. Strictly speaking, none of the patients with active metastatic disease whose plasma samples were belatedly processed up to twenty-four hours after blood draw or were diluted with salt solution fell below the copy number threshold of healthy controls. Of course, this finding should not contradict the benefits of standardized assay procedures for any kind of diagnostic test but highlights the robustness of ctDNA measurement by droplet digital PCR in clinical routine. van Dessel *et al* emphasized the impact of pre-analytical conditions on the detection of somatic variants in plasma by ddPCR (137). The authors collected blood from metastatic cancer patients, and separated plasma samples within 1, 24, and 96 hours post blood draw. They found that, the detected mutant copies in the belatedly processed plasma samples did not significantly differ from the 1-hour sample. The mutant allele fraction, however, was significantly decreased in the 96-hour sample, due to increased wild-type copies resulting from lysis of leukocytes. Additionally, Haselmann *et al* reported no differences in mutation detection results regarding differences in storage conditions of plasma (+4°C, -20°C and -80°C) and the time elapsed between storage and analysis (138). Consistent with these findings, plasma samples analyzed in this study were not significantly affected by blood processing and storage conditions.

5.2.3. ctDNA thresholds have predictive value at baseline

In contrast to previous studies, where healthy donors were used as controls to set technical detection thresholds or to determine assay specificity, I additionally considered the clinical significance of background mutations in the ctDNA of healthy individuals for statistical normalization at baseline and later on under therapy. This consideration is critical, because there is evidence that also individuals without a known diagnosis of cancer can develop mutant ctDNA throughout their lifetime, either derived from aging cells or, indeed, from undiscovered cancer cells (139). Multiple research studies showed that not all cancer driver mutations detected in a diagnostic setting truly cause cancer (140–143). For example, Anglesio *et al* identified well-known cancer driver mutations in patients with endometriosis, but without cancer

(140). In another study, somatic mutations in genes linked to hematologic cancer have been identified in 10% of the analyzed subjects over the age of 65, while the risk of cancer development in this cohort remained low (1% per year) (141). More importantly, in melanoma, mutations in *BRAF* and *NRAS* are by the far most relevant drivers of the disease, although the same mutations are frequently found and released from common benign nevi (144,145).

Regarding differences between healthy plasma donors and melanoma patients with radiologically confirmed active tumor mass, the goal was to establish a molecular cut off value for ctDNA with true clinical relevance using ROC analysis. The resulting 'baseline-prognostic' threshold was 11.74 ctDNA copies/ml for $BRAF^{V600E}$, 10.30 copies/ml for $NRAS^{Q61}$, and 13.04 copies/ml for $TERT^{prom}$. This threshold reproducibly and significantly identified high-risk patients for disease progression at baseline in the training and validation cohort. I concluded that concrete ctDNA thresholds are prognostic for outcome and represent a reliable practical tool for routine diagnostics, even in the context of background mutant ctDNA. Regarding the fact that with constant technological progress and increasing assay sensitivities, more or less every person may once be proven to carry mutant ctDNA molecules in their lifetimes (139), statistical considerations of the mutant background will become increasingly important in liquid biopsies to consolidate prognostic thresholds with true clinical relevance.

5.2.1. ctDNA thresholds have predictive value during therapy

In my study, ctDNA levels dramatically decreased under signaling targeted therapy shortly after treatment initiation (faster than under immune checkpoint inhibition). Thus, ctDNA courses match clinical observations on therapy kinetics in many ways, just earlier. Targeted therapies typically show quick tumor responses in clinical routine; however the effect is transient in many patients due to early progression (56,146). In contrast to previously published ctDNA thresholds in patients under therapy (based on median split), my goal was to establish and statistically validate a 'therapeutic-predictive' threshold based on ROC analyses of longitudinally assessed samples with timely matching CT/MRI scans. Accordingly, patients whose ctDNA levels were above a threshold of 35.85 copies/ml $BRAF^{V600E}$, 51.5 copies/ml $NRAS^{Q61}$, and 32.83 copies/ml $TERT^{prom}$ ctDNA over a period of 6-8 weeks despite therapy had significantly shorter PFS, as compared to patients whose ctDNA

remained below these thresholds. All of the ctDNA assays applied here were significantly better indicators of measurable disease compared to LDH or S100.

5.2.2. The dynamic ctDNA changes reflect response to therapy

Despite the practicability of molecular thresholds, my study indicates that the additional but still clinically practicable assessment of dynamic ctDNA changes may further foster diagnostic safety. Changes in the ctDNA level during therapy can be a sign of treatment efficacy or of clonal changes in the tumor, e.g. due to developing resistance. I found a strong correlation between ctDNA dynamics and PFS. In fact, I saw that the mean change in the ctDNA level over consecutive time points compared to the baseline represents a significant indicator of treatment effectiveness.

Furthermore, this study showed that also ctDNA changes relative to the previous sampling time point or even the rate of ctDNA increase per week can serve as the earliest hint of progression in patients receiving therapy. Indeed, ctDNA changes accurately predicted responses and disease progression significantly earlier than routine imaging in 85% of the cases (average lead-time difference 1.5 months for response and 3.5 months for progression). Haselmann *et al* reported a similar lead-time reduction (3.6 months) as compared to radiologic imaging (74). Olsson *et al* found that also in breast cancer patients, ctDNA detection precedes the clinical diagnosis of recurrence on average by 11 months (147). This highlights the true clinical benefit of ctDNA, which could be applied to change treatment management of patients in risk of developing metastasis.

Moreover, I showed in an independent cohort, that ctDNA profiles and the early changes in ctDNA levels can predict long-term response or therapy failure. Altogether, these findings highlight the clinical benefit of ctDNA, for example for prioritizing patients for more frequent clinical/radiologic assessment of their disease and guidance of therapy decision strategies.

5.2.3. Baseline NRAS^{Q61} ctDNA is an independent predictor of survival in MAPKi-treated patients

Tumor tissue-based mutational testing [e.g. by NGS with a sensitivity of 1% (121)] is currently used as clinical state-of-the-art to guide therapy selection for metastatic melanoma patients. However, it does not account for the issue of inter-tumor and

intra-patient heterogeneity. Instead, liquid biopsies should better assess the full genetic heterogeneity of solid cancers at the systemic disease level.

Here, I analyzed baseline plasma samples with ddPCR and compared the results with existing NGS-based tissue profiles. Most importantly, I found *NRAS*^{Q61} ctDNA copies in the baseline plasma of 21 out of 33 longitudinally monitored patients, who had *NRAS*^{Q61} negative tumor tissue according to NGS. At first, this may indicate that the TA-NGS protocol, which was applied to assess the mutational tumor status in our cohorts, may not be sensitive enough to detect low frequency *NRAS* mutations within bulk tumors, e.g. when originating only from minor cell subpopulations. To test this assumption, I obtained genomic DNA isolated from 51 melanoma tissue samples that previously underwent amplicon-targeted NGS and re-analyzed them on the ddPCR platform. Indeed, of 12 *BRAF*^{V600E} patients whose plasma samples were positive for *NRAS*^{Q61} ctDNA at baseline while having a negative NGS status for *NRAS*^{Q61}, 8 were also positive in their tumor tissue, when tested with the ddPCR assay. However, in another 4 cases, only plasma ddPCR could detect the positive mutational *NRAS*^{Q61} state. Altogether, this may indicate that small *NRAS*^{Q61} clones could pre-exist somewhere in the sampled tumors or outside the sampled tumors in the patients' bodies before initiation of any MAPK-pathway targeted therapy, and then outgrow upon killing of *NRAS*^{Q61} mutation-negative bulk cells.

Similar ideas have been recently reported for other cancer entities. For example, resistance to EGFR blockade in colorectal cancer is associated with cell populations carrying mutations in *RAS* family genes (*KRAS*, *NRAS*, *HRAS*) (148). Diaz *et al* have analyzed the presence of *KRAS* resistance mutations in progressing colorectal cancer patients after 5-6 month on therapy (134). Using mathematical modeling, they calculated that *KRAS* mutations were already present with high probability in the tumors before the initiation of panitumumab, i.e. in subclonal cell populations. Also in my study, the presence of baseline *NRAS*^{Q61} ctDNA in *BRAF*^{V600E} patients before initiation of MAPKi significantly correlated with shorter PFS and OS. In agreement with other reports that showed an increase of *NRAS*^{Q61} ctDNA upon MAPKi (76,82), I also observed increasing levels of *NRAS*^{Q61} during MAPKi, however, the absolute *NRAS*^{Q61} copy numbers remained lower than *BRAF*^{V600E} copies (76,82).

In sum, these results confirm that (i) cell clones, which carry genetic resistance mutations *a priori*, expand under therapeutic pressure and that (ii) resistance mutations represent promising biomarkers predicting treatment failure not only when

increased under therapy, but also when present already at baseline. The detection of these small cell populations, however, is challenging due to the heterogeneous distribution across tumor samples and the patients' bodies. Longitudinal ctDNA analysis might help in minimizing sampling bias and allow tracking of different (resistant) cell subclones simultaneously.

5.3. Future prospects

In summary, my study supports the importance of ctDNA analysis as a valid clinical tool for the provision of real-time information on current treatment responses and prediction of future response probability. In addition, the comparison of plasma-based ctDNA analysis with tumor tissue-based TA-NGS indicated considerable differences in diagnostic sensitivity and validity, particularly with regard to intra-patient tumor heterogeneity. Future studies which are powered to measure the difference between tissue-based and plasma-based diagnostics are highly needed to test if liquid biopsies represent a complementary tool or even outperform tissue-based genetic testing for primary therapeutic decision making.

The utilization of liquid biopsies in clinical practice is widely supported by many publications in the field of oncology. Over 250 clinical trials employ circulating tumor biomarkers [e.g. circulating tumor cells, ctDNA and cfDNA (44)] for the assessment of prognosis and individualized therapy, highlighting the importance and potential of this tool in standard cancer care. The ddPCR assays established in my study are suitable for fast, real-time monitoring of melanoma progression, and for evaluation of treatment response. Patients at the Department of Dermatology of the Essen University Hospital with *BRAF*^{V600E}, *NRAS*^{Q61} and *TERT*^{prom} mutations will be -from now on- prospectively monitored for occurring ctDNA changes and the results will be used to evaluate tumor load and response to treatment complementary to standard CT/MRI staging.

Based on the results obtained in my thesis, the combination of the hotspot genetic alterations in *BRAF*, *NRAS* and promoter region of *TERT* is expected to cover around 80% of all melanoma patients. To cover all melanoma patients, monitoring of total cfDNA concentrations will be tested in a follow-up study in our department. To facilitate clinical implementation of this technique, data will be evaluated based on bio-statistical methods established in my thesis. To foster the nation-wide application

of ddPCR-based ctDNA assessment in clinical practice, and support negotiations with health insurances regarding financial compensation, my thesis paved the way for a larger prospective clinical trial, which is currently designed at our department.

6. References

1. Mort RL, Jackson IJ, Patton EE. The melanocyte lineage in development and disease. Development. 2015;142(4):620–32.

2. Schadendorf D, Fisher DE, Garbe C, Gershenwald JE, Grob JJ, Halpern A, et al. Melanoma. Nat Rev Dis Prim. 2015;1(15003).

3. Goldstein AM, Tucker MA. Familial melanoma and its management. In: Genetic Predisposition to Cancer. Boston, MA: Springer US; 1996. p. 333–43.

4. Ferlay J, Soerjomataram I, Ervik M, Dikshit R, Eser S, Mathers C, Rebelo M, Parkin DM, Forman D, Bray F. GLOBOCAN 2012 v1.1, Cancer Incidence and Mortality Worldwide: IARC CancerBase No. 11. Lyon, France: International Agency for Research on Cancer. 2014.

5. http://globocan.iarc.fr/Default.aspx. Globocan.

6. Stang A, Jöckel K-H, Heidinger O. Skin cancer rates in North Rhine-Westphalia, Germany before and after the introduction of the nationwide skin cancer screening program (2000–2015). Eur J Epidemiol. 2018;33(3):303–12.

7. Ali Z, Yousaf N, Larkin J. Melanoma epidemiology, biology and prognosis. In: European Journal of Cancer, Supplement. Elsevier; 2013. p. 81–91.

8. Garibyan L, Fisher DE. How Sunlight Causes Melanoma. Curr Oncol Rep. 2010;12(5):319–26.

9. Bulliard JL, Cox B, Elwood JM. Latitude gradients in melanoma incidence and mortality in the non-Maori population of New Zealand. Cancer Causes Control. 1994;5(3):234–40.

10. Nelemans PJ, Groenendal H, Kiemeney LA, Rampen FH, Ruiter DJ, Verbeek AL. Effect of intermittent exposure to sunlight on melanoma risk among indoor workers and sun-sensitive individuals. Environ Health Perspect. 1993;101(3):252–5.

11. CANDIDO S, RAPISARDA V, MARCONI A, MALAPONTE G, BEVELACQUA V, GANGEMI P, et al. Analysis of the B-RAFV600E mutation in cutaneous melanoma patients with occupational sun exposure. Oncol Rep.

2014;31(3):1079–82.

12. Elwood JM, Jopson J. Melanoma and sun exposure: An overview of published studies. Int J Cancer. 1997;73(2):198–203.

13. White E, Kirkpatrick CS, Lee JAH. Case-Control Study of Malignant Melanoma in Washington State. Am J Epidemiol. 1994;139(9):857–68.

14. Lazovich D, Vogel RI, Berwick M, Weinstock MA, Anderson KE, Warshaw EM. Indoor tanning and risk of melanoma: a case-control study in a highly exposed population. Cancer Epidemiol Biomarkers Prev. 2010;19(6):1557–68.

15. Rastrelli M, Tropea S, Rossi CR, Alaibac M. Melanoma: epidemiology, risk factors, pathogenesis, diagnosis and classification. In Vivo. 2014;28(6):1005–11.

16. Dusingize JC, Olsen CM, Pandeya N, Thompson BS, Webb PM, Green AC, et al. Smoking and cutaneous melanoma: findings from The QSkin Sun and Health cohort study. Cancer Epidemiol Biomarkers Prev. 2018;Aug(8):874–88.

17. Cancer Genome Atlas Network TCGA. Genomic Classification of Cutaneous Melanoma. Cell. 2015;161(7):1681–96.

18. Hodis E, Watson IR, Kryukov G V., Arold ST, Imielinski M, Theurillat J-PP, et al. A landscape of driver mutations in melanoma. Cell. 2012;150(2):251–63.

19. Viros A, Sanchez-Laorden B, Pedersen M, Furney SJ, Rae J, Hogan K, et al. Ultraviolet radiation accelerates BRAF-driven melanomagenesis by targeting TP53. Nature. 2014;511(7510):478–82.

20. Hussussian CJ, Struewing JP, Goldstein AM, Higgins PAT, Ally DS, Sheahan MD, et al. Germline p16 mutations in familial melanoma. Nat Genet. 1994;8(1):15–21.

21. Zuo L, Weger J, Yang Q, Goldstein AM, Tucker MA, Walker GJ, et al. Germline mutations in the p16INK4a binding domain of CDK4 in familial melanoma. Nat Genet. 1996;12(1):97–9.

22. Potrony M, Badenas C, Aguilera P, Puig-Butille JA, Carrera C, Malvehy J, et al. Update in genetic susceptibility in melanoma. Ann Transl Med. 2015;3(15):210.

23. Schaffer J V., Bolognia JL. The Melanocortin-1 Receptor. Arch Dermatol. 2001;137(11):1477–85.

24. Aspinwall LG, Leaf SL, Dola ER, Kohlmann W, Leachman SA. CDKN2A/p16 genetic test reporting improves early detection intentions and practices in high-risk melanoma families. Cancer Epidemiol Biomarkers Prev. 2008;17(6):1510–9.

25. Tripp MK, Watson M, Balk SJ, Swetter SM, Gershenwald JE. State of the science on prevention and screening to reduce melanoma incidence and mortality: The time is now. CA Cancer J Clin. 2016;66(6):460–80.

26. Bauer J, Garbe C. Acquired Melanocytic Nevi as Risk Factor for Melanoma Development. A Comprehensive Review of Epidemiological Data. Pigment Cell Res. 2003;16(3):297–306.

27. Bevona C, Goggins W, Quinn T, Fullerton J, Tsao H. Cutaneous Melanomas Associated With Nevi. Arch Dermatol. 2003;139(12):1620.

28. Shain AH, Bastian BC. From melanocytes to melanomas. Nat Rev Cancer. 2016;16(6):345–58.

29. Gandini S, Sera F, Cattaruzza MS, Pasquini P, Abeni D, Boyle P, et al. Meta-analysis of risk factors for cutaneous melanoma: I. Common and atypical naevi. Eur J Cancer. 2005;41(1):28–44.

30. Shain AH, Yeh I, Kovalyshyn I, Sriharan A, Talevich E, Gagnon A, et al. The Genetic Evolution of Melanoma from Precursor Lesions. N Engl J Med. 2015;373(20):1926–36.

31. https://smart.servier.com/. Smart servier medical art.

32. Smoller BR. Histologic criteria for diagnosing primary cutaneous malignant melanoma. Mod Pathol. 2006;19(S2):S34–40.

33. MOWAT A, REID R, MACKIE R. Balloon cell metastatic melanoma: an important differential in the diagnosis of clear cell tumours. Histopathology. 1994 May;24(5):469–72.

34. Lucas DR, Tazelaar HD, Unni KK, Wold LE, Okada K, Dimarzio DJ, et al. Osteogenic melanoma. A rare variant of malignant melanoma. Am J Surg

Pathol. 1993 Apr;17(4):400–9.

35. BITTESINI L, TOS APD, FLETCHER CDM. Metastatic malignant melanoma showing a rhabdoid phenotype: further evidence of a non-specific histological pattern. Histopathology. 1992 Feb;20(2):167–70.

36. Cinotti E, Rongioletti F. Myxoid Melanoma. In: Rare Malignant Skin Tumors. New York, NY: Springer New York; 2015. p. 215–7.

37. Cerami E, Gao J, Dogrusoz U, Gross BE, Sumer SO, Aksoy BA, et al. The cBio cancer genomics portal: an open platform for exploring multidimensional cancer genomics data. Cancer Discov. 2012 May 1;2(5):401–4.

38. Gao J, Aksoy BA, Dogrusoz U, Dresdner G, Gross B, Sumer SO, et al. Integrative analysis of complex cancer genomics and clinical profiles using the cBioPortal. Sci Signal. 2013;6(269):pl1.

39. Ihle MA, Fassunke J, König K, Grünewald I, Schlaak M, Kreuzberg N, et al. Comparison of high resolution melting analysis, pyrosequencing, next generation sequencing and immunohistochemistry to conventional Sanger sequencing for the detection of p.V600E and non-p.V600E BRAF mutations. BMC Cancer. 2014;14(13).

40. Balch CM, Gershenwald JE, Soong S-J, Thompson JF, Atkins MB, Byrd DR, et al. Final version of 2009 AJCC melanoma staging and classification. J Clin Oncol. 2009 Dec 20;27(36):6199–206.

41. https://www.leitlinienprogramm-onkologie.de/leitlinien/melanom/. Leitlinienprogramm Onkologie: Melanom.

42. Ugurel S, Röhmel J, Ascierto PA, Flaherty KT, Grob JJ, Hauschild A, et al. Survival of patients with advanced metastatic melanoma: the impact of novel therapies-update 2017. Eur J Cancer. 2017 Sep 1;83:247–57.

43. Garbe C, Peris K, Hauschild A, Saiag P, Middleton M, Bastholt L, et al. Diagnosis and treatment of melanoma. European consensus-based interdisciplinary guideline - Update 2016. Eur J Cancer. 2016;Aug(63):201–17.

44. ClinicalTrials.gov [database on the Internet]. Bethesda, MD: US National Library of Medicine.

45. Kammula US, White DE, Rosenberg SA. Trends in the safety of high dose bolus interleukin-2 administration in patients with metastatic cancer. Cancer. 1998;83(4):797–805.

46. Kirkwood JM, Ibrahim JG, Sosman JA, Sondak VK, Agarwala SS, Ernstoff MS, et al. High-dose interferon alfa-2b significantly prolongs relapse-free and overall survival compared with the GM2-KLH/QS-21 vaccine in patients with resected stage IIB-III melanoma: Results of intergroup trial E1694/S9512/C509801. J Clin Oncol. 2001;19(9):2370–80.

47. Ribas A. Tumor Immunotherapy Directed at PD-1. N Engl J Med. 2012 Jun 28;366(26):2517–9.

48. Brunet J-F, Denizot F, Luciani M-F, Roux-Dosseto M, Suzan M, Mattei M-G, et al. A new member of the immunoglobulin superfamily—CTLA-4. Nature. 1987;328(6127):267–70.

49. Ribas A, Hanson DC, Noe DA, Millham R, Guyot DJ, Bernstein SH, et al. Tremelimumab (CP-675,206), a Cytotoxic T Lymphocyte Associated Antigen 4 Blocking Monoclonal Antibody in Clinical Development for Patients with Cancer. Oncologist. 2007 Jul 1;12(7):873–83.

50. Ishida Y, Agata Y, Shibahara K, Honjo T. Induced expression of PD-1, a novel member of the immunoglobulin gene superfamily, upon programmed cell death. EMBO J. 1992;11(11):3887–95.

51. Latchman Y, Wood CR, Chernova T, Chaudhary D, Borde M, Chernova I, et al. PD-L2 is a second ligand for PD-1 and inhibits T cell activation. Nat Immunol. 2001;2(3):261–8.

52. Dong H, Zhu G, Tamada K, Chen L. B7-H1, a third member of the B7 family, co-stimulates T-cell proliferation and interleukin-10 secretion. Nat Med. 1999;5(12):1365–9.

53. Herbst RS, Soria J-C, Kowanetz M, Fine GD, Hamid O, Gordon MS, et al. Predictive correlates of response to the anti-PD-L1 antibody MPDL3280A in cancer patients. Nature. 2014 Nov 27;515(7528):563–7.

54. https://news.bms.com/press-release/bmy/phase-12-data-combining-urelumab-opdivo-nivolumab-hematologic-and-solid-tumors-sug. Phase 1/2 Data

Combining Urelumab with Opdivo (nivolumab) in Hematologic and Solid Tumors Suggest Increased Antitumor Effect in Patients with Melanoma | BMS Newsroom.

55. Jenkins RW, Barbie DA, Flaherty KT. Mechanisms of resistance to immune checkpoint inhibitors. Br J Cancer. 2018 Jan 2;118(1):9–16.

56. Chapman PB, Hauschild A, Robert C, Haanen JB, Ascierto P, Larkin J, et al. Improved Survival with Vemurafenib in Melanoma with BRAF V600E Mutation. N Engl J Med. 2011 Jun 30;364(26):2507–16.

57. Roesch A. Tumor heterogeneity and plasticity as elusive drivers for resistance to MAPK pathway inhibition in melanoma. Oncogene. 2015;34(23):2951–7.

58. Domingues B, Lopes J, Soares P, Populo H. Melanoma treatment in review. ImmunoTargets Ther. 2018 Jun 7;Volume 7:35–49.

59. Hodi FS, Corless CL, Giobbie-Hurder A, Fletcher JA, Zhu M, Marino-Enriquez A, et al. Imatinib for melanomas harboring mutationally activated or amplified kit arising on mucosal, acral, and chronically sun-damaged skin. J Clin Oncol. 2013;31(26):3182–90.

60. Kim KB, Sosman JA, Fruehauf JP, Linette GP, Markovic SN, McDermott DF, et al. BEAM: a randomized phase II study evaluating the activity of bevacizumab in combination with carboplatin plus paclitaxel in patients with previously untreated advanced melanoma. J Clin Oncol. 2012;30(1):34–41.

61. Hayward NK, Wilmott JS, Waddell NN, Johansson PA, Field MA, Nones K, et al. Whole-genome landscapes of major melanoma subtypes. Nature. 2017;545(7653):175–80.

62. Krauthammer M, Kong Y, Bacchiocchi A, Evans P, Pornputtapong N, Wu C, et al. Exome sequencing identifies recurrent mutations in NF1 and RASopathy genes in sun-exposed melanomas. Nat Genet. 2015 Sep 27;47(9):996–1002.

63. https://www.fda.gov/MedicalDevices/. companion diagnostics.

64. Grzywa TM, Paskal W, Włodarski PK. Intratumor and Intertumor Heterogeneity in Melanoma. Translational Oncology Neoplasia Press; Dec, 2017 p. 956–75.

65. Ashworth T. A case of cancer in which cells similar to those in the tumours

were seen in the blood after death. Aust Med J. 1869;14:146–9.

66. Miller MC, Doyle G V., Terstappen LWMM. Significance of Circulating Tumor Cells Detected by the CellSearch System in Patients with Metastatic Breast Colorectal and Prostate Cancer. J Oncol. 2010;2010(617421).

67. Haber DA, Velculescu VE. Blood-based analyses of cancer: Circulating tumor cells and circulating tumor DNA. Cancer Discov. 2014;4(6):650–61.

68. González-Masiá JA, García-Olmo D, García-Olmo DC. Circulating nucleic acids in plasma and serum (CNAPS): applications in oncology. Onco Targets Ther. 2013;6:819–32.

69. Jahr S, Hentze H, Englisch S, Hardt D, Fackelmayer FO, Hesch RD, et al. DNA fragments in the blood plasma of cancer patients: Quantitations and evidence for their origin from apoptotic and necrotic cells. Cancer Res. 2001;61(4):1659–65.

70. Heitzer E, Ulz P, Geigl JB. Circulating tumor DNA as a liquid biopsy for cancer. Clin Chem. 2015;61(1):112–23.

71. Wan JCM, Massie C, Garcia-Corbacho J, Mouliere F, Brenton JD, Caldas C, et al. Liquid biopsies come of age: towards implementation of circulating tumour DNA. Nat Rev Cancer. 2017 Apr 24;17(4):223–38.

72. Bettegowda C, Sausen M, Leary RJ, Kinde I, Wang Y, Agrawal N, et al. Detection of circulating tumor DNA in early- and late-stage human malignancies. Sci Transl Med. 2014 Feb 19;6(224):224ra24.

73. Valpione S, Gremel G, Mundra P, Middlehurst P, Galvani E, Girotti MR, et al. Plasma total cell-free DNA (cfDNA) is a surrogate biomarker for tumour burden and a prognostic biomarker for survival in metastatic melanoma patients. Eur J Cancer. 2018 Jan;88:1–9.

74. Haselmann V, Gebhardt C, Brechtel I, Duda A, Czerwinski C, Sucker A, et al. Liquid Profiling of Circulating Tumor DNA in Plasma of Melanoma Patients for Companion Diagnostics and Monitoring of BRAF Inhibitor Therapy. Clin Chem. 2018 Feb 26;64(5):830–42.

75. Wong SQ, Raleigh JM, Callahan J, Vergara IA, Ftouni S, Hatzimihalis A, et al.

Circulating Tumor DNA Analysis and Functional Imaging Provide Complementary Approaches for Comprehensive Disease Monitoring in Metastatic Melanoma. JCO Precis Oncol. 2017 Jul 27;(1):1–14.

76. Girotti MR, Gremel G, Lee R, Galvani E, Rothwell D, Viros A, et al. Application of sequencing, liquid biopsies, and patient-derived xenografts for personalized medicine in melanoma. Cancer Discov. 2016;6(3):286–99.

77. Lee JH, Long G V., Menzies AM, Lo S, Guminski A, Whitbourne K, et al. Association Between Circulating Tumor DNA and Pseudoprogression in Patients With Metastatic Melanoma Treated With Anti–Programmed Cell Death 1 Antibodies. JAMA Oncol. 2018 Feb 8;4(5):717–21.

78. Lee JH, Long G V., Boyd S, Lo S, Menzies AM, Tembe V, et al. Circulating tumour DNA predicts response to anti-PD1 antibodies in metastatic melanoma. Ann Oncol. 2017 May 1;28(5):1130–6.

79. Xi L, Pham TH-T, Payabyab EC, Sherry RM, Rosenberg SA, Raffeld M. Circulating Tumor DNA as an Early Indicator of Response to T-cell Transfer Immunotherapy in Metastatic Melanoma. Clin Cancer Res. 2016 Nov 15;22(22):5480–6.

80. Lee RJ, Gremel G, Marshall A, Myers KA, Fisher N, Dunn JA, et al. Circulating tumor DNA predicts survival in patients with resected high-risk stage II/III melanoma. Ann Oncol Off J Eur Soc Med Oncol. 2018 Feb 1;29(2):490–6.

81. Santiago-Walker A, Gagnon R, Mazumdar J, Casey M, Long G V, Schadendorf D, et al. Correlation of BRAF Mutation Status in Circulating-Free DNA and Tumor and Association with Clinical Outcome across Four BRAFi and MEKi Clinical Trials. Clin Cancer Res. 2016 Feb 1;22(3):567–74.

82. Gray ES, Rizos H, Reid AL, Boyd SC, Pereira MR, Lo J, et al. Circulating tumor DNA to monitor treatment response and detect acquired resistance in patients with metastatic melanoma. Oncotarget. 2015 Dec 8;6(39):42008–18.

83. Gonzalez-Cao M, Mayo-de-Las-Casas C, Molina-Vila MA, De Mattos-Arruda L, Muñoz-Couselo E, Manzano JL, et al. BRAF mutation analysis in circulating free tumor DNA of melanoma patients treated with BRAF inhibitors. Melanoma Res. 2015 Dec 1;25(6):486–95.

84. Knol AC, Vallée A, Herbreteau G, Nguyen J-M, Varey E, Gaultier A, et al. Clinical significance of BRAF mutation status in circulating tumor DNA of metastatic melanoma patients at baseline. Exp Dermatol. 2016 Oct 1;25(10):783–8.

85. Lipson EJ, Velculescu VE, Pritchard TS, Sausen M, Pardoll DM, Topalian SL, et al. Circulating tumor DNA analysis as a real-time method for monitoring tumor burden in melanoma patients undergoing treatment with immune checkpoint blockade. J Immunother cancer. 2014;2(1):42.

86. Sanmamed MF, Fernández-Landázuri S, Rodríguez C, Zárate R, Lozano MD, Zubiri L, et al. Quantitative cell-free circulating BRAFV600E mutation analysis by use of droplet digital PCR in the follow-up of patients with melanoma being treated with BRAF inhibitors. Clin Chem. 2015 Jan 1;61(1):297–304.

87. Chang GA, Tadepalli JS, Shao Y, Zhang Y, Weiss S, Robinson E, et al. Sensitivity of plasma BRAFmutant and NRASmutant cell-free DNA assays to detect metastatic melanoma in patients with low RECIST scores and non-RECIST disease progression. Mol Oncol. 2016 Jan;10(1):157–65.

88. Schreuer M, Meersseman G, Van Den Herrewegen S, Jansen Y, Chevolet I, Bott A, et al. Quantitative assessment of BRAF V600 mutant circulating cell-free tumor DNA as a tool for therapeutic monitoring in metastatic melanoma patients treated with BRAF/MEK inhibitors. J Transl Med. 2016 Dec 19;14(1):95.

89. Booth AM, Fang Y, Fallon JK, Yang JM, Hildreth JEK, Gould SJ, et al. Exosomes and HIV Gag bud from endosome-like domains of the T cell plasma membrane. J Cell Biol. 2006;172(6):923–35.

90. Ratajczak J, Wysoczynski M, Hayek F, Janowska-Wieczorek A, Ratajczak MZ. Membrane-derived microvesicles: Important and underappreciated mediators of cell-to-cell communication. Leukemia. 2006;20(9):1487–95.

91. Raposo G, Stoorvogel W. Extracellular vesicles: exosomes, microvesicles, and friends. J Cell Biol. 2013 Feb 18;200(4):373–83.

92. Szajnik M, Czystowska M, Szczepanski MJ, Mandapathil M, Whiteside TL. Tumor-derived microvesicles induce, expand and up-regulate biological

activities of human regulatory T cells (Treg). PLoS One. 2010;5(7):e11469.

93. Skog J, Würdinger T, van Rijn S, Meijer DH, Gainche L, Curry WT, et al. Glioblastoma microvesicles transport RNA and proteins that promote tumour growth and provide diagnostic biomarkers. Nat Cell Biol. 2008;10(12):1470–6.

94. Li P, Kaslan M, Lee SH, Yao J, Gao Z. Progress in Exosome Isolation Techniques. Theranostics. 2017;7(3):789–804.

95. Peinado H, Alečković M, Lavotshkin S, Matei I, Costa-Silva B, Moreno-Bueno G, et al. Melanoma exosomes educate bone marrow progenitor cells toward a pro-metastatic phenotype through MET. Nat Med. 2012 Jun 27;18(6):883–91.

96. Bartel DP. MicroRNAs: Genomics, Biogenesis, Mechanism, and Function. Cell. 2004 Jan 23;116(2):281–97.

97. Suraj S, Dhar C, Srivastava S. Circulating nucleic acids: An analysis of their occurrence in malignancies. Biomed reports. 2017 Jan;6(1):8–14.

98. Lawrie CH, Gal S, Dunlop HM, Pushkaran B, Liggins AP, Pulford K, et al. Detection of elevated levels of tumour-associated microRNAs in serum of patients with diffuse large B-cell lymphoma. Br J Haematol. 2008;141(5):672–5.

99. Wang F, Zheng Z, Guo J, Ding X. Correlation and quantitation of microRNA aberrant expression in tissues and sera from patients with breast tumor. Gynecol Oncol. 2010 Dec;119(3):586–93.

100. Asaga S, Kuo C, Nguyen T, Terpenning M, Giuliano AE, Hoon DSB. Direct Serum Assay for MicroRNA-21 Concentrations in Early and Advanced Breast Cancer. Clin Chem. 2011 Jan 1;57(1):84–91.

101. Hindson BJ, Ness KD, Masquelier DA, Belgrader P, Heredia NJ, Makarewicz AJ, et al. High-throughput droplet digital PCR system for absolute quantitation of DNA copy number. Anal Chem. 2011;83(22):8604–10.

102. Horn S, Figl A, Rachakonda PS, Fischer C, Sucker A, Gast A, et al. TERT promoter mutations in familial and sporadic melanoma. Science (80-). 2013;339(6122):959–61.

103. Youden WJ. Index for rating diagnostic tests. Cancer. 1950;3(1):32–5.

104. DeLong ER, DeLong DM, Clarke-Pearson DL. Comparing the Areas under Two or More Correlated Receiver Operating Characteristic Curves: A Nonparametric Approach. Biometrics. 1988;44(3):837–45.

105. Altman DGDDG, McShane LLM, Sauerbrei W, Taube SSE, McShane LLM, Altman DGDDG, et al. Reporting recommendations for tumor marker prognostic studies (REMARK): explanation and elaboration. BMC Med. 2012;10(1):51.

106. De Unamuno Bustos B, Estal RM, Simó GP, De Juan Jimenez I, Muñoz BE, Serna MR, et al. Towards Personalized Medicine in Melanoma: Implementation of a Clinical Next-Generation Sequencing Panel. Sci Rep. 2017 Dec 29;7(1):495.

107. Nagore E, Heidenreich B, Rachakonda S, Garcia-Casado Z, Requena C, Soriano V, et al. TERT promoter mutations in melanoma survival. Int J Cancer. 2016;139(1):75–84.

108. Nazarian R, Shi H, Wang Q, Kong X, Koya RC, Lee H, et al. Melanomas acquire resistance to B-RAF(V600E) inhibition by RTK or N-RAS upregulation. Nature. 2010;468(7326):973–7.

109. Gangadhar TC, Savitch SL, Yee SS, Xu W, Huang AC, Harmon S, et al. Feasibility of monitoring advanced melanoma patients using cell-free DNA from plasma. Pigment Cell Melanoma Res. 2017;(May):1–9.

110. Shi H, Hugo W, Kong X, Hong A, Koya RC, Moriceau G, et al. Acquired resistance and clonal evolution in melanoma during BRAF inhibitor therapy. Cancer Discov. 2014;4(1):80–93.

111. Krauthammer M, Kong Y, Ha BH, Evans P, Bacchiocchi A, McCusker JP, et al. Exome sequencing identifies recurrent somatic RAC1 mutations in melanoma. Nat Genet. 2012;44(9):1006–14.

112. Gibney GT, Smalley KSM. An unholy alliance: Cooperation between BRAF and NF1 in melanoma development and BRAF inhibitor resistance. Cancer Discov. 2013;3(3):260–3.

113. Gide TN, Wilmott JS, Scolyer RA, Long G V. Primary and Acquired Resistance to Immune Checkpoint Inhibitors in Metastatic Melanoma. Clin Cancer Res.

2017;24(6):1260–70.

114. Manzano JL, Layos L, Bugés C, de los Llanos Gil M, Vila L, Martínez-Balibrea E, et al. Resistant mechanisms to BRAF inhibitors in melanoma. Ann Transl Med. 2016;4(12):237–237.

115. Chang-Hao Tsao S, Weiss J, Hudson C, Christophi C, Cebon J, Behren A, et al. Monitoring response to therapy in melanoma by quantifying circulating tumour DNA with droplet digital PCR for BRAF and NRAS mutations. Sci Rep. 2015 Sep 22;5(1):11198.

116. Ascierto PA, Minor D, Ribas A, Lebbe C, O'Hagan A, Arya N, et al. Phase II trial (BREAK-2) of the BRAF inhibitor dabrafenib (GSK2118436) in patients with metastatic melanoma. J Clin Oncol. 2013 Sep 10;31(26):3205–11.

117. Diaz LA, Bardelli A. Liquid biopsies: Genotyping circulating tumor DNA. J Clin Oncol. 2014;32(6):579–89.

118. Dressman D, Yan H, Traverso G, Kinzler KW, Vogelstein B. Transforming single DNA molecules into fluorescent magnetic particles for detection and enumeration of genetic variations. Proc Natl Acad Sci. 2003;100(15):8817–22.

119. Liu Q, Sommer SS. Pyrophosphorolysis-activated polymerization (PAP): Application to allele-specific amplification. Biotechniques. 2000;29(5):1072–6.

120. Vogelstein B, Kinzler KW. Digital PCR. Proc Natl Acad Sci USA. 1999;96(16):9236–41.

121. Rapisuwon S, Vietsch EE, Wellstein A. Circulating biomarkers to monitor cancer progression and treatment. Comput Struct Biotechnol J. 2016 Jan 1;14:211–22.

122. Chen Y-H, Hancock BA, Solzak JP, Brinza D, Scafe C, Miller KD, et al. Next-generation sequencing of circulating tumor DNA to predict recurrence in triple-negative breast cancer patients with residual disease after neoadjuvant chemotherapy. npj Breast Cancer. 2017 Dec 3;3(1):24.

123. Lv X, Zhao M, Yi Y, Zhang L, Guan Y, Liu T, et al. Detection of Rare Mutations in CtDNA Using Next Generation Sequencing. J Vis Exp. 2017 Aug 24;(126):e56342–e56342.

124. Shu Y, Wu X, Tong X, Wang X, Chang Z, Mao Y, et al. Circulating Tumor DNA Mutation Profiling by Targeted Next Generation Sequencing Provides Guidance for Personalized Treatments in Multiple Cancer Types. Sci Rep. 2017 Dec 3;7(1):583.

125. Yao Y, Liu J, Li L, Yuan Y, Nan K, Wu X, et al. Detection of circulating tumor DNA in patients with advanced non-small cell lung cancer. Oncotarget. 2017 Jan 10;8(2):2130–40.

126. Yang X, Zhuo M, Ye X, Bai H, Wang Z, Sun Y, et al. Quantification of mutant alleles in circulating tumor DNA can predict survival in lung cancer. Oncotarget. 2016 Apr 12;7(15):20810–24.

127. Baumgartner JM, Raymond VM, Lanman RB, Tran L, Kelly KJ, Lowy AM, et al. Preoperative Circulating Tumor DNA in Patients with Peritoneal Carcinomatosis is an Independent Predictor of Progression-Free Survival. Ann Surg Oncol. 2018 Jun 14;25(8):2400–8.

128. Fleischhacker M, Schmidt B. Circulating nucleic acids (CNAs) and cancer—A survey. Biochim Biophys Acta - Rev Cancer. 2007 Jan 1;1775(1):181–232.

129. Kaisaki PJ, Cutts A, Popitsch N, Camps C, Pentony MM, Wilson G, et al. Targeted Next-Generation Sequencing of Plasma DNA from Cancer Patients: Factors Influencing Consistency with Tumour DNA and Prospective Investigation of Its Utility for Diagnosis. Galli A, editor. PLoS One. 2016 Sep 14;11(9):e0162809.

130. Chae YK, Davis AA, Carneiro BA, Chandra S, Mohindra N, Kalyan A, et al. Concordance between genomic alterations assessed by next-generation sequencing in tumor tissue or circulating cell-free DNA. Oncotarget. 2016 Oct 4;7(40):65364–73.

131. Thompson JC, Yee SS, Troxel AB, Savitch SL, Fan R, Balli D, et al. Detection of Therapeutically Targetable Driver and Resistance Mutations in Lung Cancer Patients by Next-Generation Sequencing of Cell-Free Circulating Tumor DNA. Clin Cancer Res. 2016 Dec 1;22(23):5772–82.

132. Oxnard GR, Paweletz CP, Kuang Y, Mach SL, O'Connell A, Messineo MM, et al. Noninvasive detection of response and resistance in EGFR-mutant lung

cancer using quantitative next-generation genotyping of cell-free plasma DNA. Clin Cancer Res. 2014 Mar 15;20(6):1698–705.

133. Dawson S-J, Tsui DWY, Murtaza M, Biggs H, Rueda OM, Chin S-F, et al. Analysis of Circulating Tumor DNA to Monitor Metastatic Breast Cancer. N Engl J Med. 2013 Mar 28;368(13):1199–209.

134. Diaz LA, Williams RT, Wu J, Kinde I, Hecht JR, Berlin J, et al. The molecular evolution of acquired resistance to targeted EGFR blockade in colorectal cancers. Nature. 2012 Jun 28;486(7404):537–40.

135. Francis G, Stein S. Circulating Cell-Free Tumour DNA in the Management of Cancer. Int J Mol Sci. 2015 Jun 19;16(6):14122–42.

136. El Messaoudi S, Rolet F, Mouliere F, Thierry AR. Circulating cell free DNA: Preanalytical considerations. Clin Chim Acta. 2013 Sep 23;424:222–30.

137. van Dessel LF, Beije N, Helmijr JCA, Vitale SR, Kraan J, Look MP, et al. Application of circulating tumor DNA in prospective clinical oncology trials - standardization of preanalytical conditions. Mol Oncol. 2017 Mar;11(3):295–304.

138. Haselmann V, Ahmad-Nejad P, Geilenkeuser WJ, Duda A, Gabor M, Eichner R, et al. Results of the first external quality assessment scheme (EQA) for isolation and analysis of circulating tumour DNA (ctDNA). Clin Chem Lab Med. 2017;56(2):220–8.

139. Pantel K. Blood-Based Analysis of Circulating Cell-Free DNA and Tumor Cells for Early Cancer Detection. PLoS Med. 2016;13(12):e1002205.

140. Anglesio MS, Papadopoulos N, Ayhan A, Nazeran TM, Noë M, Horlings HM, et al. Cancer-Associated Mutations in Endometriosis without Cancer. N Engl J Med. 2017 May 11;376(19):1835–48.

141. Genovese G, Kähler AK, Handsaker RE, Lindberg J, Rose SA, Bakhoum SF, et al. Clonal Hematopoiesis and Blood-Cancer Risk Inferred from Blood DNA Sequence. N Engl J Med. 2014 Dec 25;371(26):2477–87.

142. Loeys BL, Schwarze U, Holm T, Callewaert BL, Thomas GH, Pannu H, et al. Aneurysm Syndromes Caused by Mutations in the TGF-β Receptor. N Engl J

Med. 2006 Aug 24;355(8):788–98.

143. Adjiri A. DNA Mutations May Not Be the Cause of Cancer. Oncol Ther. 2017;5(1):85–101.

144. Pollock PM, Harper UL, Hansen KS, Yudt LM, Stark M, Robbins CM, et al. High frequency of BRAF mutations in nevi. Nat Genet. 2002 Nov 25;33(1):19–20.

145. Bauer J, Curtin JA, Pinkel D, Bastian BC. Congenital Melanocytic Nevi Frequently Harbor NRAS Mutations but no BRAF Mutations. J Invest Dermatol. 2007 Jan;127(1):179–82.

146. Hauschild A, Grob JJ, Demidov L V., Jouary T, Gutzmer R, Millward M, et al. Dabrafenib in BRAF-mutated metastatic melanoma: A multicentre, open-label, phase 3 randomised controlled trial. Lancet. 2012;380(9839):358–65.

147. Olsson E, Winter C, George A, Chen Y, Howlin J, Tang ME, et al. Serial monitoring of circulating tumor DNA in patients with primary breast cancer for detection of occult metastatic disease. EMBO Mol Med. 2015;7(8):1034–47.

148. Zhao B, Wang L, Qiu H, Zhang M, Sun L, Peng P, et al. Mechanisms of resistance to anti-EGFR therapy in colorectal cancer. Oncotarget. 2017 Jan 17;8(3):3980–4000.

7. Appendices

Appendix 1 ROC analysis coordinates of *BRAF*^{V600E}, *NRAS*^{Q61} and *TERT*^{prom} ctDNA assays (related to Figure 4.11)

Biomarker	*BRAF*^{V600E}	*NRAS*^{Q61}	*TERT*^{prom}
AUC (%)	97.02	98.84	92.24
95% CI	95.48-98.56	97.22-100	88.78-95.69
Standard error	0.007	0.008	0.01
P	<0.0001	<0.0001	<0.0001
ROC curve coordinates			
Sensitivity (%)	94.96	98.09	87.58
Specificity (%)	100.00	100.00	100.00
PPV (%)	100.00	100.00	100.00
NPV (%)	82.50	90.00	55.81
Threshold (copies/ml)	11.74	10.30	13.04

AUC: Area Under the Curve, CI: Confidence Interval, P: Delong's test, PPV: Positive Predictive Value, NPV: Negative Predictive Value

Appendix 2 ROC parameters of ctDNA measurement in correlation to the radiologically assessed tumor load (CT/MRI scans) (related to Figure 4.14)

AUC of ctDNAs, LDH and S100 were calculated at 95% CI and AUC differences between ctDNA and serum markers were compared with the Delong's test.

Biomarker	***BRAF*^{V600E}**	**LDH**	**S100**
AUC (%)	87.27	63.66	66.55
95% CI	79.94-94.60	55.15-72.16	58.08-75.01
Standard error	0.03	0.04	0.04
P	<0.0001	0.001	0.0001
Biomarker	***NRAS*^{Q61}**	**LDH**	**S100**
AUC (%)	87.01	71.81	69.89
95% CI	78.56-95.47	52.90-90.72	52.84-84.87
Standard error	0.07	0.10	0.10
P	<0.0001	0.0601	0.0777
Biomarker	***TERT*^{prom}**	**LDH**	**S100**
AUC (%)	84.77	52.54	58.50
95% CI	72.61-96.93	40.35-64.72	41.15-75.85
Standard error	0.06	0.06	0.08
P	<0.0001	0.6774	0.3387
ctDNA ROC curve coordinates			
	***BRAF*^{V600E}**	***NRAS*^{Q61}**	***TERT*^{prom}**
Threshold (copies/ml)	35.85	51.50	32.83
AUC comparisons			
Pairs	**ctDNA, LDH**	**ctDNA, S100**	**LDH, S100**
Area difference (%)	23.61	20.72	-2.8900
P	<0.0001	0.0003	0.5459
Area difference (%)	15.20	17.12	1.92
P	0.1434	0.0272	0.6361
Area difference (%)	32.23	26.27	-5.96
P	0.0037	<0.0001	0.7695

AUC: Area Under the Curve, CI: Confidence Interval, *P*: Delong's test

Appendix 3 Contingency table of treatment response of *BRAF*^{V600E} patients (related to Figure 4.15E)

Tabular summary of data points of treatment response of *BRAF*^{V600E} patients categorized according to treatment response and ctDNA threshold (see Appendix 2).

Data analyzed	Non-responders	Responders	Total
<35.85 copies/ml	2	10	12
>35.85 copies/ml	34	5	39
Total	36	15	51

Fisher's exact *P*<0.0001

Appendix 4 Contingency table of 6 months PFS of *BRAF*^{V600E} patients (related to Figure 4.15F)

Tabular summary of data points of treatment response of *BRAF*^{V600E} patients categorized according to 6 months PFS and ctDNA threshold (see Appendix 2).

Data analyzed	PFS< 6 months	PFS> 6 months	Total
<35.85 copies/ml	0	12	12
>35.85 copies/ml	12	27	39
Total	12	39	51

Fisher's exact *P*=0.0468

Appendix 5 Contingency table of 6 months PFS of *NRAS*^{Q61} patients (related to Figure 4.16E)

Tabular summary of data points of treatment response of *NRAS*^{Q61} patients categorized according to 6 months PFS and ctDNA threshold (see Appendix 2).

Data analyzed	PFS< 6 months	PFS> 6 months	Total
<51.5 copies/ml	0	3	3
>51.5 copies/ml	11	3	14
Total	11	6	17

Fisher's exact *P*=0.0294

Appendix 6 Contingency table of 6 months PFS of *TERT*^{prom} patients (related to Figure 4.16F)

Tabular summary of data points of treatment response of *TERT*^{prom} patients categorized according to 6 months PFS and ctDNA threshold (see Appendix 2).

Data analyzed	PFS< 6 months	PFS> 6 months	Total
<32.83 copies/ml	1	8	9
>32.83 copies/ml	8	5	13
Total	9	13	22

Fisher's exact *P*=0.0306

Appendix 7 Contingency table of treatment response of *NRAS*^{Q61} patients (related to Figure 4.16G)

Tabular summary of data points of treatment response of *NRAS*^{Q61} patients categorized according to treatment response and ctDNA threshold (see Appendix 2).

Data analyzed	Non-responders	Responders	Total
<51.5 copies/ml	1	2	3
>51.5 copies/ml	14	0	14
Total	15	2	17

Fisher's exact *P*=0.0221

Appendix 8 Contingency table of treatment response of *TERT*^{prom} patients (related to Figure 4.16H)

Tabular summary of data points of treatment response of *TERT*^{prom} patients categorized according to treatment response and ctDNA threshold (see Appendix 2).

Data analyzed	Non-responders	Responders	Total
<32.83 copies/ml	4	5	9
>32.83 copies/ml	13	0	13
Total	17	5	22

Fisher's exact *P*=0.0048

Appendix 9 Contingency table of treatment response of patients in the validation cohort (related to Figure 4.19C)

Tabular summary of data points of treatment response of patients in the validation cohort categorized according to treatment response and ctDNA threshold according to ctDNA genotype (see Appendix 2).

Data analyzed	Non-responders	Responders	Total
Below threshold	3	12	15
Above threshold	18	2	20
Total	21	14	35

Fisher's exact *P*<0.0001

Appendix 10 Contingency table of 6 months PFS of patients in the validation cohort (related to Figure 4.19D)

Tabular summary of data points of treatment response of patients in the validation cohort categorized according to 6 months PFS and ctDNA threshold according to ctDNA genotype (see Appendix 2).

Data analyzed	PFS<6 months	PFS>6 months	Total
Below threshold	3	12	15
Above threshold	15	5	20
Total	18	17	35

Fisher's exact *P*=0.0020

8. Acknowledgements

I would like to thank the European Union's Horizon 2020 research and innovation program for the financial support of this project under the grant agreement No 641458.

I would like to express my gratitude to my supervisor Professor Alexander Roesch for his mentorship, and support during the PhD years. I would like to thank Professor Dirk Schadendorf and the Department of Dermatology for the supportive scientific environment. I also would like to acknowledge both past and present members of the Roesch lab.

I would like to thank the committee members, Professor Ralf Küppers and Professor Nelleke Gruis for reviewing my thesis. I would like to thank Antje Sucker and the personnel of the SCABIO biobank, Professor Nils von Neuhoff, Professor Jürgen C. Becker, Dr. Teo Seremet and Dr. Kilian Wistuba-Hamprecht for their collaborative efforts in this work. I would also like to express my appreciation to Professor Andreas Stang for his guidance and helpful discussions regarding the statistical aspects of my project.

I sincerely thank the MELGEN ETN project coordinators, Professor Julia Newton-Bishop and Juliette Randerson-Moor for their support and encouragement; I also thank the Leeds analysis group for providing statistical training. Many thanks go to all MELGEN students for their friendship.

My special thanks go to my family and friends all around the world. Finally, I would like to thank my wonderful “TGIT” crew: Sonia and Natalia for their friendship and outstanding support.

Végül, de nem utolsósorban, köszönöm családom és férjem odaadó szeretetét. Külön köszönettel tartozom édesapámnak, aki mindig támogatott és ellátott tanácsokkal.

9. Curriculum vitae

The biography is not included in the online version for reasons of data protection

The biography is not included in the online version for reasons of data protection

10. Statutory declarations

Erklärung:

Hiermit erkläre ich, gem. § 6 Abs. (2) g) der Promotionsordnung der Fakultät für Biologie zur Erlangung der Dr. rer. nat., dass ich das Arbeitsgebiet, dem das Thema ***„Application of circulating cell-free tumor DNA profiles for therapeutic monitoring and outcome prediction of metastatic melanoma“*** zuzuordnen ist, in Forschung und Lehre vertrete und den Antrag von ***Renáta Váraljai*** befürworte und die Betreuung auch im Falle eines Weggangs, wenn nicht wichtige Gründe dem entgegenstehen, weiterführen werde.

Essen, den _____ _____
(Prof. Dr. med. Alexander Roesch)

Erklärung:

Hiermit erkläre ich, gem. § 7 Abs. (2) d) + f) der Promotionsordnung der Fakultät für Biologie zur Erlangung des Dr. rer. nat., dass ich die vorliegende Dissertation selbständig verfasst und mich keiner anderen als der angegebenen Hilfsmittel bedient, bei der Abfassung der Dissertation nur die angegeben Hilfsmittel benutzt und alle wörtlich oder inhaltlich übernommenen Stellen als solche gekennzeichnet habe.

Essen, den _____ _____
(Renáta Váraljai)

Erklärung:

Hiermit erkläre ich, gem. § 7 Abs. (2) e) + g) der Promotionsordnung der Fakultät für Biologie zur Erlangung des Dr. rer. nat., dass ich keine anderen Promotionen bzw. Promotionsversuche in der Vergangenheit durchgeführt habe und dass diese Arbeit von keiner anderen Fakultät/Fachbereich abgelehnt worden ist.

Essen, den _____ _____
(Renáta Váraljai)